THE UNIVERSITY OF CHICAGO

DEVELOPMENT AND EXPLORATION OF NEW AUTOMATED TOOLS TO ACCELERATE RESEARCH ON TISSUE AND TUMOR MODEL SYSTEMS

A DISSERTATION SUBMITTED TO

THE FACULTY OF THE DIVISION OF THE PHYSICAL SCIENCES

IN CANDIDACY FOR THE DEGREE OF

DOCTOR OF PHILOSOPHY

DEPARTMENT OF CHEMISTRY

BY

BROOKE ELIZABETH SCHUSTER

CHICAGO, ILLINOIS

MARCH 2022

TABLE OF CONTENTS

LIST OF FIGURES

LIST OF TABLES

ACKNOWLEDGEMENTS

This thesis and my career at University Chicago would have not been possible without the involvement and support of my family, friends, and colleagues. First and foremost, I would like to thank my doctoral advisor and mentor Dr. Savas Tay for his guidance, tremendous support, and all of the wisdom he shared to help me grow as a scientist, engineer, and professional within the academic community and beyond. I appreciate his willingness to take a risk with me and providing the opportunity for me, a scientist with a chemistry and biology background with little to none engineering and computational experience, to join a lab with deep roots into both engineering and computational science. I am thankful he had faith in me and could see my willingness and eagerness to expand my knowledge and tackle new scientific challenges outside of my comfort zone. While most doctoral programs set a student up to be a "niche expert", the Tay lab provided a beautiful opportunity to not be restricted into one set box of knowledge and instead provided the opportunity to explore many different avenues of science.

I would like to significantly express my gratitude to the entire Tay Lab from my fellow graduate students to the post-doctoral staff. Each and every member helped facilitate such a welcoming and collaborative environment with a continuous excitement to learn and advance science. The initiation of the start of this organoid platform would have not been the same without the intellectual contributions and extensive mentorship provided by my post-doc mentor Michael Junkin during my first year of graduate school. I am eternally appreciative of all the time he took to teach me all that he knew and patience he had for my many novice questions. I would like to thank Jono Mathews and Parthiv Partel for sharing all their computational knowledge with me and acting as such resourceful guides to implementing the use of computational languages into my research. I also would like to highlight Nir Drayman as an additional great leader of our lab and

unreserved willingness to share his wealth of scientific expertise. We were all spoiled to have such a remarkable senior post-doc like Nir, who seemingly doubled as a second advisor and mentor to us all, and with his virology background helped transform our lab into rapidly-made viral experts as we shifted gears into the realm of COVID-19 research. I would also like to mentioned Navid Ghorashian, Luke Vistain, Minjun Son, Andrew Wang, Jing Lin, and Hoang Van Phan for also always willing to talk about microfluidics, a wide range of scientific topics, and providing support with each other's projects, even though we were all pursuing various unrelated projects and topics.

Beyond the Tay Lab, I would like to thank my additional collaborating advisors: Kevin White and Andrey Rzhetsky, for their insightful discussions and devoted contributions to my projects. I am extremely grateful to be surrounded by not just one, but multiple influential advisors to learn from and help shape me into the scientist I am today. Additional thanks to each of my organoid collaborators: Isabel Romero-Calvo, Kori Kirby, and Chris Weber with the pancreatic cancer organoids; Sonia Kupfer, Dereck Alleyne, and Maggie Bielski with the colon organoids, and Dana Ishay-Ronen and Rakefet Ben-Yishay with the lung organoids.

To all of the wonderful friends I've met during my graduate school experience and my old friends who stuck with me during this busy time of my life, thank you for providing additional emotional support and plenty of fun times to destress outside of the academic environment.

Last, but certainty not least, thank you to my family for all the never-ending love and support during my entire collegiate career. Mom, thank you for always being just a phone call away for whenever I needed any extra support and always being my number on cheerleader. Dad, thank you for always being there to be support me during my entire career journey; no matter what journey I decided to pursue next, you never doubted me. An additional shout out to my brother John, Aunt Candace, Grandma Sandy, and all my in-laws, including my second set of parents:

Tony and Jeri, for also being supportive during my graduate career. Finally, Kevin, thank you for being my strongest, most supportive partner and my never wavering rock during my entire 5 years of graduate school. It is hard to put in words how much you mean to me and how much you provided to me; this experience wouldn't have been the same without you. Thank you for always believing with me and your continuous encouragement.

ABSTRACT

Drug attrition rates for cancer are much higher than in other therapeutic areas. There is an urgent need for appropriate tumor models that can physiologically replicate the key features of human tissue to find optimal strategies to evaluate novel and effective agents and ultimately develop curative chemotherapies. Historically, 2D or traditional monolayer cancer cell lines, with limited representation of the actual tumors they are derived from, have been utilized for cancer and drug development research, as well as expensive and time-consuming patient-derived xenograft models or mutation-based rodent models. However, the realization of the vision of precision and personalized therapy urgently requires the development of individualized tumor models that are low cost, high throughput and broadly applicable to both research and clinical settings.

Organoids, multicellular constructs derived from self-organizing stem cells, are three-dimensional *ex vivo* tissue models that incorporate many of the physiological and genetic features of the in vivo tissue. Organoids promise to provide realistic research models for developmental and stem cell biology such as characterization of fundamental tumor development mechanisms, drug development and screening, and the study of basic biological processes such as cellular nutrient sensing and hormone secretion. Brain, breast, colon, prostate, lung, liver, and pancreas organoids are just some examples of tissues and tumors currently being studied. In this thesis, I will discuss and report a new solution to advance the use of organoids as a widely practical research technique. To achieve this, chemistry, biology, and engineering principles were used to design and develop a highly reproducible, standardized, miniaturized assay that can be performed in both research and clinical settings, utilizing minimal amounts of reagents in a low-cost automated system permitting screening of thousands of conditions.

First, I will discuss the optimization, characterization, and validation of an integrated microfluidic based *ex vivo* tissue and tumor modeling system that is superior to the currently available approaches in terms of ability to facilitate and accelerate both preclinical and foundational research in a high-throughput fashion with optimal user friendliness and reproducibility. Following, I will reveal a new easy to use and open source, computer vision-based platform, called OrganoID, that recognizes, labels, and tracks single organoids in brightfield and phase-contrast microscopy images. OrganoID enables straightforward and accurate analysis of organoid images to accelerate the use of organoids as physiologically relevant models in high-throughput research and compatible with both the new microfluidic culture platform as well as more traditional organoid culture methods.

CHAPTER 1

INTRODUCTION

1.1 Overview and motivation

Cancer is a highly complex disease. Identification of effective cancer therapies is constrained by the limited ability to timely screen numerous possible treatments in the required patient-specific manner. One promising new avenue to achieve this goal is via culturing of three-dimensional (3D) cancer organoids. These tissue-like systems, which can be readily created from individual patient's tumors, manifest many of the properties of primary tumors and can be maintained, expanded, and manipulated outside the body. Given these attractive attributes, identifying effective treatments still poses significant problems including the presence of biological noise, complexity of understanding multi-drug interactions, cost to conduct screens, and achieving the throughput necessary to obtain answers in a limited time frame. To address these issues, I will introduce a microfluidic organoid platform capable of housing 200 culture chambers coupled with an analysis pipeline to make sense out of multi-component drug interactions. This system provides the culturing of a high number of patient-specific replicates of cancer-derived organoids that are simultaneously subjected to different drug treatment possibilities over the course of a single

experiment. Resulting image and molecular data from experimentation is analyzed, and computational machine learning based analysis is applied to reveal the effective landscape of drug treatment. The high experimental throughput and favorable culture conditions of this platform provides the data necessary to make sense of noisy cancer data via its throughput, and the timeline of its workflow can rapidly identify potential treatments by considering a high number of conditions at a single time.

In summary, this project focused on the development of a "ready for implementation" cancer model system for screening and identifying non-trivial drug treatment possibilities in a patient specific manner. The hope is the following advanced methods, devices, and analysis framework will help the field of cancer therapeutics to solve the challenging problem of rapidly identifying the best cancer treatments (**Figure 1-1**).

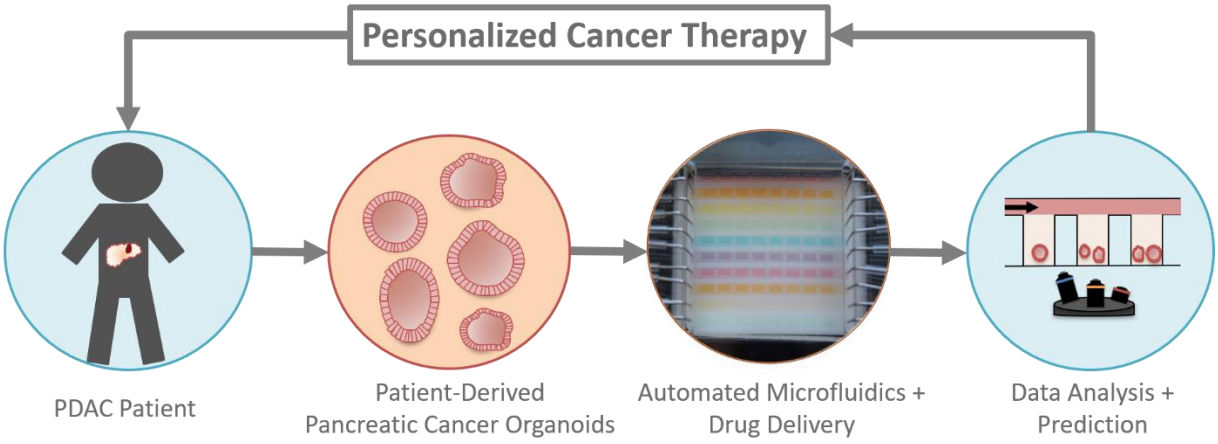

Figure 1-1: Project Overview

Brief example of how the automated organoid culture and stimulation platform integrated with a computational analysis pipeline can be applied to patient-derived organoids. Simply, patient-specific organoids are established through surgery or fine-needle aspiration from a pancreatic ductal adenocarcinoma (PDAC) patient, which are cultured in a high throughput, automated microfluidic device and subjected to a series of drug screens. The integrated system will be simultaneously imaged via phase contrast and fluorescence deconvolution microscopy to provide real-time measurements of cell reactions, movements, and proliferation to ultimately identify useful drug therapies and develop personalized treatment strategies.

1.2 Organoids: a tissue and tumor modeling system

Appropriate tumor models that can physiologically replicate a cancerous tumor may be essential in finding optimal strategies to develop curative chemotherapies. Historically, monolayer cancer cell lines, which contain limited representation of the actual tumors, along with expensive and time-consuming patient derived xenograft (PDX) models have been the focus for cancer and drug development research. However, the expense, limited realistic representation, and time barriers have produced a great need for a new model that can accurately represent real life tumors and be tested on quickly. The recent development of patient derived cancer organoids show promise to the development of individualized tumor models that are more realistic and characteristic of a human cancerous tumor[1]. Before we can take a deep dive into this thesis, we must answer the questions of what is an organoid and how does this modeling system compare to previously established models?

Organoids are multicellular constructs derived from self-organizing stem cells, embryonic, or from cells isolated from adult tissues that display the three-dimensional architecture, physiology, and genetic signatures of the intact organs[2,3]. Organoids closely recapitulate the cellular heterogeneity, structural morphology, and organ specific functions of a variety of tissues. Organoid models are established from a growth cocktail or media compromise of tissue or tumor specific growth factors and small molecules along with a basement membrane for its 3D structure support (i.e. hydrogels or Matrigel) to ultimately recreate the specific niche requirements needed for long-term flourishment.[3] Tumor organoids are clonally established from a few dissociated single cells of tumor tissue and are able to reflect the original tumor heterogeneity, which is optimal for drug sensitivities studies. Colorectal, pancreatic, liver, breast, prostate, bladder, ovarian cancers

organoids are just a few examples that were established and used to investigate drug response in comparison to corresponding patient or PDX responses[4–10]. On top of the preservation of the genetic heterogeneity, the organoid technology has been shown to exhibit cell-to-cell and cell-to-matrix interactions as well as interactions between cancer cells and other cellular components such as ones featured in the tumor microenvironment (i.e. stomal/fibroblasts and immune cells)[11].

It is important to note organoids are not limited to cancer and offer many possibilities for modeling and studying normal development and disease processes, opening up a wide range of exploratory medical research[2]. Wild-type or unaltered organoids can be genetically modified to create different disease models such as cystic fibrosis and polycystic kidney disease using gene editing methods like CRISPR[12–15]. Foundational developmental research has become emersed with the use of brain organoids or otherwise termed "mini-brains" for the study of developmental processes and neurological disorders[16], ultimately creating new avenues for a field lacking a good representative *in vitro* or *ex vivo* system. Interestingly, brain organoids have been shown to be cultured for more than 9 months, allowing for development of mature functional features such as the formation of active neurons and neuronal networks equipped with photosensitive cells that responded to light-based sensory stimulation[17].

Human organoids have also been shown to be introduced and implanted into animal models such as mice after establishment including intestinal and liver[13], even brain organoids[18], for regenerative medicine studies as well as cancer models to provide a more compensative model (i.e. immune cells and microtumor environment) and ultimately turning an *ex vivo* model *in vivo* by providing a complete vascular system. In addition to drug sensitivity studies, toxicology screens for tumorigenesis have also been implemented. Lastly, but surely not limited to, viral infections[12,19], organoid-virus co-culture models, and intestinal organoid cocultures with

microbes[20] to study microbiome relationships have been demonstrated as other capabilities of organoid models. Most recently, organoids jumped into the spot light as a model using lung or airway and colonic organoids co-cultured with SARS-CoV-2 as a model to study for the coronavirus pandemic[19,21,22]. Most uniquely, a 2020 *Cell* paper[23] even introduced the creation of snake venom gland organoids that not only was able to accurately represent the regional and cellular heterogeneity of the venom glands, but secreted functionally active toxins through venom-producing cells.

While their opportunities in both basic and clinical research seems to be endless, organoids are commonly confused with spheroids, another modern 3D cellular structure model, also known as tumorspheres. Unlike organoids, spheroids are formed from immortalized tumor cell lines and are assembled primarily via cell-to-cell adhesion to create their 3D structure[24]. Their cell line origin creates the spheroids' monoculture nature, lacking the multicellular identity that exists in organoids as well as the original tissue of interest. However, like immortalized cell lines and unlike most primary tissue cultures, once an organoid line has been established, the cultures can be cryopreserved and expanded, genotyped, and experimented on within weeks of harvesting from the original tissue source.

1.2.1 Organoids compared to other traditional tissue and tumor models

The recent boom of organoid related research in the past decade begs the question of what was the driving force to create these new models? Classically, for many decades, cell biology research, including cancer and drug development, has relied on human tumor-derived monolayer cell lines and *in vivo* xenograft mice; however, both models have drawbacks[25,26] (**Figure 1-2**). Traditional monolayer or two-dimensional (2D) cell culture ultimately lacks the 3D architecture

of the original organ tissue or tumor. Specifically, the main draw to these 3D models is the recapitulation of the original architecture shown to influence a range of cellular processes such as signaling, proliferation, viability, and drug response[27,28].

Unlike monolayer cultures, PDX or patient-derived xenograft models are able to provide complex architecture, tissue heterogeneity, as well as a complete vascular system along with tumor microenvironment[29]. However, these models are highly inefficient as they come with high labor costs, extremely prohibitive time requirements (up to 6 months), large tumor sample size requirement (typically ~100mm^3), and ultimately contain interactions from infiltration of murine stromal cells, which could affect the accuracy of drug sensitivity studies. The murine components also open the possibility of the model to become more transcriptionally "mouse-like" in comparison to the original primary tumor sample. Most importantly, the time and cost related challenges ultimately makes this system obsolete in terms of being able to use organoids on a broader scale for personalized or individualized therapies. Also, organoid establishment does not require a large tissue sample and could even be grown from a routinely collected cancer bioscopy such as endoscopic ultrasound-guided fine needle aspiration (FNA), which allows for patient specific organoid development without the requirement of a surgical resection of the tumor. Finally, dissociated tumor cells could be cultured as monolayers, however like immortalized cell lines they are unable to reflect the heterogeneity of the primary tumor due to selection in culture, lack the tissue specific architecture and mechanical cues, and are often limited on the number of passage expansions and are difficult to cryopreserve.

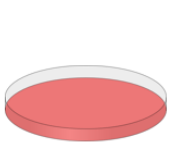
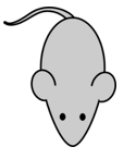
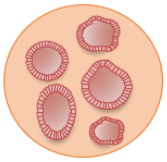

	2D Monolayers	PDXs	Organoids
Advantage	• Rapid Expansion • Less Costly	• 3D architecture • Stroma • Vascular System	• 3D architecture • Small amount of primary tumor needed (FNA) • Less Costly • Rapid Expansion • Models the tumor's cellular heterogeneity
Disadvantage	• Lack of 3D architecture • Unclear if culture conditions select for subset of tumor cells • Limited representation of primary tumor	• Rapid experimental interrogation is difficult • Time consuming and costly • Large primary tissue piece is needed • Interspecies differences • Murine stroma • Immuno-compromised mice limits the use of PDX to study immunotherapy	• Only epithelial cells

Figure 1-2: Comparison of organoids to traditional tissue cultures and models

1.2.2 Common challenges of organoid models

Development and culturing of organoids as well as other 3D cellular structures requires the use of an extracellular gel-like matrix to support cellular growth into 3D constructs. A wide range of hydrogels are commercially available to provide the support as well as some necessary proteins and growth factors needed to establish, grow, and maintain organoid cultures. Hydrogels can be synthetically derived, however the most used hydrogels for organoid studies are Basement Membrane Extract (BME) or Corning Matrigel matrix, which are purified from murine Engelbreth-Holm-Swarm (EHS) tumors. Composed primarily from type IV collagen and laminin, Matrigel, our preferred gel of choice for most of the studies featured, provides a natural extracellular matrix hydrogel that polymerizes at 37 ˚C to form a reconstituted basement membrane for organoid growth. Matrigel is handled and kept at 4 ˚C to keep it as a vicious liquid

while preparing the samples for the experiment. The use of a temperature sensitive material ends up being one of the most challenging hurtles faced in this thesis project and the methods created to conquer this hurtle will be discussed in **Chapter 2 and 4**.

Overall, organoids are a versatile technology that allows the creation of *ex vivo*, microscopic organ and tissue-like models to study a wide array of both basic and clinical research. The past decade of published organoid research has shown potentially just the "tip of the iceberg" of all the different avenues of research that could be enhanced and positively influenced by the incorporation of organoid models. Yet, challenges still remain including the need to increase the efficiency and decrease the time and costs associated with organoid generation and experimentation and developing methods to conduct experiments with organoid models in a high-throughput and automated fashion[14]. Such challenges have been addressed and solved with the following presented thesis.

1.3 Uncovering pancreatic cancer's complexity and genetic heterogeneity

As of 2021, pancreatic cancer is the third leading cause of cancer death with an overall 5-year survival rate of 10%, which is the highest mortality rate of all of the major cancers[30]. More than 90% of cases are pancreatic ductal adenocarcinoma (PDAC), which originates in the exocrine tissue of the pancreas. Pancreatectomy, surgical removal of the tumorous region of the pancreas, remains the single most effective and successful treatment, which unfortunately only ~20% of PDAC patients are even quantified candidates for. A 2013 genome study[31] noted that in a set of 99 PDAC patient samples, 2,627 mutations were detected with an average of 26 mutations per patient. Also, 1,456 of the mutations identified were classified as novel ultimately revealing the

complex heterogeneity of PDAC between the samples. Overall, the genomic landscape of pancreatic cancer identified the KRAS, TP53, CDKN2A, and SMAD4 genes as the most frequently mutated. This study highlighted the need for a better understanding of the complex molecular pathology of pancreatic cancer to elucidate the molecular phenotypes to ultimately categorize and define subgroups of patients that will respond to specific therapies.

In 2013, the Chicago Pancreatic Cancer Initiative (CPCI) led by Dr. Ralph Weichselbaum of University of Chicago Medicine and Dr. Kevin White of University of Chicago Biomedical Sciences Division and Medicine involved physicians, computational biologists, engineers, pathologists, surgical oncologist, and clinical oncologist to genomically characterize pancreatic cancers and to develop associating PDX and organoid models. Their protocols for the development of the PDAC organoids were based on and modified from the 2016 publication from the Tuveson Lab introducing the creation of human and mouse PDAC organoids[1]. The CPCI collected genomic data, biospecimens, and clinical information from more than 300 patients with pancreatic cancer. A 2018 publication summarize some of their comparison studies between the structural and genetic features of PDAC organoids and their original tissue[32]. The study concluded that histopathological features or morphologically and PDAC representative protein markers such as claudin 4 and CA19-9 showed strong concordance between the organoid and the original tissue. Specifically, with the morphology studies, they identified three major epithelial growth patterns: simple, papillary, and cribriform, between the organoid models and the primary tumor (**Figure 1-3**). DNA and RNA sequencing of single organoids or RNAseq also revealed patient-specific genomic and transcriptomic consistency. Genetic mutations were stable over time and passage number illustrating the ability to expand and cryopreserve the organoids for undefined number of experiments.

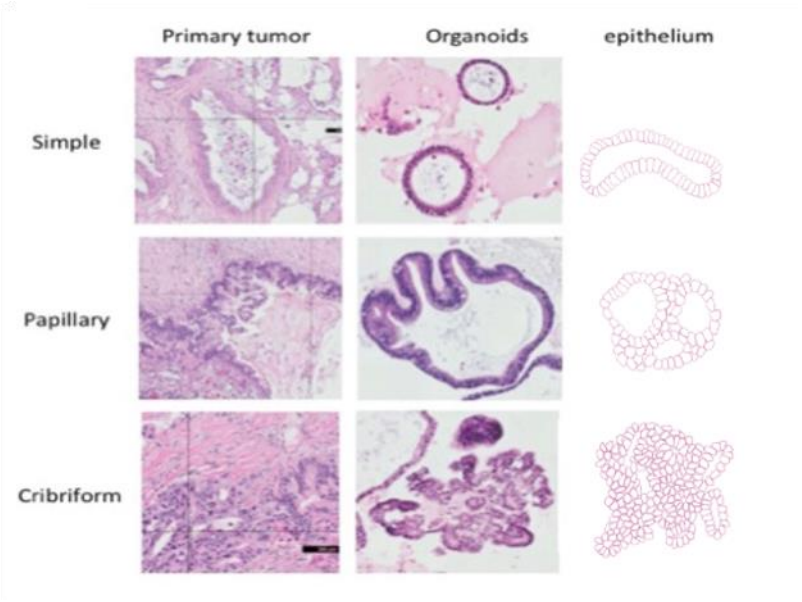

Figure 1-3: Morphologies between PDAC organoids and primary tumor samples compared

An expert GI pathologist, Dr. Christopher Weber, MD of UChicago Medicine, compared the architecture and cell morphology of the PDAC organoids established versus the primary tumor. Primary tumors and organoid morphologies were classified as Simple, Papillary, or Cribriform morphologies. The general pattern of cellular atypia and glandular architecture of the primary tumor was consistent with the morphology produced by the corresponding organoid model. Thus, this demonstrated the ability to derive PDAC organoids that morphologically recapitulate key attributes of the primary tumors. Figure created from data collected by Dr. Isabel Romero Calvo, PhD of the White Lab.

Their concluding results indicated a strong relationship of both morphological and molecular levels between the original tissue and organoid models. However, a major caveat of the study laid within their RNA sequencing analysis and claim that the cellular population of single organoids were largely clonal. Half of the organoids featured in the paper were derived from PDX models and not a direct product from the original tumor (i.e., organoids were created from tissue sample derived from PDX mouse model and not the original tissue: original tumor → PDX model → organoid). One of those PDX derived organoids was the only patient sample used for all their RNA seq analysis. The loss of heterogeneity seen within the organoid population could easily be linked with the use of PDX derived organoid instead of an organoid derived straight from the original tumor. Another 2018 organoid study published in Cell further debunked the primarily clonal

population theory with the investigation of over 100 primary and metastatic breast cancer organoid lines and their ability to broadly recapitulate the diversity and heterogenetic populations of the origan tumor[33]. DNA copy number variations and sequence changes between the tumor-organoid pairs were largely consistent, even after multiple passages. The study even concluded with an *in vitro* drug screen and compared them to PDX and the actual patients' drug responses.

This breast cancer study is not the only study published demonstrating organoid's remarkable ability to reflect tumor heterogeneity; studies regarding intestinal[34] and colorectal[35] organoids, ovarian[10] cancer, bladder[9] cancer have taken deep divides on the genetic and phenotypic relationship between organoids and their original tumor as well as drug sensitivities comparisons. Overall, these studies highlight organoids' abilities to fulfill the requirements needed to become the superior model for cancer research and drug development.

This is a good point to also mention that while PDAC and PDAC organoids were the main focus model for this thesis project, the technology and tools developed and soon to be presented are compatible with other types of cancer organoids as well as non-cancerous disease models as demonstrated later in this paper.

1.4 The use of microfluidics in cell culture

The speed and cost of organoid culture and comprehensive screening for drug sensitivities, among many other experimental explorations, is limited due to expensive reagents and labor-intensive nature of such screens. While not nearly as costly as PDX models, organoids expenses can be significantly higher than traditional immortalized cell lines due to the added reagents such as growth factors and specialty hydrogels that are needed for organoid establishment and growth.

To overcome this limitation, this project involved a creation of a standardized, miniaturized assay that can be performed in a highly reproducible environment with utilization of minimal amounts of reagents using an automated system to allow users to culture and screen thousands of conditions with minimal training and investment. All these goals are addressed through the use of microfluidics, a versatile engineering technique capable of manipulating small liquid volumes (in the range of picoliters to microliters) with micrometer-scale features. Microfluidic platforms enormously decrease experimental costs through the reduction of the sample and reagent volume needed to conduct experiments. Such platforms are easily engineered and manipulated to features a diversity of designs and integrative features to suite a wide range of experimental needs from single cell stimulation and signaling to high-throughput, multi-chambered cell culture. The integration of automation allows for easy multi-dimensional experimentation through liquid manipulation that is more precise than pipetting, accompanied with automation to greatly reduce labor and human pipetting errors.

1.4.1 Previously developed microfluidic tools

My principal investigator's, Dr. Savas Tay, lab has been active in the development of microfluidic platforms for high-throughput cell culture technologies primarily used for cell signaling studies. In 2019, an automated microfluidic device was developed by the Tay lab that contains 1,500 individually addressable and programmable micro-culture chambers capable of hosting 2D cellular populations as well as 3D neurospheres[36]. This system was used to explore the signaling landscape of neuronal stem cell differentiation through machine learning based data analysis, but unfortunately is not compatible with organoid culture due to well size and gel restrictions.

Focusing on single cell technologies, the lab has developed microfluidic devices to quantify the time-dependent secretion of cytokines from single immune cells[37] and ultrasensitive proteomic method in single-cells with a 0.5 femtomolar limit of detection for endogenous proteins[38]. Using these systems, we discovered digital NF-κB activation under inflammatory inputs[39,40], which greatly contributed to the understanding of innate immune response at the single-cell level, and allowed us to develop a comprehensive mathematical model of NF-κB. We discovered that transcription factor (p65) nuclear localization in single cells are entrained, and synchronize with a pulsatile inflammatory input[41,42]. We investigated co-stimulation of NF-κB under pathogen (LPS, PAM) inputs and showed that cells make a decision to respond to only one of the signals [43].

Most importantly, we seamlessly integrated computational methods and protocols into microfluidic experiments, such as automated cell isolation, feeding, imaging, computer aided cell tracking, and retrieval and subsequent gene expression analysis [44]. We developed custom chip and microscope control software and GUIs (simple, easy to use application platforms) for realization of truly automated experiment and systems, and developed image segmentation and single-cell tracking algorithms and statistical data analysis[39,40,43,44] . We have used machine learning based methods to analyze our data, such as the use of decision tree analysis and hierarchical clustering to analyze complex drug and signaling input stimulation of neurospheres, and identified cellular logic rules in neuronal stem cell differentiation[36].

There are various types of microfluidics (e.g., valve-based, droplet-based, paper-based, and digital microfluidics). The Tay lab has been primarily focused on value-based and droplet-based devices. Our most recent valve-based microfluidic publications include a device for ultrasensitive protein/mRNA measurements in single cells[45]. The use of previously published devices allowed us to further explore the NF-κB signaling pathway through dynamic stimulations and developed a

new machine learning or computer vision technique to predict NF-κB activation in cells. Finally, the recent adaption of microfluidic droplet technique has led to high-throughput experimentation screens of antibiotic resistant gut microbes[46] and single-cell RNA sequencing for exploration of virus infections[47].

1.4.2 Overview of the design and construction of microfluidic devices

Valve-based microfluidic devices consist of arrays of fluidic channels that can be arranged in a multitude of designs to suite your experimental needs as demonstrated by the examples given in **Section 1.4.1**. Microfluidic valves allow for precision control and movement of fluids through these channels as desired[48]. The functionality of valve-based microfluidics consists of at least two layers: a flow and control layer. These layers are often fabricated out of a polymer called polydimethylsiloxane (PDMS) through a process called soft lithography. The flow layer contains all the fluids, cells or cellular components, and desired chemical or physical stimulants. The control layer consists of a system of pressurized water that activates the microfluidic valves through pushing on and pinching off the fluidic flow of the flow layer at precise locations. Similar to an integrated electron circuit, the use of microfluidic valves expands the engineering capabilities and designs of these fluidic channels resulting in increasing complexity and development of specialized functions from on-off valves, switching valves to pumping systems[48,49].

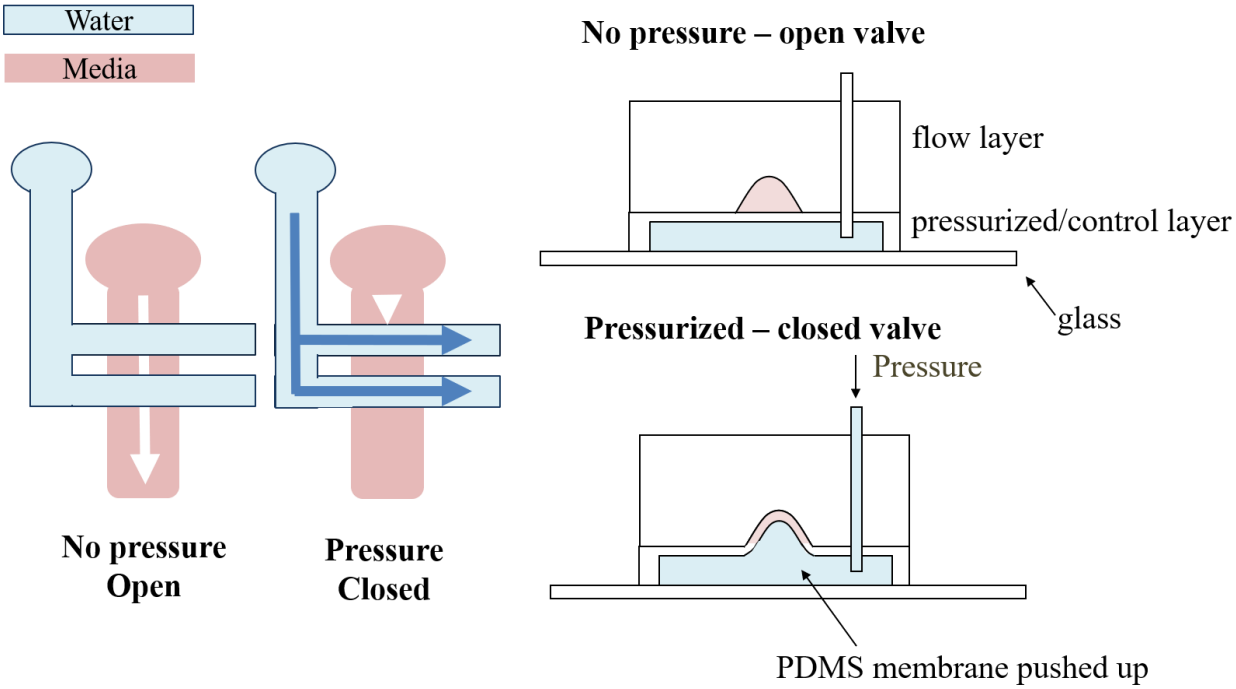

Figure 1-4: A schematic of the mechanism of a microfluidic valve

The left portion features a top view of a valve and the right shows a cross-section. The control layer features a thin layer of PDMS that can be manipulative through the presence of pressurized water. Though the influence of pressurized water, the thin PDMS membrane gets pushed up in the area of the flow layer, pinching off and closing the ability of liquids to move freely in the flow layer channels. When this pressure is released, the thin layer relaxes and the valve is opened, allowing fluidic movement in the flow channels to resume.

Our valve-based microfluidic devices are created using a replication molding approach. The molds used to create each layer of the device are fabricated using standard photolithography techniques with a combination of positive and negative photoresist on silicon wafers. The photoresist patterns on the silicon wafer are replicated and formed into layers required for the function of the device using soft lithography technique and PDMS. This technique allows for the researcher to design, print, pattern the mold, and create an entirely new device in around a day's worth of time. The ease of creating a single device by one solo researcher allows for easy changes and alterations of the device's design as needed. Following, the layers are permanently bonded using an oxygen plasma treatment process and holes are punched so the fluidic channels for both

the control and flow layers are easily accessible by external tubbing, which we call the “inlets” and “outlets” of the device. Finally, the completed PDMS based device is bonded to a glass slide suitable for microscopic imaging.

Automated and precision control of microfluidic valves are externally actuated using electronic solenoid valves connected to pressurized air and tubing pre-filled with water, where valves are activated or “closed” by the initiation of air pressurizing the water into the control fluidic channels and the valves are “opened” with the release this pressure (**Figure 1-4**). The control layer consists of a thinner PDMS layer in comparison to the flow layer in order to be manipulative by the pressurized water, which also provides separation between the fluids of the control and flow layers, preventing any unwanted cross-talk. These actions are easily controlled using MATLAB based GUIs or other computational interfaces. Overall, these features allow for precise and automatic delivery of reagents to independent chambers of cells as well as labor-free, error-free, and time-dependent delivery, and the additional of a cluster of valves creates peristaltic pumps designed to provide even more dynamic and specific volume control (examples can be seen in **Section 1.4.1**).

Finally, the valve control system, equipped with solenoid valves, along with the corresponding control computer are easily portable for use on different microscopes. The imaging microscopes themselves are fully motorized and contained their own incubation system to control temperature, humidity, and CO_2 for long term culture capabilities as pictured in **Figure 1-5**.

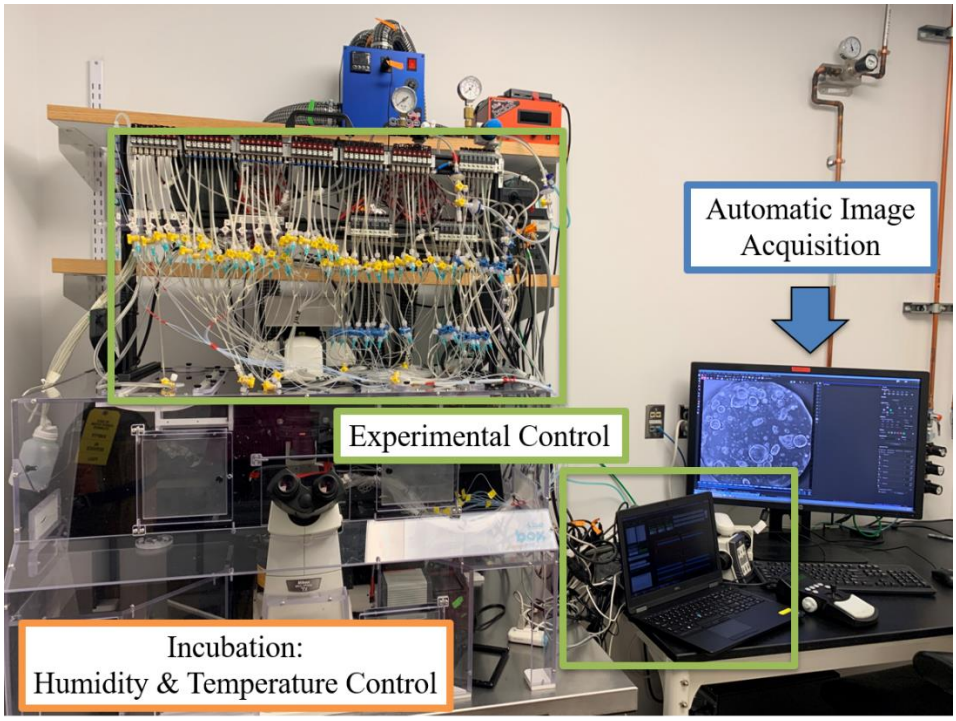

Figure 1-5: Photo of microfluidic culture system setup

A brief system overview: Experimental control is obtained using an array of solenoid valves connected to a pressurized air source and control by a USB controller box operated by a standard laptop control. A separate computer controls a fully motorized and automated inverted fluorescence microscope. A customized incubation system surrounds the microscope to provide consistent humidity, temperature, and CO_2 control.

1.5 Summary and Aims

Overall, a major bottleneck in precision oncology is the development of reliable, fast, and inexpensive assaying using *ex vivo* cancer models. An ideal system would minimize measurement noise, robustly measure effects of single drugs and drug cocktails, and be applicable to primary patient tumor and tissue samples. Such variability necessitates screening each drug or therapeutic condition with many multiple replicates creates a significant burden on studies relying on traditional low-throughput cell or organoid platforms and systems. Further, combinatorial and temporal screening of drugs and biologics have previously only been possible through the use of

complex and expensive robotic systems, which are also not suitable for real-time monitoring and probing of cellular and molecular features. The use of robust microfluidic technologies, already established by the laboratory, provides the potential engineering technical capabilities to bring to life a "turnkey" integrated cancer or tissue model platform to facilitate preclinical research and development of personalized treatment strategies and overall ease the ability to use organoids in a wide range of experiments. Here, I will introduce a platform with the ability to automatically stimulate, image, and then analyze within one microfluidic based system by real-time imaging of primary human tumor or tissue samples with integrated capabilities of high-throughput measurements of features such as tumor growth or drug responses (**Figure 1-6**).

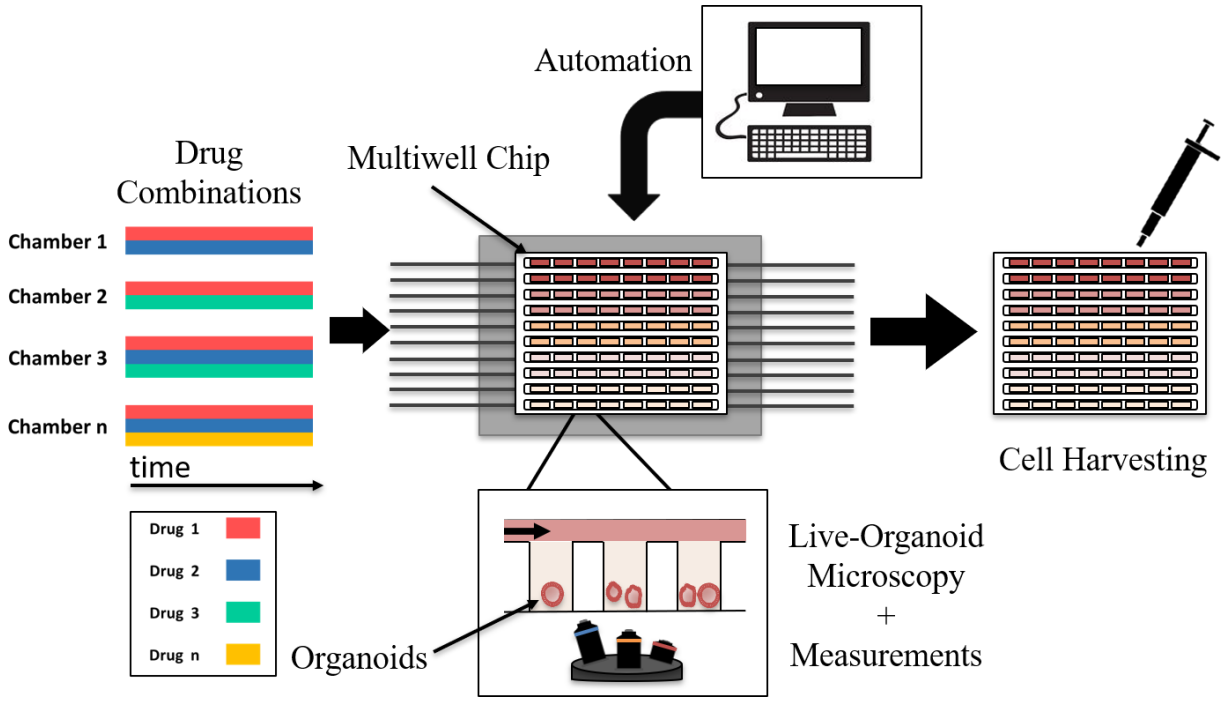

Figure 1-6: Overview of platform for organoid growth, culture, and stimulation

A simplified schematic of the presented microfluidic device capable of housing patient-derived organoids coupled with automated programing of dynamic and combinatorial drug stimulation profiles to well array subsets producing many parallel experiments simultaneously. Organoids are observed before, during, and after stimulation to quantify drug effects. After an experiment is completed, organoids can be easily harvested out of the device for further analysis.

1.5.1 Aim 1: Establishment of a Platform for Organoid Growth and Culture

The first goal of this project is to develop the necessary engineering principles to design microfluidic devices that are capable of housing, growing, and stimulating multiple organoids or other 3D cell-based structures and, ultimately, to evaluate the efficacy of an integrated microfluidic system for research applications. This can be validated using traditional plate-based techniques for comparison and validation that the use of this platform does not affect the growth and development of the organoids.

1.5.2 Aim 2: Automatic and Dynamic Stimulation and Screening

The devices described in Aim 1 will be equipped with automatic and dynamic stimulation and screening capabilities to facilitate organoid growth and high-throughput delivery of reagents in a robust, simple, precise, time-specific manner with low labor intensity and minimized potential for human error. This platform will be combined with high-throughput and automated image acquisition compatible with fluorescence probes or immunofluorescence to record and quantify organoid responses. Aim 1 and Aim 2 will be discussed in greater detail in **Chapter 2**.

1.5.3 Aim 3: A Machine Learning Pipeline for Automated Organoid Image Analysis

Finally, a computational machine-learning based pipeline capable of automatically analyzing groups of diverse organoid images to simplify and accelerate the ability to process large amounts, terabytes in size, of organoid based images obtained from the high-throughput platform discussed in Aim 1 and 2. The specific capabilities of said pipeline will be discussed further in **Chapter 3**. Overall, the platform in conjugation with the computational analysis pipeline has the

potential to provide a complete system superior to currently available approaches for a wide range of studies including, but not limited to, (a) studying the developmental trajectory of specific tissues and the factors that contribute to it, (b) genetic manipulation of biological systems to probe the mechanisms of various cellular processes, and (c) preclinical cancer or disease research on organoids and other 3D cell culture lines. In the following chapters, I will introduce and present a new novel platform capable of culturing and stimulating individualized human-derived tumor or tissue models that are low cost, high throughput and broadly applicable to both research and clinical settings.

CHAPTER 2

A NEW TOOL FOR ORGANOID EXPERIMENTATION AND DISCOVERY

Portions of this chapter was published in *Nature Communications*: Brooke Schuster, Michael Junkin, Sara Saheb Kashaf, Isabel Romero-Calvo, Kori Kirby, Jonathan Matthews, Christopher R. Weber, Andrey Rzhetsky, Kevin P. White, and Savaş Tay. "Automated microfluidic platform for dynamic and combinatorial drug screening of tumor organoids." *Nature communications* 11, no. 1 (2020): 1-12. doi:10.1038/s41467-020-19058-4

A U.S. patent for the following device was filed on 2019-12-12 titled *microfluidic devices, systems, and methods for investigating three-dimensional structures*. U.S. patent number 7973989.

2.1 Summary

Three-dimensional (3D) cell culture technologies, such as organoids, are physiologically relevant models for basic and clinical applications. Automated microfluidics offers advantages in high-throughput and precision analysis of cells but is not yet compatible with organoids. Here, we present an automated, high-throughput, microfluidic 3D organoid culture and analysis system to facilitate preclinical research and personalized therapies. Our system provides combinatorial and dynamic drug treatments to hundreds of cultures and real-time analysis of organoids. We validate our system by facilitating individual, combinatorial, and sequential drug screens on human-derived pancreatic tumor organoids. We observe significant differences in the response of individual patient-based organoids to drug treatments and find that temporally-modified drug treatments can be more effective than constant-dose monotherapy or combination therapy with *in vitro* organoid drug screening. This integrated platform advances organoid models to screen and mirror real patient treatment courses with a future potential to facilitate treatment decisions for personalized therapy.

2.2 Introduction

Cell culture techniques are important tools in both basic and clinical research ranging from personalized or regenerative medicine to more fundamental research like developmental biology. The need for more biologically relevant tissue models has driven interest away from traditional two-dimensional platforms and towards three-dimensional cell culture systems that more accurately simulate cell and tissue morphology, proliferation, differentiation, and migration[14,50,51].

3D culture and organoid based systems have been widely used for the study of different disease states, personalized drug screening, discovery drug safety and efficacy studies, and manipulations of cellular environment, ultimately providing more physiologically relevant information and more predictive data for *in vivo* tests than traditional methods[52,53].

Patient-derived organoids have several advantages as personalized tumor models. Primary cancer tumor cells cultured as 2D monolayers do not reflect the heterogeneity of the primary tumor due to selection in culture, tissue-specific architecture, and mechanical stresses, while tumor organoids can overcome these deficiencies[27,28,32]. Patient-derived cancer tumor organoids can be established in a shorter period and are much more economical than costly patient-derived xenograft (PDX) models, which requires a large tissue sample, up to 6 months to establish tumor growth, and retains complications from infiltrating murine stromal cells[29,54]. Tumor organoids can also be cryopreserved, expanded, genotyped, and challenged with therapies within weeks of the initial culture. Additionally, tumor organoids can be cultured from a routine cancer biopsy, such as an endoscopic ultrasound-guided fine needle aspiration, with a high success rate, making it ideal for probing changes involved at different stages of tumorigenesis. Patient-derived organoids also open the possibility of clinical benefits when the response to therapy mimics the parent tumor and allow for deep genomic characterization and *ex vivo* therapeutic testing in classes of patients that have traditionally been understudied in research settings[54].

It is desirable to improve the speed, cost, and reproducibility of culture and comprehensive screening of organoids for phenotypes such as drug sensitivity or tissue development. One way to achieve these objectives involves the creation of standardized, parallelized, and miniaturized assays that can be performed in a highly reproducible environment with the utilization of minimal amounts of reagents, using an automated system that allows users to culture and screen thousands

of conditions with minimal training and investment. Microfluidics can provide dynamical screens with drug cocktails and signaling molecules, where the concentration, timing, and duration of fluidic delivery can be precisely controlled in an automated fashion. Similar systems have already been developed and commercialized for 2D cultures, but fail to accommodate many 3D cell culture structures due to several limitations of existing microfluidic systems[36–38]. Most importantly, organoids and other 3D cell structure models often require the use of an extracellular matrix that interacts with the cells and tissue to provide both mechanical support and biochemical cues. Naturally-derived matrices (e.g. Matrigel) are widely used, however their physical and chemical properties (such as temperature sensitivity and clogging of microfluidic channels) make current microfluidic and other high-throughput techniques obsolete.

Current microfluidic literature has demonstrated the use of organoids with microfluidics, but either contains very low throughput methods (less than eleven chambers per device), incompatibility with Matrigel, little to no automation, and/or with small chamber depths that are unable to accommodate the large 3D organoid size (~400 μm diameter)[53,55,56]. Other microfluidic-related devices called organ-on-a-chip or body-on-a-chip platform have used tissue-specific cells and their extracellular matrixes to remodel 3D tissues architectures and physiological conditions, such as shear stress and fluidic flow, within a tissue-specific microfluidic structure and system[57–59]. However, while extremely useful for certain research studies, in comparison to organoid based microfluidics, these systems are limited when reconstituting the biological complexity of tissue development. Also, body-on-a-chip systems and other commercially available automatic and high throughput methods often required complex or extremely expensive robotic based systems, have complications or incompatible with gel scaffolds, and not always suitable for real-time monitoring of cellular and molecular features[60,61].

Finally, some of the most common and effective chemotherapies are administered in a specified temporal sequence[62–64], however culture devices that can accommodate 3D gel-based cultures are typically not automated and do not support the on-demand perfusion of drugs and signaling factors that could provide preclinical drug screens in a time-dependent manner. Furthermore, time-dependent analysis of 3D organoids is extremely challenging, especially when the fluidic conditions need to be dynamically altered during experiments.

To address these limitations, we have developed a robust and streamlined automated microfluidic platform that allows high-throughput culture, stimulation, assaying, and harvesting of organoids and other 3D culture models under dynamic conditions. Our system is compatible with gel-based culture and dramatically decreases the labor-intensive and time-consuming tasks of 3D cellular culture, human error, and minimizes the consumption of expensive reagents, while being able to continuously monitor the cultures for long periods of time. Most importantly, the automated fluidic architecture built into the system facilitates dynamic programmed changes to the culture conditions and enables real-time screening of different sequences of drugs or signaling factors in parallel culture chambers. The dynamical control of fluidic conditions allows testing of thousands of drug stimulations in a single experiment. Once an experiment is completed, the cultures can be easily harvested for additional genomic analysis, expansion, or grafting. Ultimately, this system can increase and accelerate the use of organoids and other 3D culture-based systems (e.g. spheroids or cellular aggregates), enhancing their ability to become an essential tool for both basic and translational research.

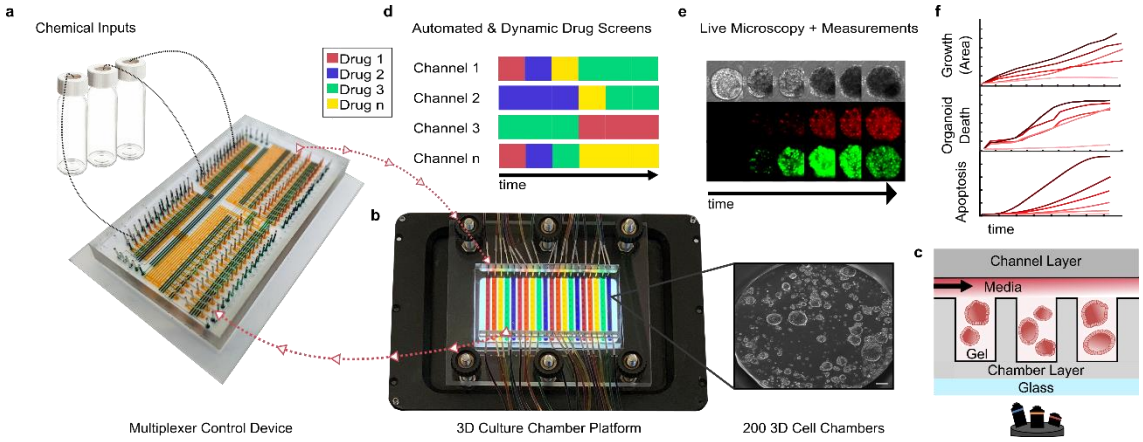

Figure 2-1: Automated microfluidic 3D cellular and organoid culture platform for dynamical drug perturbations.

a) A programmable membrane-valve based microfluidic chip (multiplexer control device) provides automated stimulation profiles to various chambers of a separate 3D culture platform (b) to produce many parallel and dynamical culture experiments. b-c) The 3D culture chamber platform contains 200 individual chambers that are compatible with temperature sensitive gels (i.e. Matrigel), and an overlaying channel layer enables 20 independent fluidic conditions (scale bar $100\ \mu m$). The channel layer is reversibly clamped on top of the chamber layer to provide media and other chemical stimulation without leakage. c) A cross-section of the two-layer multichambered PDMS-based 3D culture chamber device d) 30 chemical inputs and 30 outlets of the multiplexer control device (a) are preprogrammed to provide combinatorial and time-varying stimulations to the 3D culture chamber device (b) e-f) Organoids or 3D cellular structures are continuously observed through time-lapse imaging for quantification; fluidic culture conditions can be changed on demand. The 3D culture chamber device can also be disassembled for cell harvesting and further cellular assays.

2.3 Results

2.3.1 Design of an automated platform for 3D cellular cultures

We developed an automated high-throughput microfluidic platform capable of culturing organoid and other 3D cellular cultures for continuous monitoring of 3D growth, morphology, and biochemical analysis. The platform consists of two integrated devices, a 3D culture chamber device and a multiplexer fluid control device, custom software for automated and programmable experimental control, and live-cell time-lapse fluorescence microscopy.

The reversibly clamped two-layer chamber chip consists of a 200-well array and an overlying layer of fluidic channels. Each well unit in the lower layer serves as a culture for organoids or other 3D cellular structures grown inside a gel-like extracellular matrix such as Matrigel or hydrogel (**Figure 2-1**). A second channel layer compliments the chamber array and is reversibly bonded together, along with a glass slide, through a clamping-based system to provide fluidic channels. The array is divided into 20 different subsets of 10 individual chamber units to accommodate up to 10 different patient samples (**Figure 2-1b-c, Figure 2-2**).

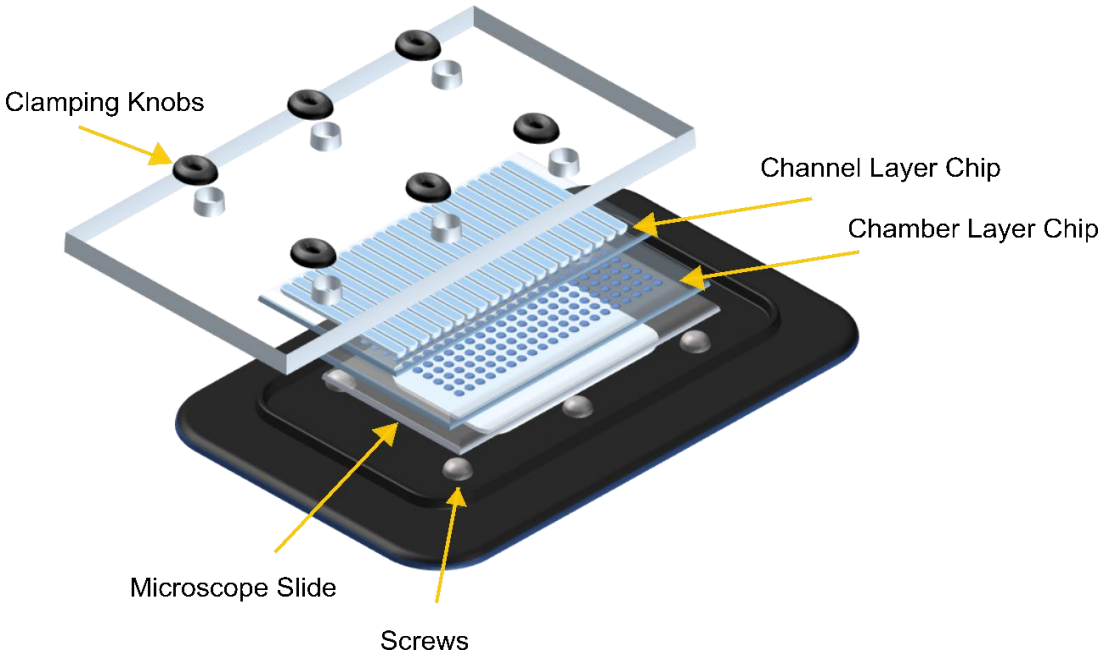

Figure 2-2: Overview of 3D culture chamber platform.

A microscope stage customized with 6 screws and a 50x75 mm glass slide nested inside provides the base of the clamping system. On top of the glass slide, lies the first thin layer of an air permeable silicone material (PDMS) encapsulating miniature chamber wells, 1.5 mm in diameter and 610 µM deep, which houses the 3D, gel-compatible, environment for the culture. Complementing the chamber layer, a second PDMS based channel layer goes on top for the fluidic supply to the 3D cellular culture. Finally, a clear piece of polycarbonate applies even pressure by reversibly bonding the layers with knobs screwed down to prevent any leakage or cross-contamination between the channels.

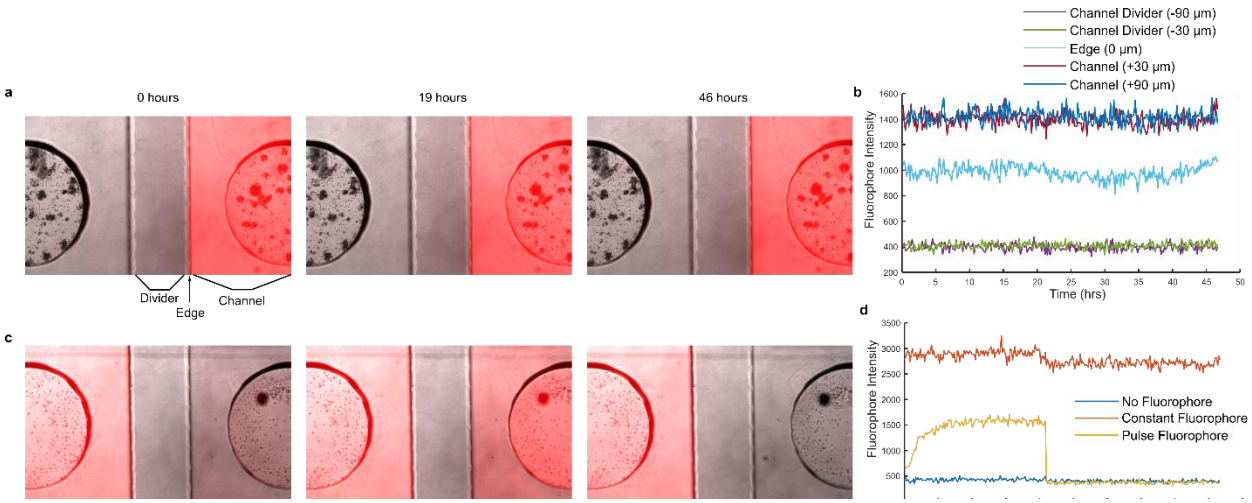

Figure 2-3: Lack of leakage, drug absorption, and cross contamination between microfluidic channels.

Alexa Fluor 647 fluorescent dye (Sigma Aldrich GE25-9004) was added to specific channels and fluorescence intensity was monitored overtime to assess leakage and any cross-talk/drug contamination between channels. a-b) With the edge of a channel with the fluorophore at constant pressure as the starting point, 30 µm and 90 µm to the left of the edge in the divider region and 30 µm and 90 µm to right of the edge in the channel region was assessed for fluorescent intensity. c-d) A channel with the fluorophore, the divider between the channels (no fluorophore), and a channel that received a pulse of the fluorophore solution was measured over 48 hours. In additional to the use of fluorescent to access leakage, all drugs used in our study except paclitaxel and docetaxel are hydrophilic, and their concentrations are expected to be unchanged. For paclitaxel (and its derivative docetaxel), a study[65] found less than 5% absorption of the drug into the PDMS device. We therefore estimate that the drug concentrations inside the chambers are as expected, with no more than 5% difference than the concentrations of the stock solution.

The 3D culture chamber platform was geometrically engineered to reduce bubble formation and prevent leakage between channels (**Figure 2-3**). Uniquely, the channel and chamber heights were specifically engineered to provide a suitable 3D environment for the large mature organoids that average around 500 µm in diameter. The fluidic channels are 455 µm in height in order to provide enough liquid nutrients to the growing organoids and to prevent disruption of the gel-based environment in the chambers. The chamber units are 610 µm in height, on average, which is significantly larger than most microfluidic devices (typically between 100-200 µm, although heights of up to 350 µm have been reported[55]). Additionally, previously published high-throughput microfluidic devices are not compatible with temperature-sensitive Matrigel, which quickly solidifies at room temperature and difficult to flow through microfluidic channels and

valves. Our two-part, valve-less, non-permanently bonded organoid culture device allows for easy accommodation of Matrigel into the wells through manual pipetting and the clamping feature allows for reversible bonding without the possibility of any leakage of the device after the cells are added, eliminating the need for a permanent bonding method or complicated/unfeasible Matrigel loading methods.

The variable fluidic conditions are supplied to the well chambers via channels that pass over the top of the chambers. This configuration creates 20 independent experimental conditions that are controlled with a second multiplexer device. To formulate automated, complex, and dynamic fluidic flow to the system, we designed a valve-based, reusable multiplexer control device composed of a system of fluidic channels and valves to provide culture control to the valve-less 3D culture chamber device (**Figure 2-1a, Figure 2-4**). The multiplexer device is automated and controlled by solenoid valves and custom software to carry out preprogrammed experiments and deliver precise fluid sequences to the culture device. The experimental conditions supplied to organoids consist of specific temporal profiles of chemical inputs (i.e. medium, drug cocktails, chemical signals) that are prepared and connected through fluid vials with their delivery pre-programmed through a simple tab-delimited text file (e.g. Excel). The desired solutions are preloaded (up to 30 solutions) to the multiplexer device, which in return provides the automation by acting as the fluidic guide to provide each desire solution to the specific designated channel in a time specific manner. The level of automation allows easy programing and application of any number of dynamic conditions and overcomes the limits of manual pipetting by limiting errors and standardizing timing of media delivery. While the 3D cellular cultures are being exposed to predetermined experimental regimes, they are simultaneously imaged in 3D via phase contrast and fluorescence deconvolution microscopy to provide real-time measurements of cell reactions,

movements, and proliferations (**Figure 2-1d-f)**. The programmable microscope is also equipped with an environmental chamber (incubator) for continuous temperature and climate control. Once an experiment is completed, the design of the 3D culture chamber device allows the upper fluidic supply channels to be removed exposing the well array with cell-containing gel for facile harvesting of 3D cultures/organoids for subsequent analysis (sequencing, expansion, etc.). Moreover, during the entire culturing period, we can use fluorescent cellular protein markers for continuous time-dependent analysis (**Figure 2-1e, f**).

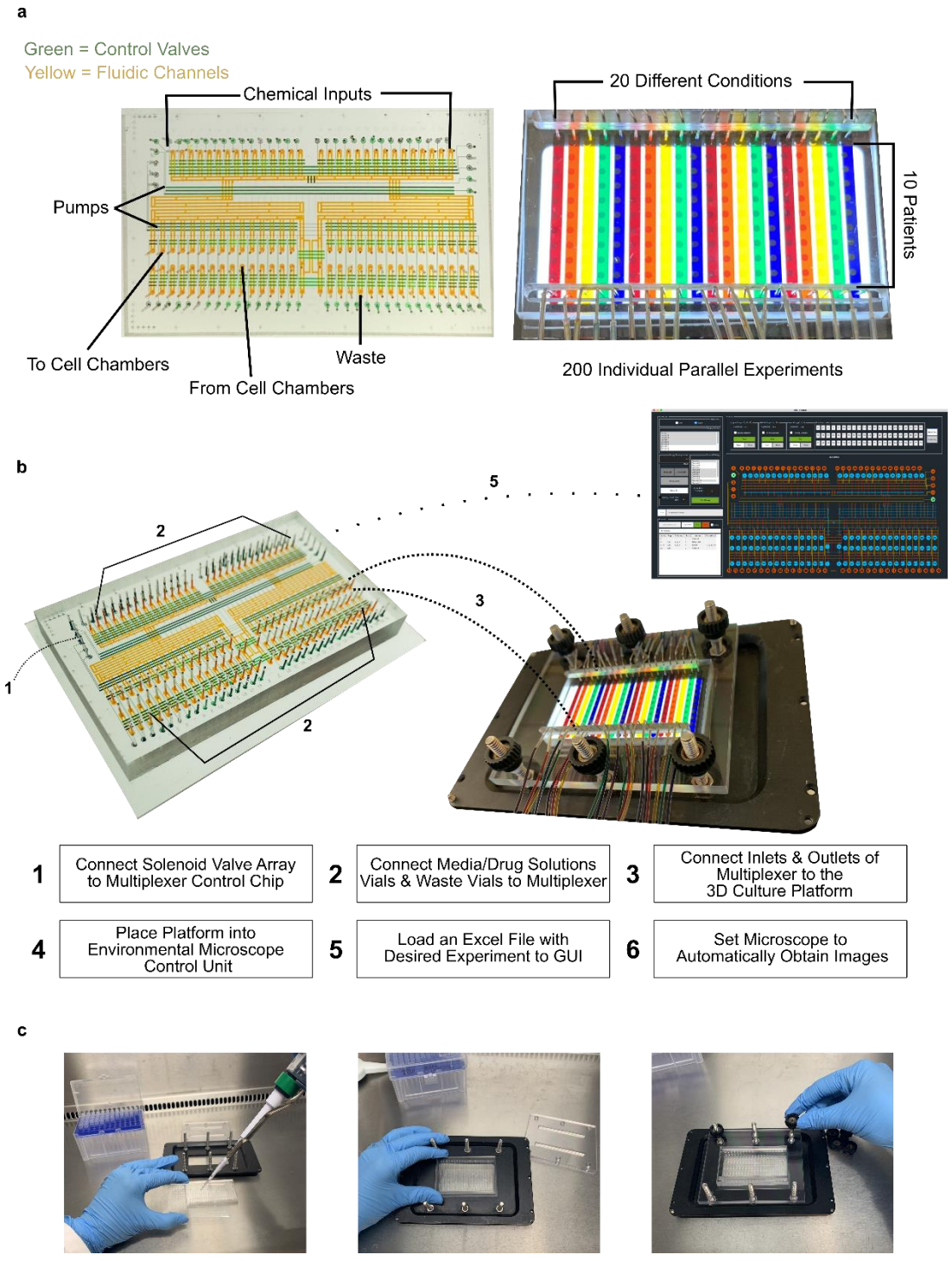

Figure 2-4: Experimental setup

a) Features of the multiplexer control device (left) and the 3D culture chamber device (right). b) The multiplexer control chip is connected to a solenoid valve array through the outer inlets and pressurized at around 40 psi. Solutions (pressurized at 5 psi) and waste vials are connected to the appropriate inlets on the chip. The multiplexer is then connected to the culture platform before being placed onto a microscope equipped with an environmental control unit. The desired experiment is uploaded to both the solenoid valve

Fig. 2-4, continued: array control computer and microscope for automatic fluidic delivery and image acquisition. c) Organoids embedded in Matrigel or other 3D cellular culture are easily pipetted into the chamber layer, followed by assembly of the channel layer reversibly bonded with the clamping system.

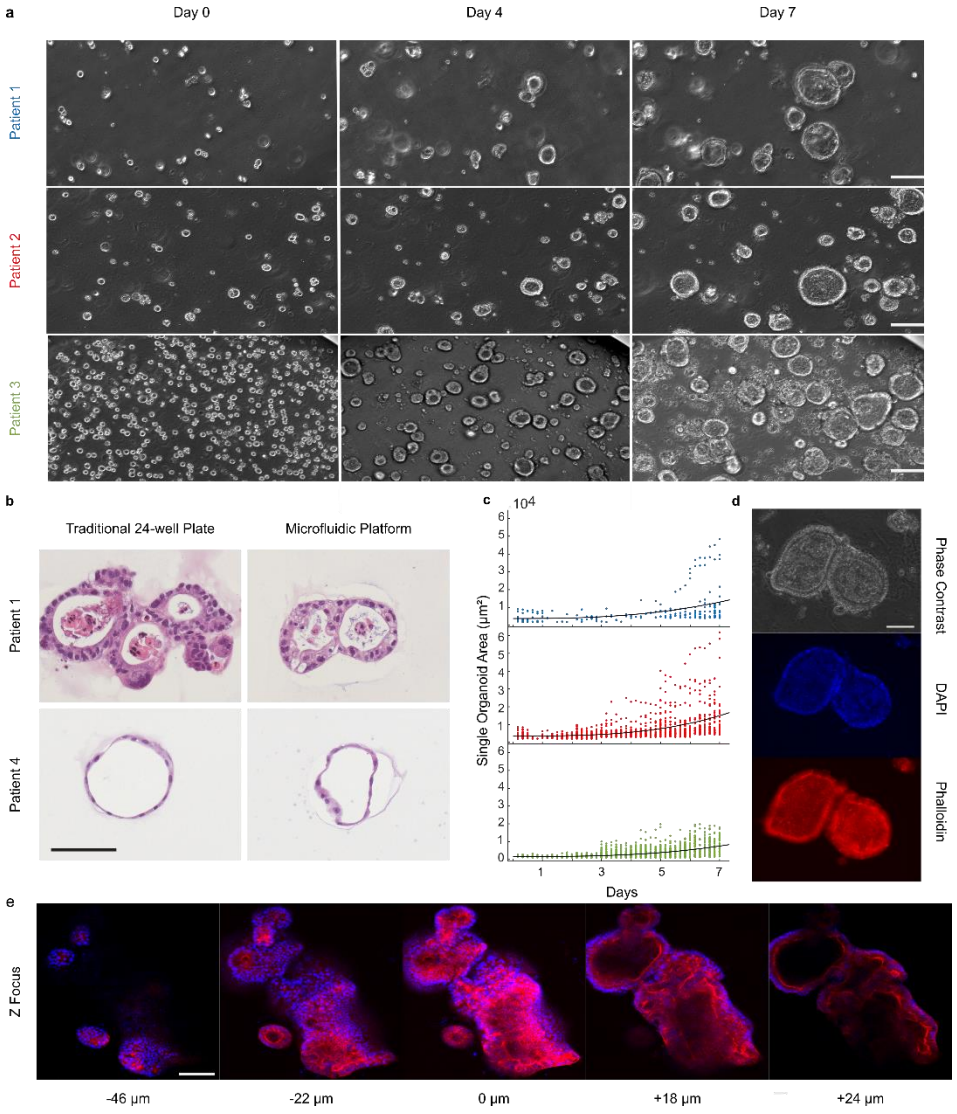

Figure 2-5: Human tumor organoid culture and growth on microfluidic platform

a) On-platform growth of organoids: three separate patient-derived pancreatic ductal adenocarcinoma (PDAC) organoids in Matrigel from single cells to formation of differentiated morphology of complex 3D structures (scale bar 100 µm). b) Organoids from two patients were grown in parallel in a traditional 24-well plate and on our microfluidic platform (scale bar 100 µm). After mature organoid formation, organoids were harvested, H&E stained, and their morphologies compared and analyzed. In both platforms, organoids from patient 1 exhibited back-to-back glands with a high degree of nuclear atypia and pleomorphism with an accumulation of apoptotic luminal necrotic cells. Organoids from patient 4 demonstrated a well-differentiated morphology with simple spherical organoids and uniform nuclear and cytoplasmic features with little or no accumulation of necrotic luminal cells. c) Organoid growth curves of PDAC organoid samples derived from three patients grown from single cells for 7 days on the platform. Each dot represents

Fig. 2-5, continued: the cross-sectional area of an individual organoid. Patient 1 (blue), Patient 2 (red), Patient 3 (green). d) Long-term culture, growth, and fluorescent staining of fixed PDAC organoids on the platform. Nuclei staining (DAPI) and F-actin (Phalloidin) are demonstrated (scale bar 100 μm). e) Multiple *Z* image slices or stacks of a group of fixed and fluorescently stained organoids with DAPI and phalloidin (scale bar 100 μm).

2.3.2 Individual cells develop into organoids on the platform

Our 3D culture platform has been used to grow a variety of 3D cell structures from a cancer cell line (MDA-MB-231) grown into aggregates, pancreatic tumor organoids from patient derived samples, and colon organoids from human-derived normal (i.e. non-diseased) colon tissue samples (**Figure 2-5a,c**, **Figure 2-6**). The application of the same platform to grow different 3D models provides an easy means of standardization and allows culturing of dynamic conditions for long time periods (14+ days). For example, pancreatic ductal adenocarcinoma (PDAC) organoids from patient-derived samples are grown from single cells to a stage where tissue-level structures are observable. During the entire culturing period, we conducted continuous visual monitoring of cells and stained cellular components on the platform (**Figure 2-5d**). Timing and feeding were optimized using the high-throughput features of the system to ensure a suitable environment where the cells could proliferate and ultimately grow into 3D glandular structures.

The cellular phenotypes of PDAC organoids grown on our platform were then compared to traditional plate-based experiments and other known tumor tissue characteristics for these same organoids in previously published work[32] (**Figure 2-5b**). To validate the tumor pathology, a gastrointestinal pathologist compared the architecture and cell morphology of two organoids with very different histological appearances grown on both platforms and then stained with hematoxylin and eosin (H&E) for histopathological evaluation There was a remarkably good correlation between the organoids grown on different platforms for both patients based on the H&E cell appearance and glandular structure of the tumor organoids. The formation of multilumen structures with a high degree of cytologic atypia seen in patient 1 in contrast to the well-

differentiated cysts in patient 4 were consistent between platforms. The contrasting patient morphologies are a reflection of the organoids ability to reflect the individualized characteristics of the tumor they are derived from, which is retained between the platforms[32]. To accommodate the entire 3D structure, we took multiple *Z* image slices or stacks to fully image the entire volume of each organoid (**Figure 2-5e**). Selected *Z* stacks with the largest diameter of the organoid were analyzed by measurements accumulated through image segmentation. The cross-sectional area of multiple individual PDAC organoids was measured over the course of 7 days for three different patients to obtain growth rates (**Figure 2-5a,c**).

2.3.3 Growth and drug screening of primary human tumor organoids

Once the culture of organoids was established on our platform, we developed a robust high-throughput assay of organoid growth and cellular apoptosis for drug-treated and untreated samples to demonstrate the experimental and potential biomedical utility of our platform. We used FDA-approved and standard of care chemotherapy regimens for pancreatic cancer to design drug screening assays on human-derived pancreatic cancer organoids using our platform. A set of fluorescent dyes were used to monitor the drug sensitivity of each organoid continuously using live cell imaging. Our design accommodates up to 20 different regimens and 10 different patient samples to be tested in parallel.

To verify the drug screening capabilities of the platform, we treated PDAC organoids, obtained from three different patients, with clinically relevant doses of gemcitabine (100nM), paclitaxel (10nM), 5-fluorouracil (5FU, 100nM), docetaxel (10nM), irinotecan (CPT-11) (100nM), oxaliplatin (100nM), and cisplatin (100nM). The PDAC organoids were grown on the platform for a minimum of 7 days prior to drug exposure or until organoids were visibly mature.

We quantified the organoid growth and reactions to drug exposure continuously through automated image analysis using apoptosis and cellular death fluorescent dyes (**Figure 2-7a-b**). During the entire course of organoid culture and treatment, image stacks taken of the chamber arrays provided real-time 3D monitoring of organoid size, number, and morphology. The monitoring continued during drug exposure and images were automatically analyzed in combination with fluorescent markers for size and viability using MATLAB based image analysis (**Figure 2-7c-f**). To mimic previously used plate-based methods, the organoids were continuously exposed to individual drugs for 72 hours (**Figure 2-7c,e**) or exposed for a 4 hour drug/s pulse (**Figure 2-7d,f**) followed by a wash and replacement with normal growth media for the duration of the treatment. At the 48-hour mark, all treatment and control groups were supplied with either drug-containing or normal growth media to replenish growth nutrients and prevent non-drug related cell death. We also compared clinically relevant combinations of the chemotherapy drugs administered for 4 or 72 hours (**Figure 2-7e-f, Table 2-1**). This screen allowed for multiple conditions to be automatically supplied to different subsets of organoids, providing an easy means to simultaneously compare multiple treatments in a single experiment. Overall, we found that combination chemotherapy treatment resulted in significantly increased apoptosis in tumor organoids compared to monotherapy as expected.

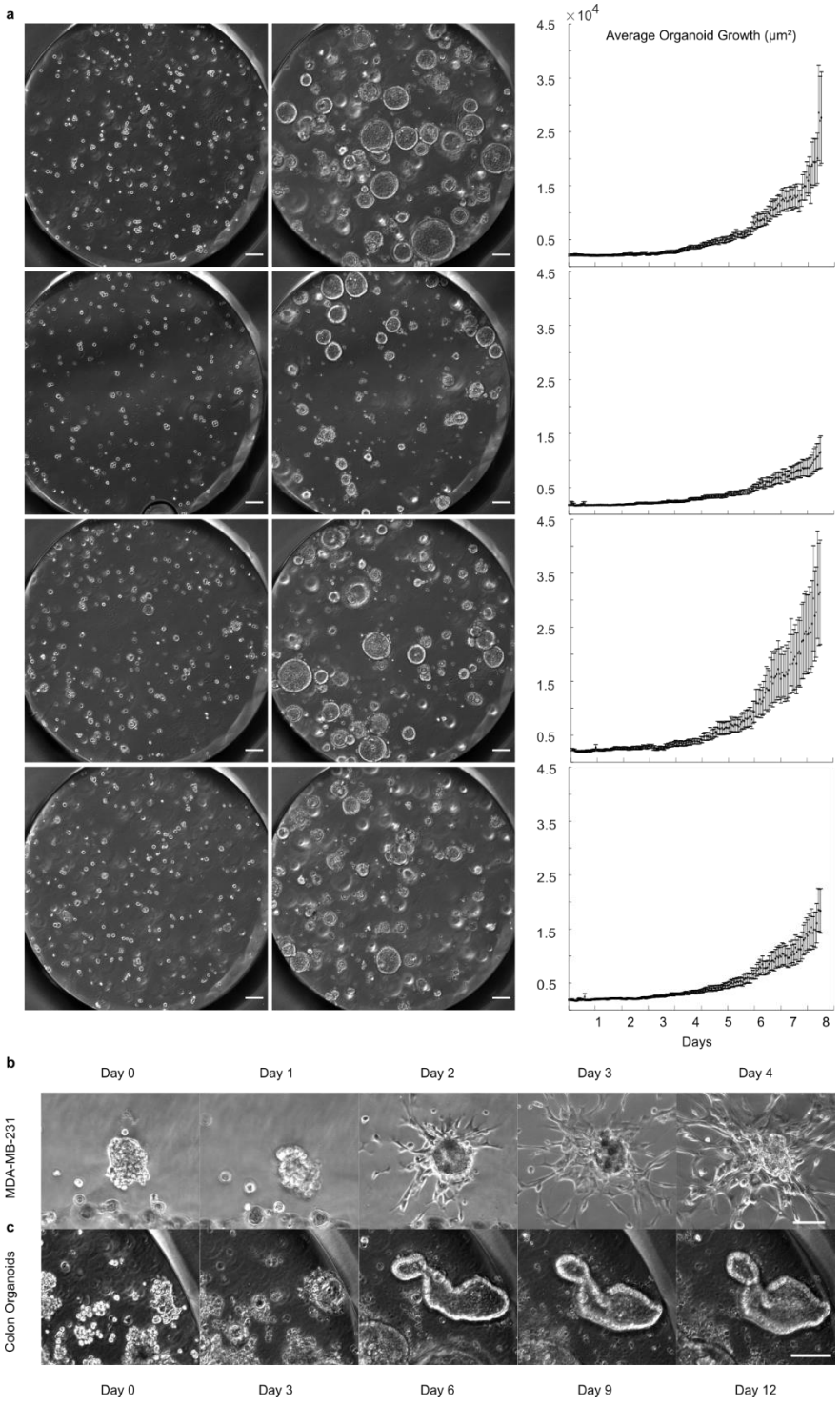

Figure 2-6: Pancreatic cancer organoid and other 3D cellular cultures grown on platform

a) Examples of four different cell culture chambers growing from single cells to mature pancreatic ductal adenocarcinoma (PDAC) organoids in 8 days on the platform in parallel (scale bar 100 μm). b) Immortalized cancer cell lines such as MDA-MB-231, a breast cancer line, can be grown and stimulated on the platform to form cellular aggregates for drug screening or migration studies. Other cancer organoids

Fig. 2-6, continued: and non-cancer/diseased organoids such as the human normal colonic organoids shown are also compatible with this system (scale bar 100 μm*)*.

2.3.4 Dynamic drug screening of human cancer organoids

Some of the most common and effective combination chemotherapies for cancer are clinically administered to the patient in a specified temporal order[62–64]. Our platform can automatically create such dynamic chemotherapy regimens in many parallelized organoid cultures and analyze organoid response in real time. To investigate the efficacy of such treatments, we leveraged several standard medical chemotherapy practices for PDAC to design five temporal chemotherapy regimens. With our platform, we exposed organoids to these regimens to mirror real treatments given to PDAC patients in the clinic[18–21]. Unlike traditional plate-based methods, our platform allows for combination chemotherapy to be sequentially delivered in pulses to the desired array of organoids without human intervention, drastically reducing laborious pipetting steps and human error while maintaining a real-time organoid imaging process.

In the clinic, FOLFIRINOX is a frequently used combination chemotherapy regimen that consists of two hours of intravenous irinotecan (CPT-11), followed by two hours of oxaliplatin, continued with a high dose burst of 5-fluorouracil (5-FU, 1 μM), and finished with a continuous infusion of low-dose 5-FU (100 nM) for 46 hours. Our platform mirrored this clinical treatment strategy by exposing the organoids to 2 hours of CPT-11, 2 hours of oxaliplatin, 30 minutes of a high dose of 5-FU, and then a continuous low dose of 5-FU until the end of the 72-hour experiment. We then compared the temporally and sequentially delivered FOLFIRINOX treatment to a static FOLFIRINOX treatment, where the organoids received the complete FOLFIRINOX cocktail at once and continuously for 4 or 72 hours, mimicking the capabilities of traditional plate experiments. This process was repeated for four more common combination therapies: FOLFIRI,

FOLFOX, gemcitabine + 5-FU, and gemcitabine + paclitaxel as outlined in **Table 2-1** and illustrated in **Figure 2-8**.

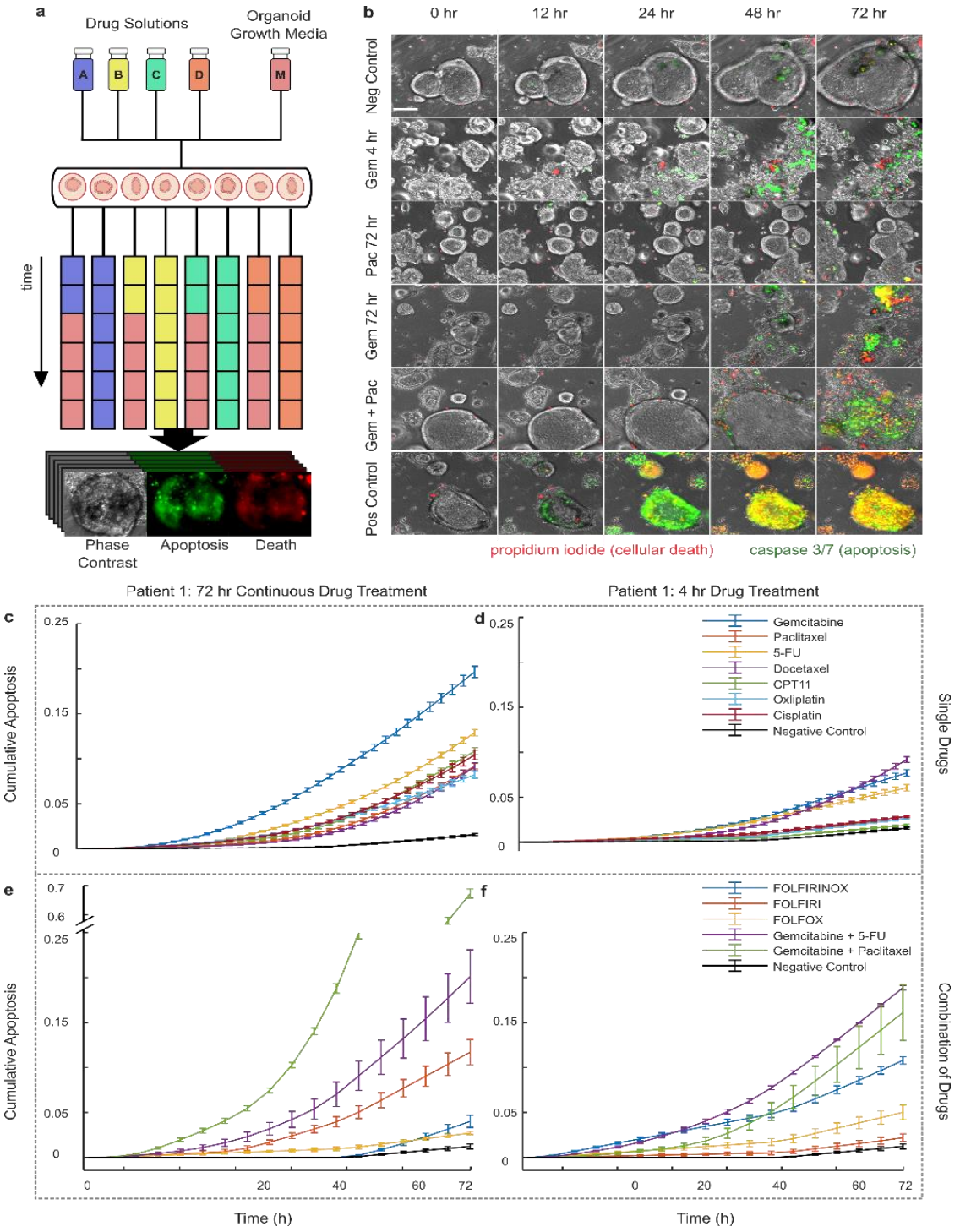

Figure 2-7: Combinatorial drug treatment of human tumor organoids on microfluidic platform

Fig. 2-7, continued: a) On-platform drug treatment and stimulation with continuous fluorescence and phase imaging of organoids for the treatment duration. Each color represents a different drug formulation. Drug treatments on each channel can be changed on demand, creating time-varying drug treatments. Organoids can be analyzed for growth, morphology changes, or death. b) Representative images (10x) of gemcitabine (100nM) treated organoids for a 4-hour drug pulse followed by normal growth media, continuous treatment of paclitaxel (10nM) for 72-hours, continuous treatment of gemcitabine (100nM) for 72-hours, a combination dose of gemcitabine (100 nM) + paclitaxel (10nM) for 72-hours, and negative and positive controls (staurosporine 10mM). Caspase 3/7 reagent (green) used for apoptosis detection and propidium iodide (red) for dead cells along with phase contrast images (scale bar 100 μm). c) Average caspase 3/7 signal over 72-hour period of continuous single drug treatments for patient 1 d) Average caspase 3/7 signal over 72-hour period for a 4-hour pulse of a single drug treatment followed by normal growth media for patient 1 e-f) 72-hour (e) and 4-hour (f) drug treatments similarly examined for multiple known combinations of drugs. c-f) All data presented as mean values +/- SEM, n=3, and normalized to positive control. Overall, combination chemotherapy treatment resulted in significantly increased apoptosis in tumor organoids compared to single drug treatments as expected.

2.3.5 Temporal drug delivery can be more effective than constant

Analysis of combinatorial and dynamic drug treatment experiments revealed notable differences between constant and temporally pulsed drug treatments for certain patients. For patient 1, temporally modified delivery of FOLFIRINOX, FOLFIRI, FOLFOX, gemcitabine + 5-FU and gemcitabine + paclitaxel were the only treatments that produced significantly different responses from the control groups (repeated measurement ANOVA *p*-values were, respectively, 0.0098, 8.39E-07, 0.02, 7.05E-07, 2.31E-05). Patient 1 also demonstrated significantly greater drug sensitivity (i.e. increased apoptosis) to almost all the sequentially-administered combination therapies compared to their 4- and 72-hour simultaneous administration counterparts (**Figure 2-8h**). Overall, the gemcitabine/paclitaxel treatment sequence was the most effective on the organoids derived from patient 1. Retrospective clinical data reports that patient was treated with a Whipple procedure, followed by one round of adjuvant gemcitabine after surgery. A final round

of gemcitabine + paclitaxel was given, but the patient was transferred to hospice shortly after.

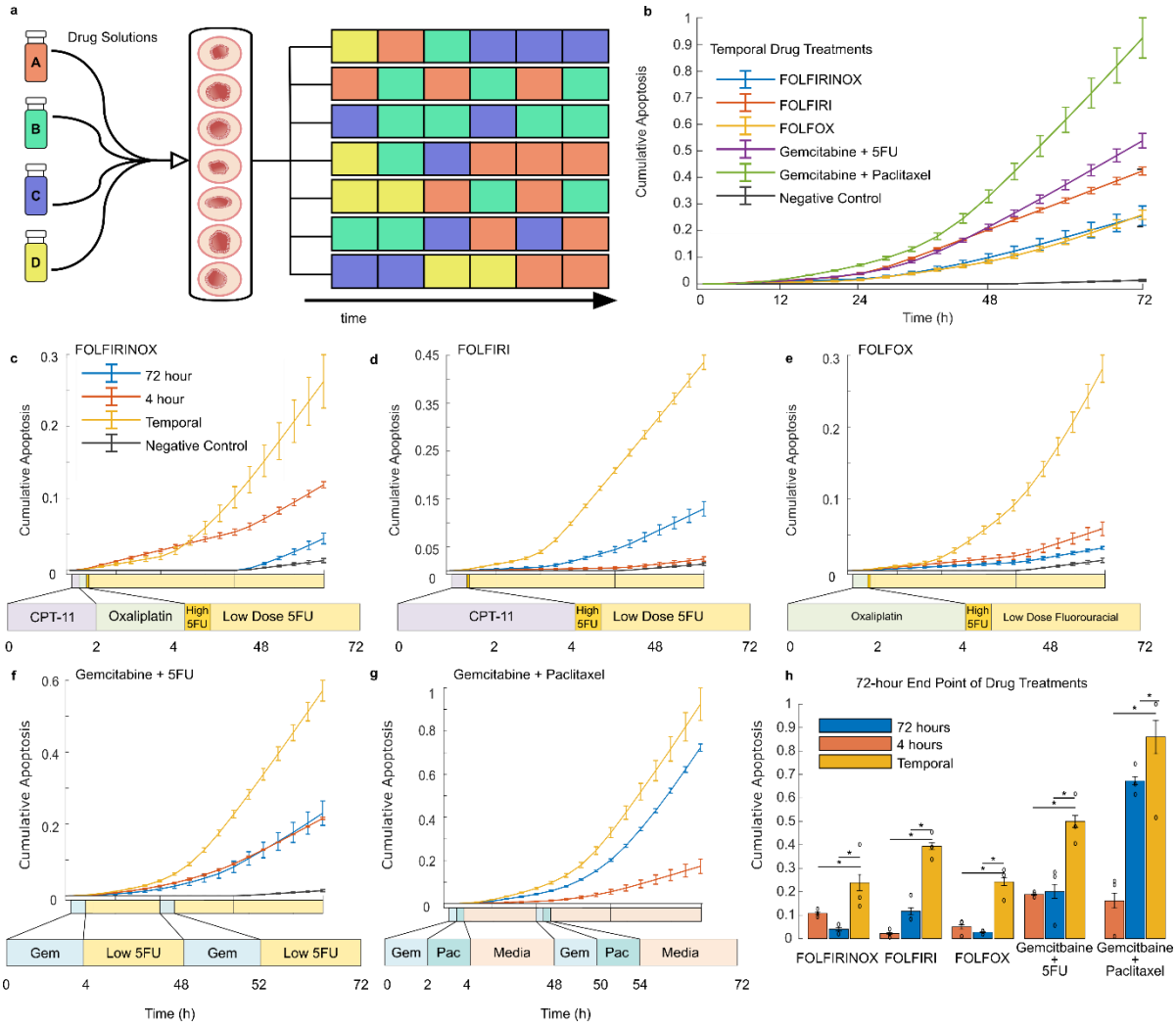

Figure 2-8: Sequential and temporal drug treatment on the microfluidic platform reveals the efficacy of dynamic temporal drug treatment for personalized therapy

a) Schematic of sequential drug delivery schedules of single drugs delivered temporally in pulses to recapitulate dynamic combination chemotherapy with the platform. Colors in each row represent a different drug formulation, which can be changed on-demand. b-h) Comparison of the temporal delivery for five combination chemotherapies using average caspase 3/7 signal to detect apoptosis for patient 1. All data presented as mean values +/- SEM, n=3, and normalized to positive control c-g) Comparison of temporal delivery for each of the five combination chemotherapies to their 72-hour and 4-hour constant delivery counterparts (i.e. all drugs in the sequence at once). Details of the drugs used in each therapy regimen are shown below the graph and described in more detail in Table 2-1. Time course of each drug on the x-axis is to scale. h) Comparison of all investigated therapies at the end of the 72-hour drug treatment period (*denotes significant differences from temporal treatment, two-way ANOVA, p valves from left to right; FOLFIRINOX: 8.3E-07, 7E-07; FOLFIRI: 1.7E-06, 7E-07; FOLFOX: 0.03, 0.01; Gem+5FU: 3.9E-05, 8.3E-05; Gem+Pac: 9.6E-10, 6.16E-06). Sequentially-administered combination therapy is more efficient in inducing tumor cell death.

The capacity to conduct experiments in parallel allowed us to compare three different patients simultaneously without human intervention (**Figure 2-9**). Patient 2 showed significant drug sensitivity to a 72-hour treatment of gemcitabine, FOLFIRINOX delivered both temporally and for 72 hours, and temporally-delivered gemcitabine + 5-FU compared to the control (*p*-values=, respectively, 7E-07, 9.61E-05, 3.04E-06, 0.01). Patient 2 was the most sensitive to the 72-hour Gemcitabine and temporally-delivered Gemcitabine + 5FU. This is consistent with previously published organoid sensitivity data[8] using traditional plate-based testing methods. In the clinic, patient 2 received adjuvant rounds of gemcitabine followed by FOLFIRINOX with dose reduction before ultimately being transferred into hospice. It was also noted that the patient was delayed in receiving chemotherapies due to surgical complications. Gemcitabine + paclitaxel was also planned, but never administered due to fast progression of the disease.

Revealing more additional patient-specific drug sensitivity, patient 3 showed all gemcitabine-based treatments and durations significantly differ from the control (Ctrl vs. Gem *p*=8.39E-07; Ctrl vs. Gem+5FU 4hr *p*=6.72E-05, 72hr *p*=0.0004, Temporal *p*=1.65E-06). In clinic, patient 3 was administered a round of neoadjuvant FOLFIRINOX, followed by a round of adjuvant gemcitabine after the Whipple procedure, but the tumor ultimately metastasized to the liver. A round of gemcitabine + paclitaxel was administered but discontinued due to patient's intolerance and quick decline in health. Overall, these results demonstrate the importance of studying personalized drug responses, as individual patients exhibit different responses to drug treatment regimens.

In order to assess reproducibility and the effect of passage number, we repeated this experiment with patients 1 and 3 (**Figure 2-10**). Two different passage numbers (41 and 15) for patient 1 were compared and still revealed the most significant sensitivity to temporally derived gemcitabine + 5-FU over the 72 and 4-hr durations in both experiments. Similar passage numbers

(24 and 27) for patient 3 were also compared in two different experiments; again, both passages showed similar significant drug sensitivities for all four gemcitabine treatment groups, with temporal delivery as the most effective. The consistent response across passages highlights the reproducibility of the platform.

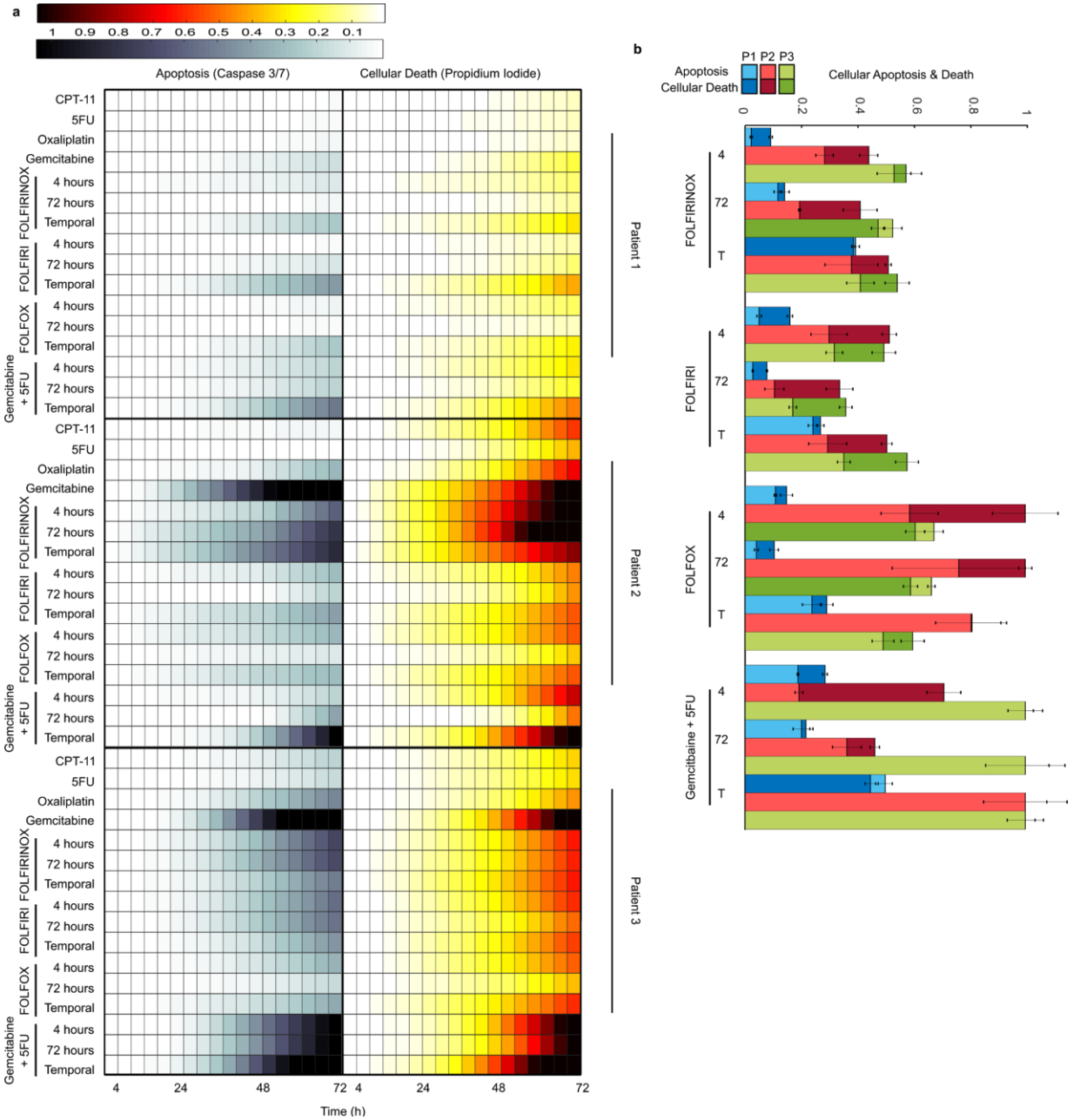

Figure 2-9: High throughput drug testing of multiple patients in a single experiment

Fig. 2-9, continued: a) Heat maps of organoids from three patients grown and stimulated in a simultaneous experiment. Cellular apoptosis (caspase 3/7) and death (propidium iodide) were recorded over the 72-hour drug treatment period to assess drug sensitivity. b) End-point analysis of average organoid cellular apoptosis and death for each patient and combination treatment group. All data presented as mean values +/- SEM, n=3, and normalized to positive control. Response comparisons between the different patients revealed distinct sensitivities to specific drug regimens across both independent cell viability assays.

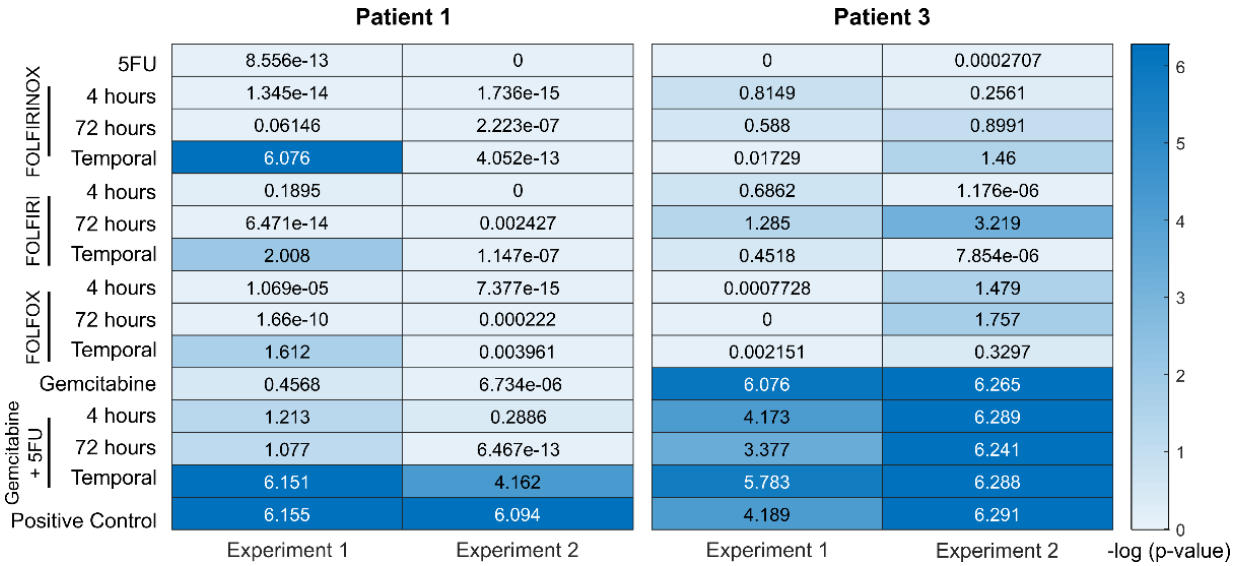

Figure 2-10: Reproducibility of the platform.

An identical experiment was repeated with two of the patients shown with a heat map of -log (p-value) of each drug treatment compared to the negative control (no drug/s). Patient 1 was repeated with varying passage numbers (Experiment 1: P41 and Experiment 2: P15), while patient 3 were both similar passages (Experiment 1: P24 and Experiment 2: P27). Overall, both patients retained the most significant and effective drug (Patient 1: gemcitabine + 5FU Temporal; Patient 2: all gemcitabine treatments; repeated measures ANOVA, n=3) for both experiments. For both experiments, the passage number did not affect the experimental results as expected[32].

Table 2-1: Temporal drug combinations

Combinatorial Chemotherapy	Constant Drug Combination Description	Temporal Drug Combination Description	Temporal Delivery Description
FOLFIRINOX	CPT-11(100 nM), Oxaliplatin (100 nM), Fluorouracil (100 nM)	CPT-11(100 nM), Oxaliplatin (100 nM), High Dose Fluorouracil (1 μM), Low Dose Fluorouracil (100 nM)	CPT-11 (2 hours), Oxaliplatin (2 hours), High Dose Fluorouracil (30 minutes), Low Dose Fluorouracil (48 hours)
FOLFIRI	CPT-11(100 nM), Fluorouracil (100 nM)	CPT-11(100 nM), High Dose Fluorouracil (1 μM), Low Dose Fluorouracil (100 nM)	CPT-11(4 hours), High Dose Fluorouracil (30 minutes), Low Dose Fluorouracil (48 hours)
FOLFOX	Oxaliplatin (100 nM), Fluorouracil (100 nM)	Oxaliplatin (100 nM), High Dose Fluorouracil (1 μM), Low Dose Fluorouracil (100 nM)	Oxaliplatin (4 hours), High Dose Fluorouracil (30 minutes), Low Dose Fluorouracil (48 hours)
Gemcitabine and Fluorouracil (5FU)	Gemcitabine (100 nM), Fluorouracil (100 nM)	Gemcitabine (100 nM), Fluorouracil (100 nM)	Gemcitabine (4 hours), Low Dose Fluorouracil (48 hours) repeated twice
Gemcitabine and Paclitaxel	Gemcitabine (100 nM), Paclitaxel (10 nM)	Gemcitabine (100 nM), Paclitaxel (10 nM)	Gemcitabine (4 hours), Paclitaxel (4 hours), normal growth media (24 hours) repeated twice

Table 2-2: Retrospective clinical data compared to corresponding patient's organoid drug sensitivity results

	Clinical Results	Organoid Results
Patient 1	Whipple procedure with an adjuvant round of gemcitabine. Liver metastases emerged and a round of gemcitabine + paclitaxel (otherwise known as gemcitabine + abraxane in clinic) was given right before the patient expired. Total duration was 11 months.	Organoids were most sensitive to a treatment of gemcitabine + paclitaxel
Patient 2	Whipple procedure followed by delayed adjuvant round of gemcitabine due to surgical complications. Liver metastases emerged and FOLFIRINOX with dose reduction was administered, before the patient expired. Gemcitabine + paclitaxel was planned, but never administered. Total duration was 16 months.	Organoids were most sensitive to gemcitabine and gemcitabine + 5FU.
Patient 3	Patient received neoadjuvant FOLFIRINOX before the Whipple procedure, followed by an adjuvant round of gemcitabine. Local recurrence and liver metastases emerged. A round of gemcitabine + paclitaxel was administered, but was discontinued due to intolerance before the patient expired. Total duration was 10 months.	Organoids were most sensitive to all gemcitabine-containing therapies

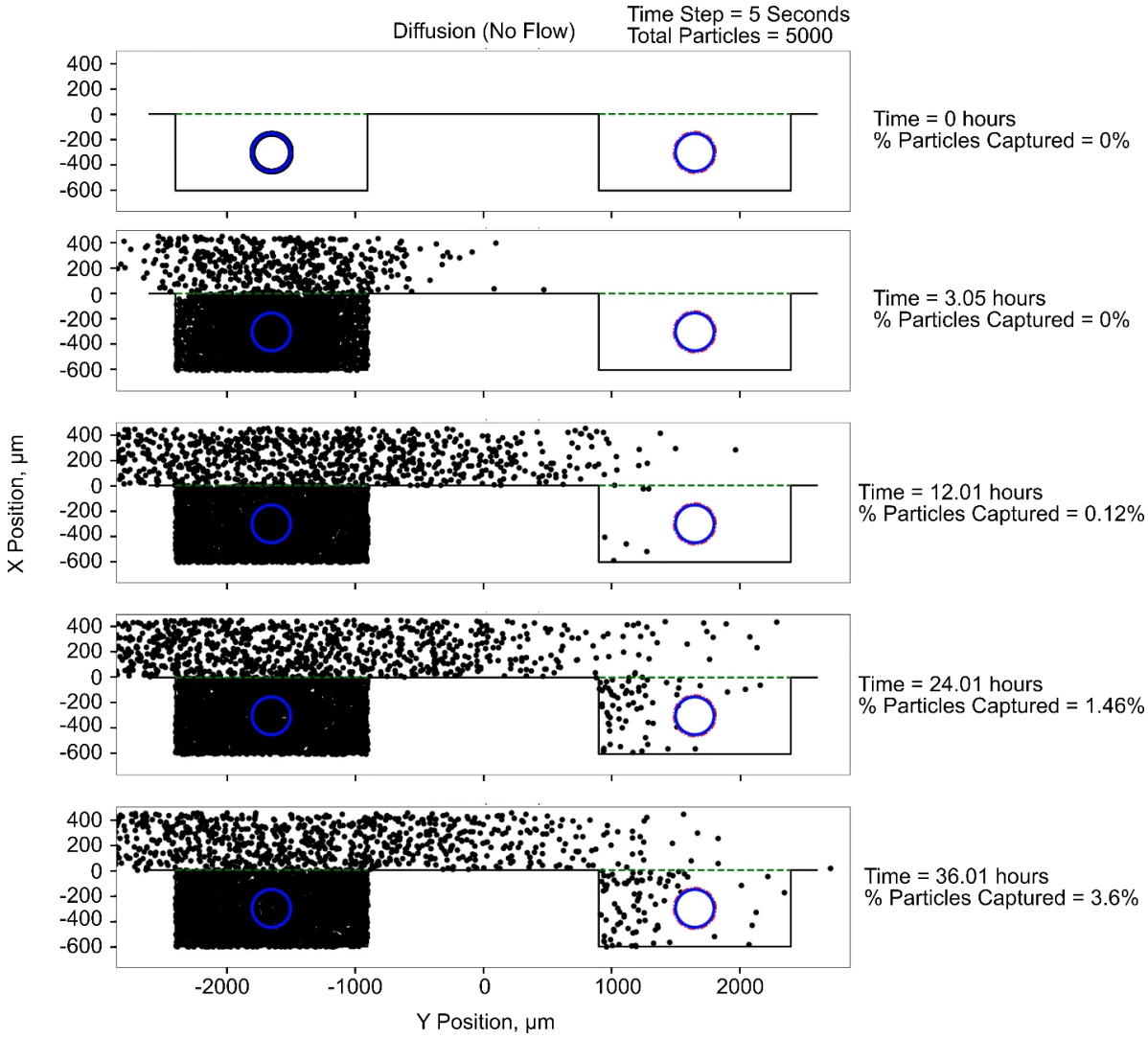

Figure 2-11: Mathematical modeling of potential organoid cross-communication between microfluidic wells

A model simulates the movement of 5,000 cytokine particles between two individual wells of organoids within one microfluidic channel. Using a time step of 5 seconds, the model simulated 36 hours of cytokine secretion and the potential capture of those particles to the neighboring well of organoids. The model demonstrated that low overall cytokine cross talk (3.6%) occurs between neighboring wells of organoids. Full explanation featured in **Experimental Methods Section 2.6**.

2.4 Conclusion

Here, we have developed an automated organoid culture platform for dynamic and combinatorial drug screening to aid in the research and modeling of human organ development and human pathologies. Our microfluidic platform enables highly reproducible, dynamic, and robust experimental analyses of organoids, while also accommodating the use of complex treatment combinations and temporal sequences of culture conditions. Traditional 2D immortalized or primary monolayer cell lines do not reflect the heterogeneous structure of *in vivo* tissue, while recently developed approaches for culturing 3D models, such as organoids, can overcome these limitations. The many potential applications of these new models are only just beginning to be explored and the described platform is a means to accelerate the use of organoids and other 3D cellular structures in fundamental and pre-clinical research.

As demonstrated here, the automated, high-throughput, and dynamic capabilities of the platform allow simultaneous parallel comparison between organoids grown from multiple patients under a variety of individual and combination drug therapies, as well as using predetermined temporal sequences of drug treatments. This design allows robust determination of drug effects in three ways. First, the complex addition of reagents in precise amounts at precise times would be a major source of error if attempted manually. Using our microfluidic architecture, volumes are simply metered by the number of pump cycles or level of pressurized flow and the device geometry. Reagent additions (e.g. drug exposure times, number of drug pulses, drug combinations) are programmed into the control system, that is error free as it is specified in a control file and then translated into the fluidic control architecture, thus the accuracy depends only upon correct connection of supply fluid vials.

The second way in which this experimental platform provides robustness is via the large number of repeated conditions and the intrinsic inclusion of controls through identical well units exposed to identical conditions. This strategy provides the necessary data to obtain statistically relevant quantifications of experimental outcomes. Finally, the temporal capabilities of the platform to deliver drugs individually in a sequential manner enables testing thousands of drug combinations to procedurally mirror real life patient treatments.

Our results showed significant differences in the drug response of individual patients, highlighting the importance of studying drug treatments at the individual level, particularly in cancer. We also found that temporal drug delivery may be more effective for certain patients than continuous or single-pulsed simultaneous drug treatment administered during organoid screening. This temporal effect warrants continued exploration and could lead to clinical trial hypothesis by testing a larger number of patient organoids, different type of cancer organoids, and testing different sequence variations of standard of care drug combinations.

In comparison to the clinical retrospective data, patient 1's organoids were most sensitive to gemcitabine + paclitaxel and unfortunately this treatment was delivered late in the treatment regimen as the last chemotherapy administered to the patient. This was also at a point of advance progression of the disease, where as soon as the chemotherapy administration was completed, the patient was transferred to hospice. Given the organoids' sensitivity results, the patient could have potentially benefited by receiving the chemotherapies earlier in the treatment plan. Patient 2 received gemcitabine and FOLFIRINOX post-surgery before being transferred to hospice. Gemcitabine and Gemcitabine + 5FU were the most effective with the organoids and the patient could have benefited from receiving another round of gemcitabine or a gemcitabine combination instead of switching to FOLFIRINOX, which was unsuccessful in the patient and the

corresponding organoids. The patient also suffered from surgical complications, ultimately preventing timely administration of chemotherapies after surgery. Patient 3's organoids showed sensitivity to all gemcitabine-based treatments, while in clinic, the patient received a round of FOLFIRINOX before surgery followed by round of gemcitabine and gemcitabine + paclitaxel, but seemingly too late as the patient's tumor metastasized to the liver. Given the results of the organoids, Patient 3 could have potentially benefited from receiving both gemcitabine treatments earlier in the treatment instead of FOLFIRINOX, which was ineffective for both the patient and the organoids. The late prognosis and noticeably rapid progression and short duration from diagnosis to patient's death also makes pancreatic cancer difficult to compare with in clinic results. Ideally, a cancer with a slower progression with a more controlled, in parallel clinical trial would be needed to further confirm that temporal preclinical testing is better at predicting drug sensitives compared to continuous delivery of treatment.

A current limitation of organoid technology is that it provides an incomplete representation of the tumor microenvironment such as blood vessels, stromal components, and immune cells. Recent research has demonstrated that organoids can thrive in co-cultures with other cellular components such as patient derived T-cells[24,66,67], fibroblasts[68–70], or even microbial and viral components[12,71]. Specifically, PDAC has been characterized by a preponderant stromal component that largely exceeds the epithelial component, and the PDAC associated fibroblasts are known to secrete factors that stimulate tumor growth, cell survival, and metastasis[14,24]. Another caveat to acknowledge is the use of Iriontecan (CPT-11) instead of its active metabolite SN-38 that is bioactivated through hydrolyzation in the liver, the use of this compound instead would further improve the accuracy of our model. In future research, improvements could be made to our platform through the incorporation of other cellular elements such as patient-derived stromal

fibroblasts or immune components to further create a more realistic tumor microenvironment. Through this incorporation, our platform could potentially accelerate investigations into how the stroma modulates disease progression, imparts resistance to drugs, and affects therapeutic response.

2.5 Experimental Methods

Design and fabrication of the platform

We designed and fabricated both devices based on previously developed standard microfluidic protocols[72]. In summary, both devices were designed using AutoCAD (Autodesk Inc. San Rafael, CA, USA) and processed using photolithography techniques to make silicon-based molds that were then used to cast the devices from polydimethylsiloxane (PDMS) using standard soft lithography procedures. The design of the multiplexer control device was based on previously developed techniques allowing for multiple fluidic configurations and control with a minimal number of valves[40,72–75]. The multiplexer control device is composed of two PDMS based layers, a flow layer and a control layer, bonded together onto a glass slide to produce push-up valve configuration for fluidic control. The 3D culture chamber device consisted of two PDMS slabs: the channel layer for fluidic exchange and chamber layer consisting of the 200 well array. Both the channel layer and the chamber layer molds were constructed out of SU-8 3050, while the control layer and flow channels of the multiplexer control device were produced with SU-8 3025 (MicroChem, Westborough, MA, USA). Additionally, AZ-50x (AZ Electronic Materials, Luxembourg) was used to construct the valves of the multiplexer control device. The photoresists were spun to a minimal height of 450 μm for the channel layer and 600 μm for the chamber wells.

The multiplexer device was spun to 75 μm for the control layer and the AZ based valves and 90 μm for the fluidic flow layer. Using standard soft lithography procedures, 72 g of PDMS (10:1 monomer/catalyst ratio) was mixed, debubbled, and poured over the trimethylchlorosilane-treated silicon mold for both the channel layer and flow layer of the multiplexer device. The thinner chamber array used 15 g of PDMS. The control layer of the multiplexer mold was spin coated at a speed of 1800 rpm. The PDMS for all molds was cured at 80°C for at least an hour. The channel layer was punched for inlet and outlet holes when the curing process was completed. While, the flow and control layer of the multiplexer were plasma treated, aligned, and set with at least 4 hours of thermal bonding before the inlet and outlet holes were punched. The multiplexer control device was then bonded to a glass slide and cured overnight at 80°C before use. These methods produce devices with low variation and high reproducibility with less than 2% coefficient of variation (CV, n=6) for the height of the chamber and channel and almost 0% (0.4, 0.002) for the width (x and y dimensions) of the wells and channels.

Human specimens, isolation and culture of cancer organoids

Between 2014 and 2017, tumor samples were collected from human pancreatic ductal adenocarcinoma cancer (PDAC) patients under IRB12-1108 and IRB13-1149. Samples were obtained from patients undergoing pancreatic resections at The University of Chicago Medicine (UCM) facilities. Tumor samples were digested and established into organoids according to established protocols previously published[9]. Briefly, organoids were grown and cultured by embedding dissociated tumor cells in growth-factor-reduced (GFR) Matrigel (Corning, 356231) and cultured in complete media (Intesticult [Stemcell Technologies, 6005], A83-01 [0.5 μM, Sigma, SML0788], fibroblast growth factor 10 [FGF10, 100 ng/ml, Gibco, PHG024)], Gastrin I

[10 nM, Sigma, 17105-041], N-acetyl-L-cysteine [10 mM, Sigma, A9165], Nicotinamide [10 mM, Sigma, N0636], B27 supplement [1x, Gibco, 17504-044], Primocin [1 mg/ml, InvivoGen, ant-pm-1] and Y-27632 [10.5 µM Tocris, 1254]). Organoids were passaged via mechanical dissociation and TrypLE Express (Fisher Scientific, 12605-010) to single cells before being loaded on to the platform.

Cell culture and organoid loading on platform

The chamber array layer is placed on a glass slide (75 x 50 x 2 mm) and single cells or premature organoids were embedded in 70% cold Matrigel and 30% organoid growth media and manually pipetted into each individual chamber. The chamber layer with the corresponding channel layer are placed together and nested inside the microscope plate holder (Nikon), which has been drilled to specifications to accommodate the 6 screws that corresponded with a machine-shopped process piece of polycarbonate to apply an even pressure on the two piece PDMS layer that in return reversibly bond the device with knobs screwed down on each of the screws.

Multiplexer Control Device Setup

Valve control channels of the multiplexer control device were connected to miniature pneumatic solenoid valves (Festo, Switzerland) that were controlled with a custom designed MATLAB (MathWorks, USA) graphical user interface with tab-delimited text (e.g. Excel) or csv compatible file for automation instructions. Through visual confirmation and fluidic testing, optimal closing pressures for the push-up valves were typically between 35 to 40 psi. The solutions were connected to the inlets of the multiplexer and pressurized at 5 psi. Vials to collect excess waste and solutions from wash steps are also connected. The multiplexer control device is then connected to the

organoid culture chip by both the inlets and outlets of the chip. If bubbles accidently arise in the channels full of media, pressurization of the media from the inlet with the outlet valve closed can remove them. Once connected, the custom MATLAB software delivers the desired fluidic supply to the organoids or other 3D cellular culture. Before the drug treatment experimental, optimal growth media exchange/feeding occurred automatically every 38 hours.

Live-cell fluorescence microscopy and environmental control

The completed two-part organoid culture platform was housed on an automated translational stage of an inverted microscope (Nikon Eclipse Ti) that is encased inside an enclosure designed for cellular environmental control (Life Imaging Service GmbH, Basel, Switzerland). The enclosure features machinery to control the temperature, humidity, and CO2 gas composition to maintain the cell culture[12]. The optimal parameters consist of constant 37°C temperature, 5% CO2 level, a humidity flow rate of 25-30 l/hr, and a relative humidity level set to 100%. The media reserves for the organoids are also kept inside the enclosure to be maintained at ample temperature. Images of the organoids in the platform during the experiment were acquired via the supplied microscope software that is capable of automatically acquiring images at different positions, *Z*-planes/stacks, and in multiple color channels (NIS-Elements software, Japan). A digital complementary metal-oxide semiconductor (CMOS) camera (ORCA-Flash 4.0, Hamamatsu, Japan) imaged the organoids using a x10 objective at 2 to 4-hour intervals. To monitor and measure the organoid growth over time, the acquired phase contrast images were analyzed using an automated organoid segmentation pipeline with manual curation of segmented images. For quantification of cellular death and apoptosis, the fluorescent images were analyzed using a MATLAB script that extracts the average fluorescence intensity of the desired fluorescent marker for each segmented organoid and each time-lapse image.

Qualification of H&E architecture

Organoids were fixed with 10% formalin, paraffin embedded and sectioned (5μm) then stained with hematoxylin and eosin (H&E) for histopathological evaluation. A gastrointestinal pathologist classified the organoids based on tumor cell appearance, differentiation, and gland structure. Previously published data on the same organoids used here (Romero Calvo et al., 2019, *Molecular Cancer Research)* showed a more valuable overall representation of tumor differentiation with H&E tumor cell appearance and gland structure than individual immunohistochemical markers.

Culture of Other 3D Cellular Structures and Organoids

Human colonic organoids cultured similarly to PDAC organoids in Matrigel on platform with growth media as described in reports documenting previously established methods[76]. The MDA-MB-231 human breast cancer cell line was maintained in DMEM, high glucose/pyruvate, (11995115, Gibco) containing 10% fetal bovine serum (FBS). Cells were resuspended in 1:1 Matrigel: Growth Media Solution before being seeded into the platform. Growth protocol was then carried out in a similar fashion as the organoid culture with feeding every 48 hours.

Drug Screening Experiments

Real time viability: Relative apoptosis and viability of organoids was determined by measuring apoptosis with a caspase 3/7 fluorescence marker (Essen Bioscience 4400) and cellular death with propidium iodide fluorescence maker (Thermo Fisher P3566) simultaneously in real-time using the described microscope platform. After one to two weeks of growth on our platform, the organoids were treated with desired chemotherapy drugs once they reached around 100 μm diameter in size. Cells were incubated with the caspase 3/7 (5 μM) and propidium iodide (1.5 μM)

along with the desired drug or drug combination. The desire drug solution was automatically delivered with the multiplexer control device according to the pre-set program. Imaging began 30 minutes after the first drug delivery to ensure proper incorporation of the fluorescent markers and continued for the complete 72-hour time period every 2 or 4 hours. The fluorescence time-lapse images intensities were measured, acquired with MATLAB, and normalized to the positive control (staurosporine, 10 mM). The acquired apoptosis (caspase 3/7) fluorescent intensities were analyzed using the trapezoid rule for numerical integration and averaging of the three independent experimental replicates for each subset of treatments along with the standard error of the mean of the replicates (s.e.m.). The wash and waste capabilities of the multiplex control device allowed thorough wash and cleansing of the fluidic controller between different drug treatments. Fluorescent intensity of the entire experiment for each patient and replicates were averaged and presented in drug sensitivity heat map (n=3).

All treatments were normalized to each patient's corresponding positive control and to the first time point to prevent any possible well to well variation. To resemble traditional plate-based, SOC drugs were used to treat the tumor organoids at 4- and 72-hour durations. To mimic and mirror real-life patient chemotherapy treatments, combination treatments were given temporally/sequentially as outlined in Table 2-1. Tumor organoid culture variation between the wells were measured based on the organoid size distribution with a coefficient of variation (CV, n=6) of 12.8%, which was accounted for during the image analysis with replicates and normalization to positive control and to the first time point in each treatment group. Docetaxel (01885, Sigma); Paclitaxel (T7191, Sigma); Gemcitabine Hydrochloride (G6423, Sigma); 5-Fluorouracil (F6627, Sigma); Cisplatin (232120, Sigma); Oxaliplatin (AG-CR1-3592, AdipoGen);

Irinotecan Hydrochloride (CPT-11) (I1406, Sigma); Staurosporine (NC0748115, Fisher Scientific).

Statistics and Reproducibility

Statistical analysis was performed with MATLAB and repeated measures ANOVA and one-way ANOVA was used as indicated ($p<0.05$). All experiments were conducted with samples sizes of a minimum of three. All microscopic images provided in the figures are representative of the entire sample size and have been reproducible in independent replicates and experiments.

Modeling Organoid Cytokine Cross-Talk within One Microfluidic Channel

In order to determine if an organoid culture in a single well could be influenced by cellular factors secreted by neighboring wells of organoids in the same microfluidic channel, we developed a python-based model to simulate the transfer and capture of cytokines from one organoid chamber to its neighboring chamber. The model was formulated by simulating two neighboring well chambers and the flow channel above them with the same well dimensions as the actual device. The number of cells per well were estimated to be 2,500 cells with the organoids having an average diameter of 300 μm. The program simulates the release of cytokines from the surface of the left organoid over a period of 36 hours. The cytokines will diffuse slowly via a random walk in the well until they transition above the green dotted line (representing the Matrigel barrier) and then enter the main flow channel, continue to diffuse, and cross into the gel of a neighboring well. If they go into the second well, they are considered as captured once they come in contact with the second organoid (the red dotted line), are removed from the simulation, and the capture counter is updated. This process is simulated for 36 hours as at each 36-hour cycle the feeding or drug

medium is exchanged and that would remove any cytokines in the channels. Degradation or half-life of cytokine was not considered. Diffusion coefficient for the medium: 3E-10 (m^2/sec). Difussion coefficient for the matirgel: 5.15e-12 (m^2/sec). The model demonstrated that low overall cytokine cross talk (3.6%) occurs between neighboring wells of organoids. Given that cancer organoids are not composed of cells that are specialized secretors of signaling factors (i.e. immune cells), and that the overall molecular transport is very small, it is believed that the drug studies will not be influenced in a significant way by secreted cross-talk factors.

CHAPTER 3

A DEEP LEARNING PLATFORM FOR ORGANOID IMAGE ANALYSIS

As of December 2021, portions of this chapter are in the publication process: Brooke Schuster[†], Jonathan Matthews[†], Sara Saheb Kashaf, Mustafa Bilgic, Andrey Rzhetsky, and Savaş Tay. "OrganoID: a versatile deep learning platform for organoid image analysis."

[†] These authors contributed equally to this work.

3.1 Summary

Organoids are three-dimensional *ex vivo* tissue models that can closely represent the native heterogeneity, microanatomy, and functionality of a particular organ. One unique hurdle to overcome is the analysis of microscopy images of these 3D cellular cultures, due to the diversity in the shape and size of organoids, as well as their movement through focal planes. Here, we present OrganoID, a user-friendly and open-source organoid image analysis platform that recognizes, labels, and tracks single organoids in brightfield and phase-contrast microscopy images. The platform can identify morphologies of detected organoids pixel by pixel and can

accurately analyze a wide range of organoid types out of the box and without the need of fluorescence or transgenic labeling. The neural network is modified from the U-Net architecture and has 98% fewer parameters than the original structure to encourage model generalization and allow fast execution on a standard laptop CPU. The network was trained on 66 manually annotated images of human pancreatic cancer (PDAC) organoids. Validation on separate images from pancreatic, lung, colon, and adenoid cystic carcinoma (ACC) organoids demonstrated a mean intersection-over-union (IOU) of 0.77. Lastly, an assignment algorithm was used to follow identified organoids across a series of time-course images for single-organoid tracking. This platform enables straightforward and accurate analysis of organoid images to accelerate the use of organoids as physiologically relevant models in high-throughput research.

3.2 Introduction

Three-dimensional (3D) cell culture systems can serve as more physiologically relevant models than traditional human cell monolayers for both basic and clinical applications[77]. Organoids are multicellular 3D structures derived from primary or stem cells that are embedded into a biological hydrogel matrix to create an extracellular environment that provides structural support and key growth factors. Organoids are a particularly useful culture system, as they closely recapitulate cellular heterogeneity, structural morphology, and organ-specific functions of a variety of tissues[33,50,78,79]. Live-cell imaging can reveal important organoid dynamics, such as growth, apoptosis/necrosis, and movement, which putatively reflect physiological and pathological behaviors and responses. While organoids have been successfully used to investigate

important phenomena that might be obscured in simpler models, their use in data-intensive applications, such as high-throughput (HT) screening, is limited.

A major challenge for such experiments is the measurement of organoid responses, which must be computed for a large number of microscopy images. Response measurement is particularly difficult for organoid experiments due to 3D movement in their hydrogel matrix environment across focal planes and variability in organoid size and shape between different tissue types, within the same tissue type, and within the same single culture sample[80,81]. Cells can be genetically modified to express fluorescent proteins[82–84], yet the transformation process increases experimental time and complexity and may alter cellular dynamics[85,86]. Small fluorescent dyes can penetrate cell membranes to stain intracellular structures, however live-cell staining is especially inadequate for organoid culture due to cumulative toxicity over longer growth times and limited diffusion through the hydrogel matrix[87]. As such, there is a critical need for a HT imaging platform that can measure organoid responses without the use of potentially toxic or otherwise confounding live-cell fluorescence techniques.

Several software platforms have been developed to automate the process of organoid image analysis. These platforms use conventional image processing methods, such as adaptive thresholding and mathematical morphology[88], or convolutional neural networks[89,90] to identify organoids in sequences of microscopy images. Despite their advantages, most existing platforms require cellular nuclei to be transgenically labeled[90], which increases experiment time and complexity and may modify cellular dynamics, require manual parameter tuning for each image[88], or are limited to bounding-box detection[89], which leads to failure of capturing a considerable amount of morphological information. Changes in organoid shape can reveal their important responses to external stimuli or internal changes. For example, organoids can blebb or merge,

which might be missed with bounding-box measurements. Importantly, existing platforms were developed for analysis of organoids derived from a single type of tissue and for images obtained with one specific geometric configuration. A robust analysis platform that can handle a variety of organoid types and microscopy setups would promote broad adoption of organoids in HT experiments.

To address these challenges, we have developed a software platform, OrganoID, that can identify and track organoids from a wide range of tissue types, pixel-by-pixel, in both brightfield and phase-contrast microscopy images. OrganoID consists of (i) a convolutional neural network, which processes raw microscopy images to produce an "organoid probability score" for each pixel, (ii) an edge detection and labeling module, which identifies individual organoids in each image, and (iii) a tracking module, which matches and follows single organoids in image sequences. The neural network structure was derived from the *u-net* architecture[91] and uses far fewer feature channels than the original implementation to allow network inference to be executed in a few seconds on a standard laptop computer. OrganoID is publicly available both as an open-source code, and as a standalone executable. The distribution package also includes sample datasets and detailed usage instructions. The software is ready to be used for organoid research overcoming a major hurtle in experimental analysis to support wider integration of use of organoid models in HT applications.

3.3 Results

3.3.1 A generalizable convolutional neural network for per-pixel organoid detection

We developed a deep learning-based image analysis pipeline, OrganoID, that recognizes and tracks individual organoids, pixel-by-pixel, for bulk and single-organoid analysis in brightfield and phase-contrast microscopy images **(Figure 3-1)**. The platform employs a convolutional neural network to transform microscopy images into organoid probability images, where brightness values represent the network belief that an organoid is present at a given pixel. The network structure was derived from the widely successful *u-net* approach to image segmentation[9] **(Figure 3-1b-d).** The *u-net* approach first passes each image through a contracting series of multidimensional convolutions and maximum filters to extract a set of deep feature maps that describe the image at various scales of detail and spatial contexts. Then, the feature maps are passed through an expanding series of transposed convolutions, which learn to localize the features and assemble a final output that matches the resolution of the input image. The OrganoID neural network uses the *u-net* structure; however, each layer uses far fewer parameters (2% of the original implementation parameter count), which limits overfitting and minimizes the amount of memory and computational power required to use the network in the final distribution **(Figure 3-1d)**. Additionally, all hidden convolutional layers were set to compute outputs with the exponential linear unit (ELU) activation function[92], which has demonstrated higher accuracy than the rectified linear unit (ReLU) and avoids vanishing gradient problems during network training. Neurons in the final convolutional layer were set with a sigmoid activation function to produce a normalized output that corresponds to the probability that an organoid is present at each pixel in the original image.

An original dataset of 75 brightfield and phase-contrast microscopy images of organoids were manually segmented to produce black-and-white ground truth images for network training, validation, and testing **(Figure 3-2a,b)**. Each image featured 5 to 50 organoids derived from human pancreatic ductal adenocarcinoma (PDAC). Organoids were either grown on a standard tissue culture plate or on our previously published microfluidic organoid platform[93] (Table 2). To teach the network that segmentations should be independent of imaging orientation, field-of-view, lens distortion, and other potential sources of overfitting, the training dataset was augmented with random rotation, zoom, elastic distortion, and shear transformations to produce a total of 2,000 images **(Figure 3-1c)**.

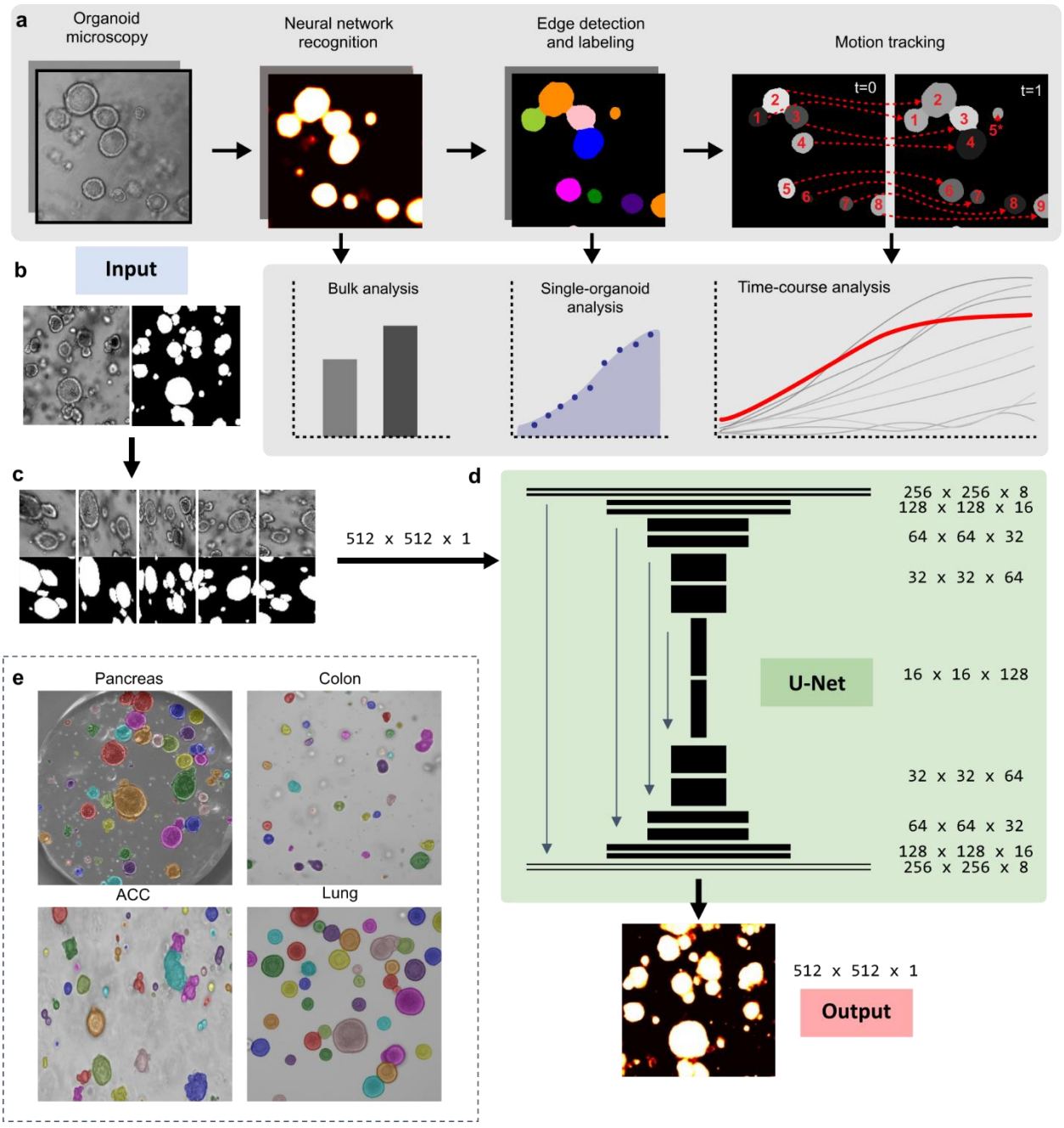

Figure 3-1: OrganoID automates pixel-by-pixel analysis of organoid microscopy images

(a) The platform uses a convolutional neural network to recognize live organoids pixel by pixel. An edge detection module identifies individual organoids for single-organoid analysis. A tracking algorithm matches identified organoids in time-lapse microscopy image sequences to follow single-organoid responses over time. (b-d) Training and structure of the OrganoID convolutional neural network. (b) The network was trained on 66 manually-labeled brightfield or phase-contrast microscopy images of pancreatic cancer (PDAC) organoids. (c) The images were passed through a series of random transformations to produce an augmented dataset of 2,000 images. (d) The neural network is based on the *u-net* architecture, which applies a series of trainable convolutions to produce an organoid probability score for each pixel. (e) Despite training on only PDAC organoids, OrganoID was able to generalize to organoids derived from other tissue

Fig. 3-1, continued: types, including colon epithelia, distal lung epithelia, and salivary adenoid cystic carcinoma (ACC).

Network training halted after 37 epochs, once segmentation error (binary cross-entropy) on the validation dataset converged to a minimal value **(Figure 3-2c-d)**. After hyperparameter tuning, the final model performance was assessed on a novel PDAC testing dataset, previously unseen by the network. The intersection-over-union (IOU), defined as the overlap between the predicted and actual organoid pixels divided by their union **(Figure 3-2e)**, was used to quantify network performance**.** An IOU greater than 0.5 is generally considered to reflect a good prediction; we chose this value to be the minimal benchmark for satisfactory model performance. The mean IOU for the PDAC testing dataset was 0.74 (*SD = 0.080*) **(Table 3-1)**. Each image was segmented in ~300 milliseconds on a laptop CPU (Intel i7-9750H, 2.6GHz) with less than 200 megabytes of RAM usage. The network was also evaluated for appropriate exclusion of non-organoid artifacts. Air bubbles in culture media or gel matrix were rarely detected by OrganoID with a false positive rate of 4.2% **(Figure 3-3a)**. We observed that OrganoID segmentations also avoided cellular debris or dust embedded into the gel, ignored chamber borders, and performed robustly across microscope resolutions, organoid concentrations, and organoid shapes **(Figure 3-3b-g)**.

Because the network was trained and assessed solely with images of PDAC organoids, we were curious to evaluate its capacity to generalize to organoids derived from other tissue types. 18 microscopy images of organoids derived from the distal airway tissue from the lung, colon epithelia and salivary adenoid cystic carcinoma were manually segmented and assembled into an expanded dataset **(Figure 3-1e, Figure 3-2f)**. Analysis of network performance on this dataset demonstrated a mean IOU of 0.79 (*SD=0.094)* **(Table 3-1)**. These results demonstrate the capability of the OrganoID neural network to accurately detect organoids from various tissues of origin in a pixel-by-pixel manner.

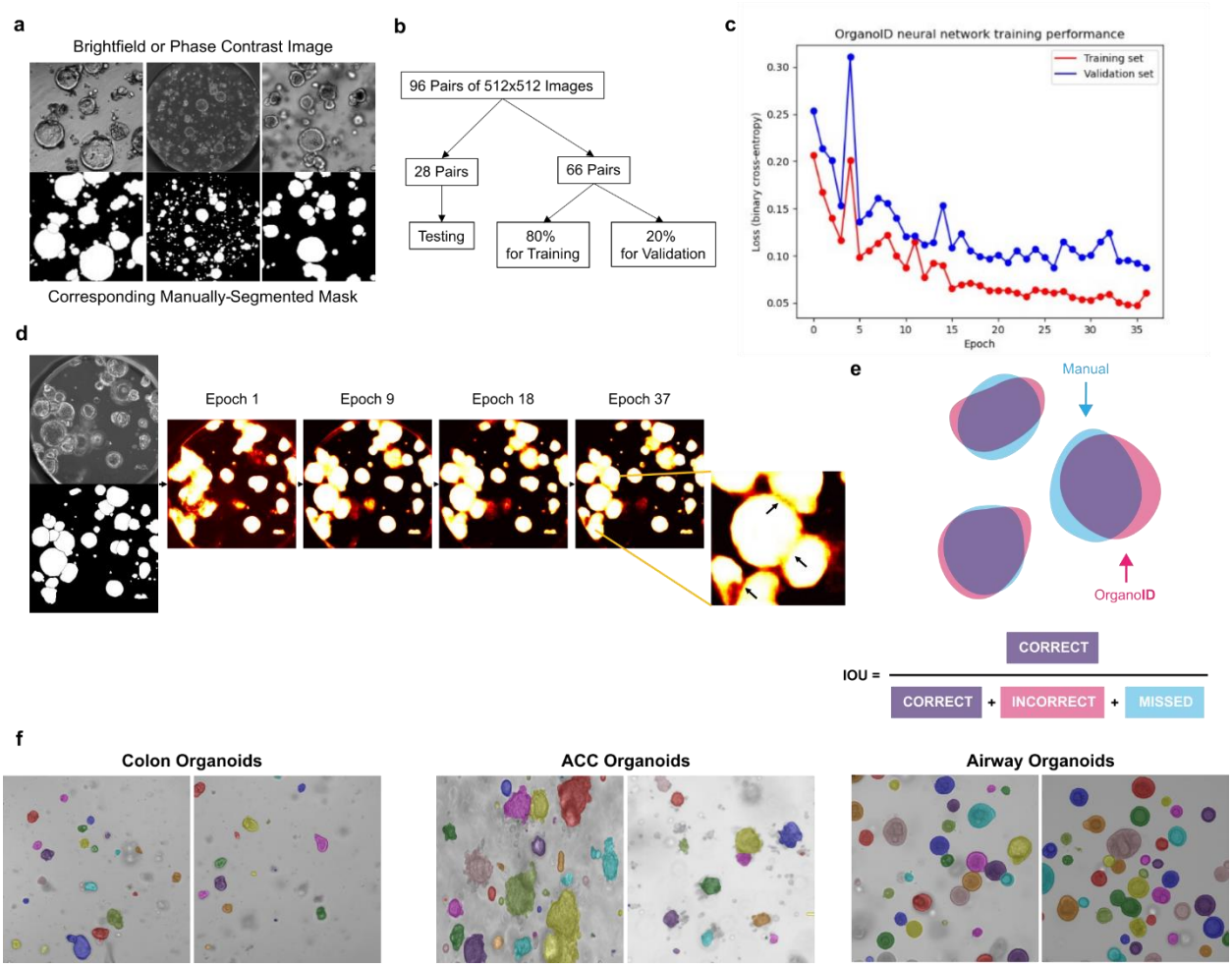

Figure 3-2: Neural network training, validation, and generalization.

(a) 94 (76 pairs were only pancreatic cancer (PDAC) organoids) ground-truth segmentations were created from brightfield and phase-contrast microscopy images. Three representative examples are shown. (b) Ground-truth data was randomly split into datasets for training (52 image pairs), validation (14 image pairs), and testing (28 image pairs: 10 pairs of PDAC, 6 pairs Colon, 6 pairs ACC, 6 pairs Airway)). (c) Network training was stopped after 37 epochs, once a minimum binary cross-entropy loss on the validation dataset was reached. (d) The OrganoID neural network predicts the probability that an organoid is present at each pixel. Shown are network predictions produced by intermediate models at selected epochs through the training process. The zoomed-in view shows that the network produces slightly less confident predictions at organoid boundaries (black arrows). This phenomenon is used to separate organoids in physical contact. (e) The intersection-over-union (IOU) metric is used to quantify network performance on testing datasets. (f) OrganoID can process a wide range of organoid types, morphologies, and sizes.

Table 3-1: Analysis of the OrganoID's network performance

The intersection-over-union (IOU), defined as the overlap between the predicted and actual organoid pixels divided by their union, was used to quantify network performance. An IOU greater than 0.5 is generally considered to reflect a good prediction. SD is standard deviation.

Organoid source (image count)	Mean IOU	SD
All (28)	0.77	± 0.092
Pancreatic ductal adenocarcinoma (10)	0.74	± 0.080
Tissues not used for training/validation (18)	0.79	± 0.094
Benign distal respiratory epithelial tumor (6)	0.87	± 0.040
Benign colon epithelial tumor (6)	0.72	± 0.082
Salivary adenoid cystic carcinoma (6)	0.78	± 0.086

3.3.2 Identification of individual organoids with diverse morphology and size

The convolutional neural network detects organoids in an image on a pixel-by-pixel basis, which can be used to measure bulk responses. For single-organoid analysis, high-belief pixels must be grouped together to identify individual organoids. This task is straightforward for isolated organoids, where all high-belief pixels in a cluster correspond to one organoid but is more difficult for organoids that are in physical contact. To address this challenge, we developed an organoid separation pipeline that uses raw neural network predictions, edge detection, and a watershed transformation to group pixels into single-organoid clusters **(Figure 3-4a-f)**.

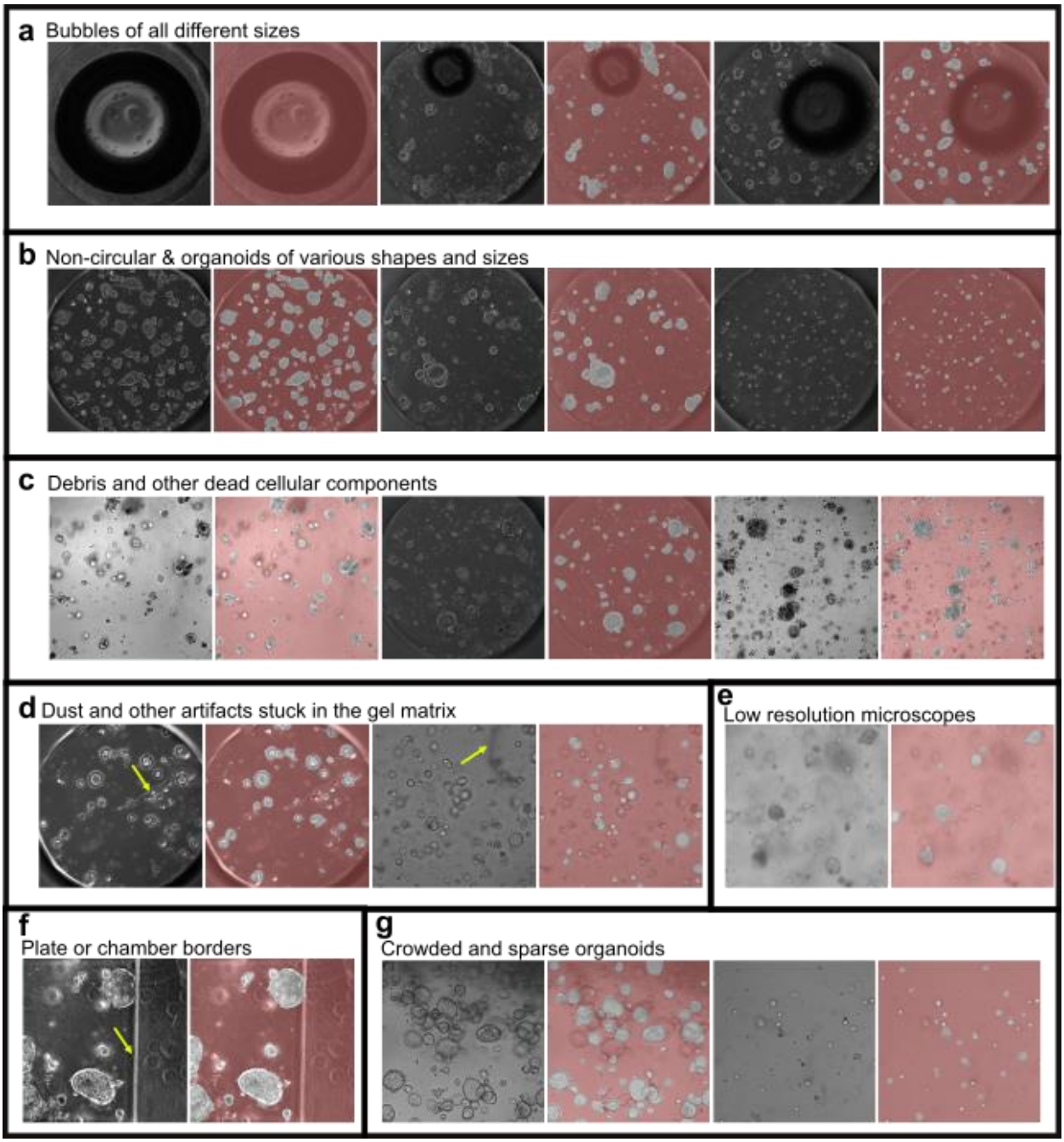

Figure 3-3: Exclusion of non-organoid structures and artifacts

OrganoID was able to ignore bubbles (a), debris (c-d), and plate or microfluidic chamber borders (f) to accurately identify organoids that exhibit diverse morphology and sizes, even within a single sample (b). OrganoID can also handle various optical configurations, including low-resolution or poorly lit images (e). Gel droplets can support densely packed or isolated organoids, which can all be detected with OrganoID (g).

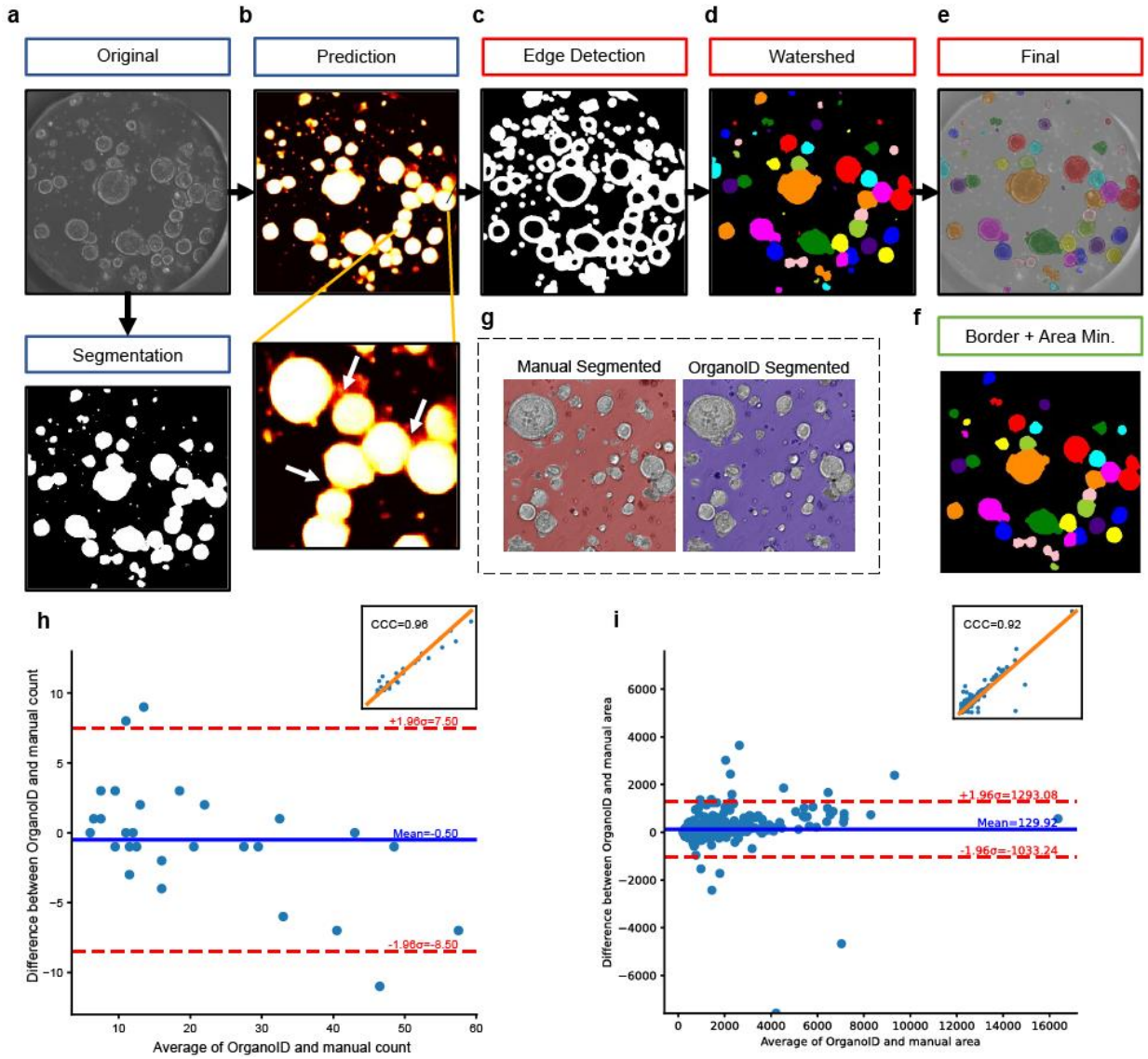

Figure 3-4: Network predictions are used for single-organoid identification

(a-f) OrganoID can identify individual organoids and distinguish organoids in physical contact. (a) Neural network predictions are commonly thresholded to produce a binary segmentation image that does not discern between individual organoids. (b) To identify individual organoids, OrganoID takes advantage of marginally less confident predictions at organoid borders. White arrows in the zoomed-in image point to organoid borders. (c) Prediction images are first processed with a Canny edge detector to identify organoid borders and centers. (d) A watershed algorithm fills organoid contours to produce unique labels. (e) The final labels can be overlayed onto the original image. (f) An organoid area threshold and border removal can refine analysis. (h-i) The single-organoid pipeline was validated through comparison to manually-labeled images. (h) A Bland-Altman plot shows bias and limits of agreement between the number of organoids identified manually and with OrganoID. Inset is a plot of OrganoID count versus manual count (orange line is displayed as y=x, CCC=concordance correlation coefficient). (i) A Bland-Altman plot shows bias and limits of agreement between the area of each organoid as identified manually and with OrganoID. Inset is a plot of OrganoID count versus manual count (orange line is displayed as y=x, CCC=concordance correlation coefficient).

Conventionally, neural network image segmentation methods set an absolute threshold on predicted pixels to produce a binary detection mask **(Figure 3-4a)**. This approach is effective but discards useful information about the strength of predictions. The segmentations that were used to train the neural network were produced with a thin boundary between organoids in contact. As a result, the network predictions were marginally less confident about pixels near organoid boundaries **(Figure 3-4b)**. We took advantage of this phenomenon to identify and separate organoid contours with a modified Canny edge detector[94]. Our detector sequentially applies (i) a pair of Sobel operators, which compute the image intensity gradient; (ii) a Gaussian filter, which smooths noisy regions; and (iii) a hysteresis-based threshold, which identifies locally strong edges. Edges are etched into a thresholded prediction image to mark the centers of each organoid **(Figure 3-4c)**. These centers are used as initializer basins for a watershed transformation that is then applied to the raw prediction image **(Figure 3-4d)**. This step results in a labeled image, where the pixels that represent an individual organoid are all set to a unique organoid ID number (**Figure 3-4e, Figure 3-5**). In addition, these results can be further refined to remove any organoids touching the border that may be only partially seen or cut off by the field of view and/or thresholding the minimum size of organoids detected to filter out single cells or smaller organoids as desired (**Figure 3-4f**).

For quantitative validation, OrganoID single-organoid measurements were compared to measurements obtained from manually-labeled images (**Figure 3-4g-i**). The two methods were used to count the number of organoids in each image and measure the area of each detected organoid. Comparison of organoid counts resulted in a concordance correlation coefficient (CCC) of 0.96 [95% CI 0.92-0.98] and a Pearson correlation coefficient of 0.97 [95% CI 0.94-0.99]. OrganoID, on average, detected 0.5 fewer organoids per image than manual counting. The limits

of agreement between OrganoID and manual counts were between -8.5 and 7.5 organoids (**Figure 3-4h**). Organoid area comparison resulted in a CCC of 0.92 [95% CI 0.91-0.94] and Pearson correlation coefficient of 0.93 [95% CI 0.92-0.94]. OrganoID area measurements were biased to be 130 pixels larger on average, per organoid, (0.05% of total image area) and the limits of agreement were from -1033 to 1293 pixels (-0.4% to 0.5% of total image area) (**Figure 3-4i**). For reference, the total area for each image is standardized to 262,144 pixels (512^2). The measurements produced by OrganoID were in considerable agreement with those obtained by hand, which supports the use of OrganoID for automated single-organoid analysis.

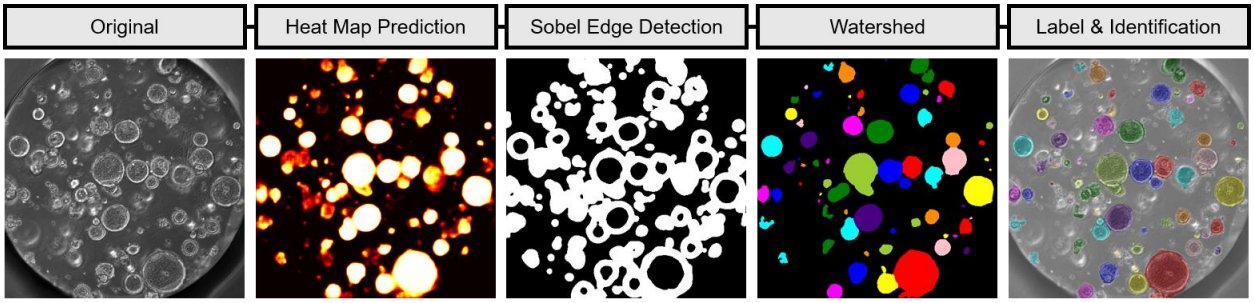

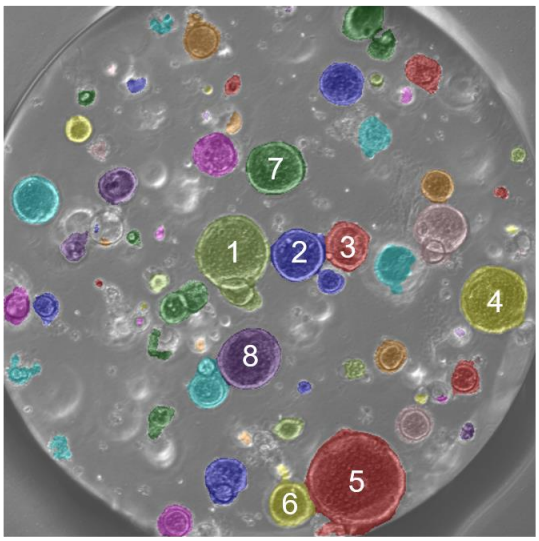

Organoid ID	Area (μm²)
1	32,381
2	18,177
3	11,207
4	23,390
5	51,986
6	11,277
7	16,399
8	19,815

Figure 3-5: Full example of single-organoid detection and labeling.

A brightfield microscopy image is processed by the OrganoID neural network to recognize organoids pixel-by-pixel. An edge detection algorithm uses a Sobel filter to recognize boundaries between organoids in the prediction image and mark organoid centers. The watershed method then expands organoid centers to find filled and labeled organoid contours. Identified organoids can be morphologically analyzed to compute various properties, such as 2D area.

3.3.3 OrganoID measures bulk and single-organoid growth and death over time

We used OrganoID to automatically process time-lapse image sequences obtained with our previously published microfluidic organoid platform[93]. PDAC organoids were grown in microfluidic wells and imaged every 2 hours over the course of 4 days. 8 wells from the dataset were randomly selected for analysis (**Figure 3-6a-c, Figure 3-7**). For each phase-contrast image, OrganoID was used to calculate the number of organoids, total organoid area, and individual organoid areas. The measured total organoid area trended monotonically upwards over time in accordance with organoid growth **(Figure 3-6a)**. Transient fluctuations in total area were observed due to movement of organoids across the image borders and on the cusp of the focal plane. The number of organoids in each well decreased over time, which reflected growth of a few large organoids that appeared to dominate the image area's focal plane forcing the smaller or non-growing organoids out of view **(Figure 3-6b, Figure 3-7)**. Single-organoid analysis recapitulated bulk measurements with monotonically increasing mean organoid areas and emergence of a small proportion of particularly large organoids **(Figure 3-6c)**. The variety of organoid growth curves and sizes between the samples grown in identical conditions highlights the diversity seen among organoids from a single patient in a single experiment.

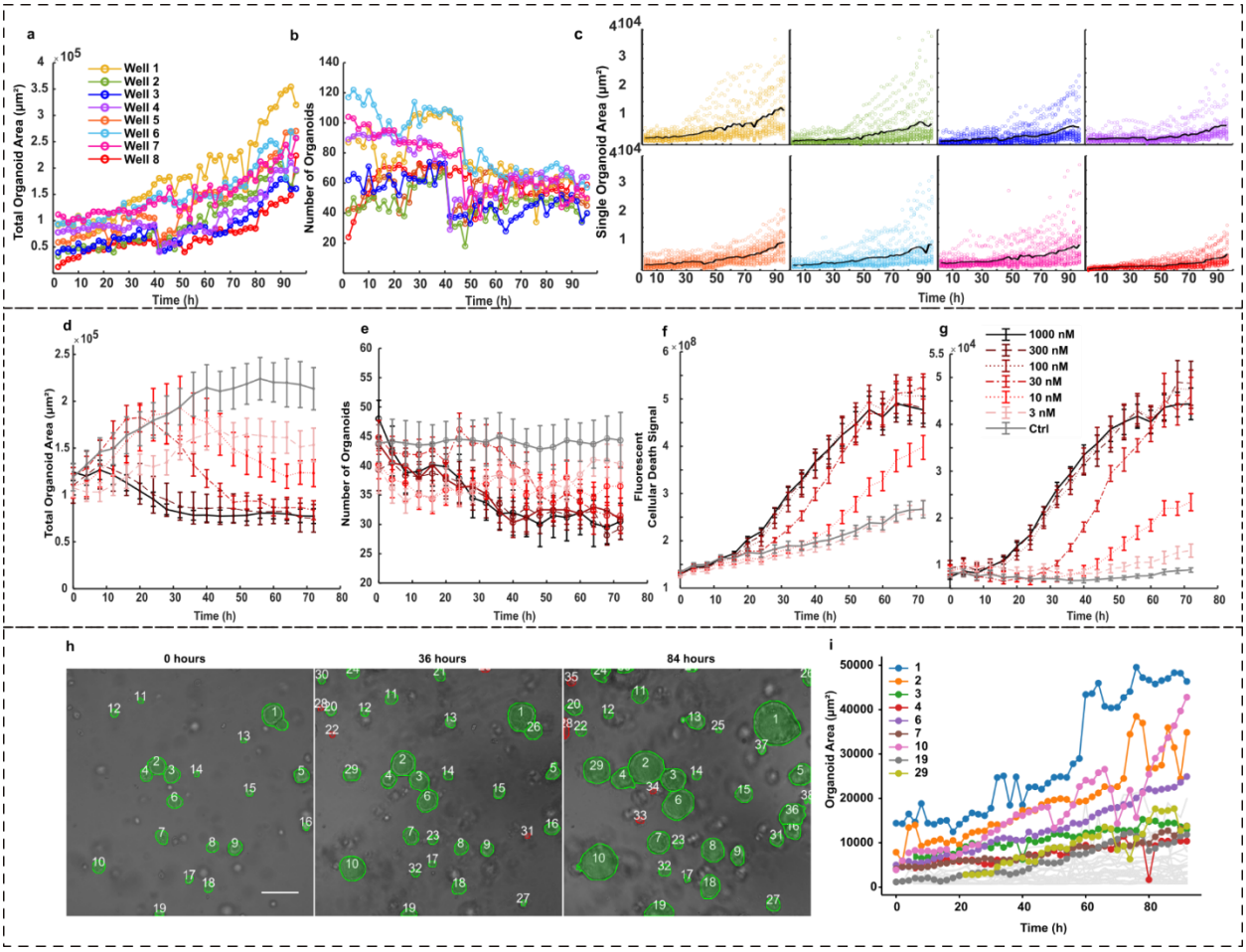

Figure 3-6: OrganoID enables time-course analysis and assay normalization

(a-c) Organoids derived from pancreatic ductal adenocarcinoma (PDAC) were grown in microfluidic wells for 4 days under normal growth conditions and analyzed with OrganoID. (a) The total image area of OrganoID-identified organoids in each microscopy image over time. (b) The number of OrganoID-identified organoids per well at each time point. (c) The image area of individual OrganoID-identified organoids per well. The black line follows the mean organoid area at each time point for each sample. (d-g) PDAC organoids were treated with serial dilutions of gemcitabine and imaged over 72 hours. Propidium iodide (PI) was used to fluorescently label dead organoids. Data points are mean values and error bars are standard error of the mean (n = 6). (d) The total area of OrganoID-identified organoids for each concentration of gemcitabine. (e) The number of OrganoID-identified organoids for each concentration of gemcitabine. (f) Total fluorescence intensity of PI for each concentration of gemcitabine. (g) Normalization of PI measurements with total area of OrganoID-identified organoids increases separation of responses to distinct treatments. (h-i) The OrganoID tracking module matches identified organoids in image sequences to follow individual responses over time. (h) Time-lapse microscopy images from a PDAC organoid experiment are analyzed with OrganoID. Organoids are detected pixel by pixel and individually numbered. Labeled organoids in subsequent images are optimally matched to organoids in previous images. Green overlay highlights identified organoids. Red overlay highlights organoids that were identified in a previous image but are missing in the current image. Overlayed numbers are organoid labels. Error bar is equal to 100 µm. (i) Tracked area of individual OrganoID-identified organoids over time in the data shown in (h).

We then leveraged OrganoID to investigate PDAC organoid death responses to serial dilutions of gemcitabine, an FDA-approved chemotherapeutic agent commonly used to treat pancreatic cancer. Organoids were grown in well plate chambers and respectively dosed with 6 serial dilutions of gemcitabine (3nM-1000nM) with control. Brightfield images were obtained every four hours over the course of 72 hours and processed with the OrganoID platform to compute the total area and number of living organoids. The total area of living organoids for all conditions increased for the first several hours, which reflected initial organoid growth, but then decreased to a value and at a rate inversely proportional to gemcitabine concentration **(Figure 3-6d)**. Organoid counts also followed trends that were in accordance with dosage **(Figure 3-6e)**. To further investigate responses to gemcitabine, propidium iodide (PI, a fluorescent reporter of cellular necrosis) was added to the culture media **(Figure 3-6a, Figure 3-8a)**. To account for the wide distribution in number and size of organoids between samples, we used OrganoID to normalize the fluorescence measurements. For each time point, the total intensity of the fluorescent cellular death signal was computed and divided by the OrganoID-computed total area measurement. Normalization increased the separation of responses between each treatment group compared to non-normalized data **(Figure 3-6f-h, Supp. Figure 3-8b-c)**. These results were compared to normalization with an MTS proliferation assay, which is a gold-standard method to measure endpoint viability for drug testing studies. At the 72-hour time point, the non-normalized PI assay identified 12 significantly different organoid responses to different gemcitabine concentrations **(Supp. Figure 3-8b)**. Normalization with the MTS assay revealed 4 additional significant response differences**;** these differences were also captured through normalization with OrganoID area measurements **(Figure 3-8b-d, Table 3-2).** Through this approach, OrganoID was able to generate useful measurement curves for time-course experiments that can capture bulk and single-organoid

growth and death dynamics without live-cell fluorescence techniques or limitation to only end point analysis.

We next aimed to use OrganoID for longitudinal single-organoid analysis of time-course experiments, where changes in various properties, such as size and shape, of individual organoids are measured and followed over time. We developed a tracking module to match organoid labels across image sequences based on similarities in position and size. The module builds a cost matrix and uses the Hungarian method[95], an optimization algorithm that assigns each organoid to a label with cost of mismatch minimized, to link identified organoids in a given frame to organoids in a previous frame. By matching organoid labels across image frames, the software produces data tracks that can analyze properties of single organoids over time. A representative series of microscopy images were passed through the entire OrganoID detection, identification, and tracking pipeline to produce growth curves that visually followed single-organoid changes in position and size over time **(Figure 3-6i-j)**. The tracking module was also able to resume tracking of any organoids transiently lost to detection due to bubble interference or change in focal plane.

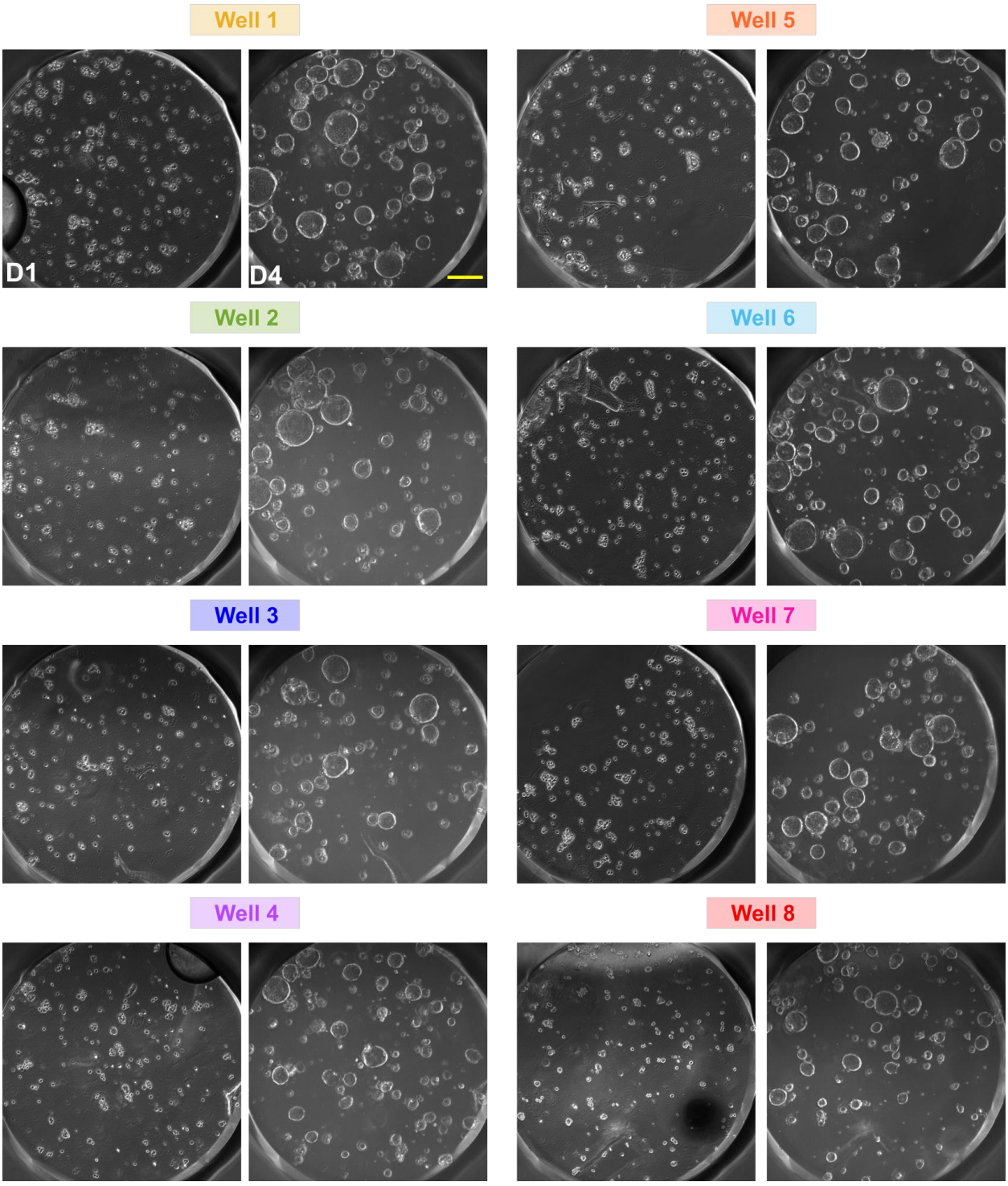

Figure 3-7: Pancreatic cancer (PDAC) organoids growth over 4 Days

Example images of PDAC organoids grown on a microfluidic device over a time period of 4 days. The organoids were supplied with fresh media every 36 hours and imaged every 2 hours. Yellow Scale bar = 200 µm.

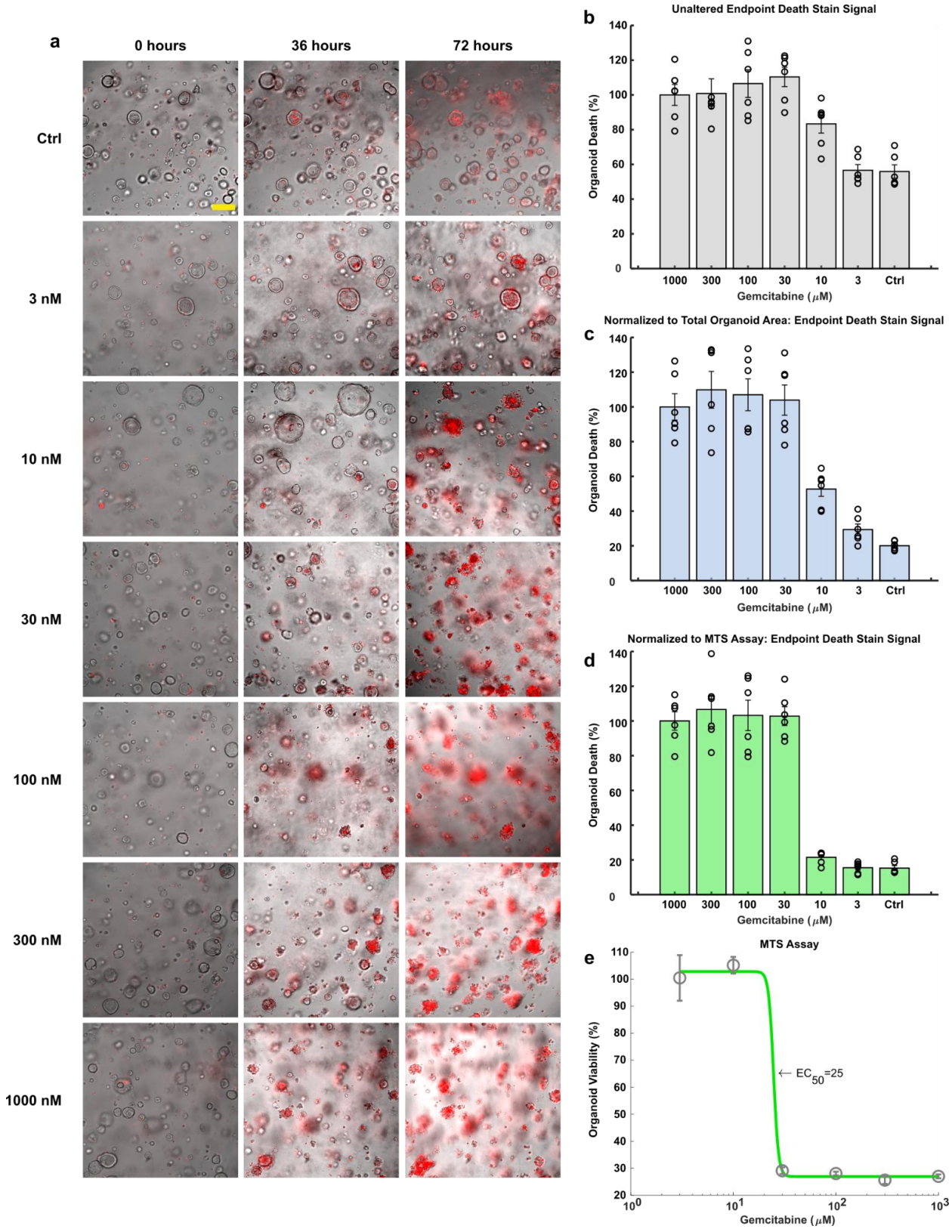

Figure 3-8: Comparison of drug treatment data analysis normalized with OrganoID

Fig. 3-8, continued: (a) Example brightfield images of pancreatic cancer (PDAC) organoids drug treated for 72 hours with a 10-fold serial dilution of gemcitabine, a chemotherapeutic agent commonly used to treat PDAC. Fluorescence of propidium iodide (PI), a reporter of cellular necrosis, is overlayed in red. The control was given only PDAC organoid growth media. Yellow scale bar = 100 μm. (b) Intensity sum of PI fluorescence at the end of the 72-hour drug treatment period for each concentration of gemcitabine. (c) Intensity sum of PI fluorescence divided by the total organoid area, computed with OrganoID, in each sample at the 72 hour time point, which normalizes for differences in the baseline number and sizes of organoids in each replicate. (d) A gold standard endpoint proliferation assay, MTS, was conducted to measure total organoid viability in each sample. Here, the intensity sum of PI fluorescence was instead normalized with the MTS readout for comparison to OrganoID normalization. (b-d) All PI measurements were normalized to the readout from the strongest drug concentration (1000 nM) and presented as mean values ± SEM, n = 6. One-Way ANOVA statistical results in Table 3-2. (e) A viability curve was computed from the MTS assay and demonstrated a half-maximal effective concentration (EC50) of 25 μM.

Table 3-2: One-Way ANOVA calculated P-Values (P<0.001)

Condition 1	Condition 2	PI Data	PI Data Normalized with Area	PI Data Normalized with MTS
1000nM	**300nM**	1	0.956628	0.975909
1000nM	**100nM**	0.987028	0.992248	0.999517
1000nM	**30nM**	0.884143	0.999688	0.999789
1000nM	**1 nM**	0.465339	0.0008	3.72E-08
1000nM	**3nM**	0.000246	8.84E-07	3.71E-08
1000nM	**Ctrl**	0.000191	9.51E-08	3.71E-08
300nM	**100nM**	0.993637	0.999953	0.999353
300nM	**30nM**	0.918481	0.996913	0.998727
300nM	**1 nM**	0.407788	4.48E-05	3.71E-08
300nM	**3nM**	0.000185	8.68E-08	3.71E-08
300nM	**Ctrl**	0.000143	4.08E-08	3.71E-08
100nM	**30nM**	0.999275	0.999928	1
100nM	**1 nM**	0.125988	0.000104	3.71E-08
100nM	**3nM**	2.52E-05	1.49E-07	3.71E-08
100nM	**Ctrl**	1.95E-05	4.52E-08	3.71E-08
30nM	**1 nM**	0.04618	0.000255	3.71E-08
30nM	**3nM**	6.55E-06	3.07E-07	3.71E-08
30nM	**Ctrl**	5.08E-06	5.62E-08	3.71E-08
10nM	**3nM**	0.050677	0.272317	0.985243
10nM	**Ctrl**	0.041342	0.040022	0.982259
3nM	**Ctrl**	1	0.966961	1

3.4 Conclusion

Organoids have revolutionized biomedical research through improved model representation of native tissues and organ systems. However, the field has yet to fully enter the high-throughput experimental space. A central bottleneck is the challenge of automated response measurement and analysis in large numbers of microscopy images. Organoids exhibit striking diversity in morphology and size and can move through their 3D environment into and out of the focal plane, while current image processing tools have not quite been able to capture these aspects in a robust manner. We developed OrganoID to bridge this gap and automate the process of accurate pixel-by-pixel organoid identification and tracking.

Additionally, we have contributed an organoid image segmentation dataset for use in other computational platforms. OrganoID has demonstrated compatibility with organoids of various sizes, shapes, and sample concentrations as well as various optical configurations. Most excitingly, the OrganoID model was trained and validated on only images of pancreatic cancer (PDAC) organoids but still demonstrated excellent performance on images of other types of organoids, including those derived from colon tissue, lung tissue, and adenoid cystic carcinoma (ACC).

Experimental replicates in organoid studies can display a wide range of number and size distribution of organoids per well. This difference between assumed identical samples can pose significant challenges to comparative analysis. As an example, drug testing experiments require per-sample normalization of response measurements in order to account for differences in baseline growth of organoid colonies. This requirement is less critical for traditional 2D monolayer cell culture due to more consistent growth patterns and uniform morphologies. As well, there are several commercially available live-cell assays that can facilitate normalization in 2D culture.

However, these same assays have proven to be difficult for organoid use due to the production of toxic photobleaching byproducts, limited diffusion through the gel matrix, and nonspecific staining of the gel matrix that results in a considerable background signal. Another available option is to genetically modify each organoid sample to express fluorescent proteins, which greatly increases experimental time and complexity, limits the ability to test straight from the original tissue and may alter cellular dynamics. Our vision is to combine the OrganoID platform with other organoid assays to enable high-throughput experiments with non-invasive and 3D culture-compatible measurement normalization. OrganoID could also be used to quantify morphological features and investigate organoid differentiation and growth phases for developmental studies. The platform overcomes a major hurdle in experimental analysis to support wider integration of the organoid model into HT applications.

Our approach was limited in the number of images we were able to obtain from our culture platform and from collaborating laboratories. Despite the suggested generalizability of OrganoID to various samples and optical configurations, performance may still differ with other types of organoids or microscopes. We have released the entire platform, including the training module, fully open-source with documentation to leave open the possibility of retraining the model to expand functionality if needed. Platform performance could also be improved through expansion of the training dataset or by increasing model complexity, albeit at the cost of deployability.

3.5 Experimental Methods

Organoid culture and image acquisition

Tumor organoid cultures derived from PDAC patients were isolated and prepared as previously described[32]. PDAC organoids were cultured and imaged in a microfluidic platform[93] or a 24-well suspension culture plate (Thermo Fisher, 144530). Human colonic organoids were cultured similarly to PDAC organoids, with Matrigel and growth media as described in established methods[76]. Distal respiratory organoids were obtained from the Ishay-Ronen Lab at the Sheba Medical Center and cultured through a previously described protocol[7] in 24-well plates. Images of adenoid cystic carcinoma (ACC) organoids were directly obtained from Dr. Weber and colleagues from University of Chicago Medicine. The pancreatic and airway lung organoids were cultured and imaged on an automated translational stage of an inverted microscope (Nikon Eclipse Ti) enclosed in an environmentally-controlled chamber (Life Imaging Service GmbH, Basel, Switzerland). The enclosure provides temperature, humidity, and CO2 gas control to maintain adequate cell culture conditions for the organoids. Organoids were cultured at a constant 37°C, 5% CO2, a humidity flow rate of 25-30 L/hour, and 95-100% relative humidity. Images of the organoids were acquired through the standard microscope software that is capable of automatically acquiring images at different positions, *Z*-planes/stacks, and multiple fluorescent filters (NIS-Elements software, Japan). The microscope was equipped with a digital complementary metal-oxide semiconductor (CMOS) camera (ORCA-Flash 4.0, Hamamatsu, Japan), which imaged the organoids using a x10 objective at 2 to 4-hour intervals.

Neural network design and implementation

The neural network architecture was based on the *u-net* encoder-decoder network, which has produced incredibly successful results for a variety of biomedical image segmentation tasks[9]. *u-net* uses several convolutional filters for each layer of neurons and doubles the number of filters per-channel for each sequential layer. The original *u-net* implementation uses 64 filters in the first layer, which results in a large number of trainable parameters across the full network (over 30 million). We sequentially reduced the number of filters in the first layer by powers of two to reach a minimal value that preserved performance on the validation dataset. The final OrganoID *u-net* structure uses only 8 filters in the first layer, which results in a network structure with less than 500,000 trainable parameters (a 98% reduction when compared to the original implementation). This simplification reduces the computational power needed to train and use the network and, in theory, decreases network overfitting. All convolutional neurons were set to compute outputs with the exponential linear unit activation function[10]. The final 1x1 convolution was set with a sigmoid activation function to produce a normalized output that corresponded to the probability of an organoid at each pixel. All images are auto-contrasted and resized to 512x512 pixels before training and inference. Python was used for the entire OrganoID platform and Keras (an interface to the TensorFlow library) was used for network expression, training, and operation. The TensorFlow Lite API was used to minimize the memory footprint and number of software dependencies required for network inference in the OrganoID standalone distribution.

Training procedure and ground-truth dataset creation

Ground-truth segmentations were created by hand with Pinta and Aseprite, two open-source image editing programs. 66 ground-truth segmentations were created from brightfield and phase-contrast microscopy images of PDAC organoids and was randomly spilt into datasets for training (52 image pairs) and validation (14 image pairs). The Augmentor Python package[96] was used to apply random rotation, zoom, shear, elastic distortion, and skew operations to the training dataset for data augmentation. The neural network was trained with the Adam stochastic optimization algorithm[97] at a learning rate of 0.001. Unweighted binary cross-entropy between predicted and ground-truth segmentations was used for the loss function. Layer weights were initialized with the He method[98]. An early stopping rule was used to halt training once performance on the validation dataset reached a minimum (i.e. once 10 epochs pass with no improvement in validation loss). The batch size was set to train on 8 augmented images for every round of backpropagation. Dropout regularization was introduced after all convolutions to randomly set 12.5% of neurons to zero after each batch. After each epoch, a copy of the model was saved for additional evaluation of the training process.

Dataset for evaluation of network performance and generalizability

The network structure and training process were manually tuned for performance on the PDAC validation dataset. After optimization, we locked out any further changes to all hyperparameters and evaluated final network performance and generalizability on a separate dataset of 28 organoid microscopy images. The dataset included images of organoids derived from PDAC (10), benign colon tumor cells (6), long epithelia (6), and salivary adenoid cystic carcinoma (6). The images were obtained through brightfield and phase-contrast microscopy from multiple microscopy cores and manually labeled by two independent reviewers.

Single-organoid identification and segmentation refinement

The *scipy*[99] and *scikit-image*[100] packages were used to identify individual organoids from the network detection images. Detection images were thresholded (T=0.5) and passed through a morphological opening operation to remove weak and noisy predictions. Partial derivatives were computed with a Sobel filter, passed through a Gaussian filter (σ=2), and converted to an edge mask with a hysteresis threshold filter (T_{hi}=0.05, T_{lo}=0.005), which was then was used to mark organoid centers. The watershed method was used to identify filled organoid contours, with the organoid centers as label initializers and the network prediction image as an inverted heightmap. Labeled organoids were morphologically filled and discarded if the total area was below 100 pixels.

Tracking of individual organoids over time

Images were morphologically processed with *scikit-image* to record the centroid and area of each detected organoid. The centroids and areas of organoids in the next image are then computed and used to build a cost-assignment matrix, where each row corresponds to an organoid from the previous image and each column corresponds to an organoid in the next image. Each matrix entry is the cost of assigning a given organoid detection in the current image to a detection in the previous image. The cost function was designed to be proportional to the Euclidean distance between the two detection centroids as well as the difference between the detection areas. As such, the assignment cost between two detections will be minimal for those that are close and similar in size. The cost-assignment matrix is also padded with additional rows and columns to allow for "pseudo-assignments" that represent missing or newly-detected organoids. These additional entries were filled with constants that were manually tuned for stable tracking in 512x512 pixel images (-5

pixels for a missing organoid and -200 pixels for a new organoid). Finally, the Munkres variant of the Hungarian algorithm[95] was used to minimize the cost-assignment matrix to find an optimal matching between organoid detections in the previous image and the detections in the current image

Statistical Methods for OrganoID Platform Verification

Statistical analysis was performed with the *numpy* and *scipy* packages in Python. Network performance on the testing dataset was evaluated as the pixel-wise intersection-over-union (IOU) of predictions compared to ground-truth segmentations. A single IOU value was computed for each prediction/ground-truth pair and summarized as a mean IOU and 95% confidence interval over the dataset. For agreement of single-organoid counts and measurements, the Lin concordance correlation coefficient (CCC) was computed as

$$CCC = \frac{2s_{xy}}{{s_x}^2+{s_y}^2+(\bar{x}-\underline{y})^2}.$$

The Fisher transformation (*artanh(CCC)*) and the inverse Fisher transformation (*tanh(*z_{LO}*,* Z_{HI}*)*) were also used to obtain a z-value and construct a 95% confidence interval for CCC statistics. Bland-Altman plots were generated with *matplotlib* in Python.

Drug Screening Experiments

The pancreatic organoids were grown for a week in normal growth conditions and then were treated with gemcitabine hydrochloride (G6423, Sigma) at 10-fold serial dilutions from 3 nM to 1000 nM. Propidium iodide (Thermo Fisher P3566) was used to fluorescently measure cellular death and relative viability of organoids in real-time at 4-hour intervals over 72 hours. The

fluorescence time-lapse image intensities were either measured as is or normalized with the total area of organoids in each sample, which is the raw fluorescence divided by total area of organoids per time point. The end point measurements were also further normalized to 100% cellular death with the fluorescence measurement of the 1000 nM treatment group in order to further compare the different measurement methods (total area normalization vs raw fluorescence data). The six independent experimental replicates for each condition were averaged and presented along with the standard error of the mean of replicates (s.e.m.).

The MTS assay, an end point assay, was also performed at the end of the experiment to further determine the relative number of viable cancer cells per each condition by measuring the optical density using CellTiter 96 Aqueous One Solution Cell Proliferation Assay kit according to manufacturer's instructions (Promega, G3580). Statistical analysis for the drug experiments was performed with MATLAB and one-way ANOVA was used as indicated ($p<0.001$).

CHAPTER 4

CONCLUSIONS AND FUTURE OUTLOOKS

4.1 Reflections and Troubleshooting

4.1.1 Challenges of the Microfluidic Organoid Platform

High-throughput and automated microfluidic devices are not novel as demonstrated by the published one featuring 1,500 individually addressable micro-culture chambers[36] that were exposed to various drug combinations. However, to achieve the ability to culture organoids in a similar fashion, new microfluidic and engineering methods were needed to accommodate the larger size of the 3D structures, be compatible with a 3D environment and the gel structural components that come with it (i.e. Matrigel or hydrogel), and allow for easy extraction of the cells after the experiment is completed for further sequencing analysis, while retaining the ability for high-throughput stimulation, assaying, and harvesting of organoids under dynamic conditions. While designing such a device, the biggest challenges resided in solving both media and gel-based bubble related issues and prevention of leakage.

First, the required organoid media was unusually bubble-prone. Most likely due to the additional supplements added to facilitate organoid establishment and culture such as the B-27

supplement, a cocktail of antioxidants to reduce reactive oxygen damage. Dealing with micro-sized devices, the addition of bubbles can prevent adequate liquid media exchange and exposure of the desired reagents to specific organoid filled chambers. In addition, bubbles can highly distort and block the field of view captured in the images collected during the experiment. In the beginning prototype phases of this device, bubble "infestations" would destroy entire experiments and once the bubbles appeared it was quite difficult to remove them with the first versions of the platform. To prevent or remove any bubbles that occurred, three different methods were optimized: the geometric shape of the wells, the addition of "bubble traps", and design optimization of our clamping system for the culture chamber device. The first version of the device contained chambers or wells in the shape of squares and channels featuring square edges (**Figure 4-1**). The change to both rounded wells and channel edges allowed for a greatly reduced amount of bubble accommodation in the device. This is predicted to be linked to the limitation of bubbles getting stuck and ultimately trapped in the edges of the square chambers or channels.

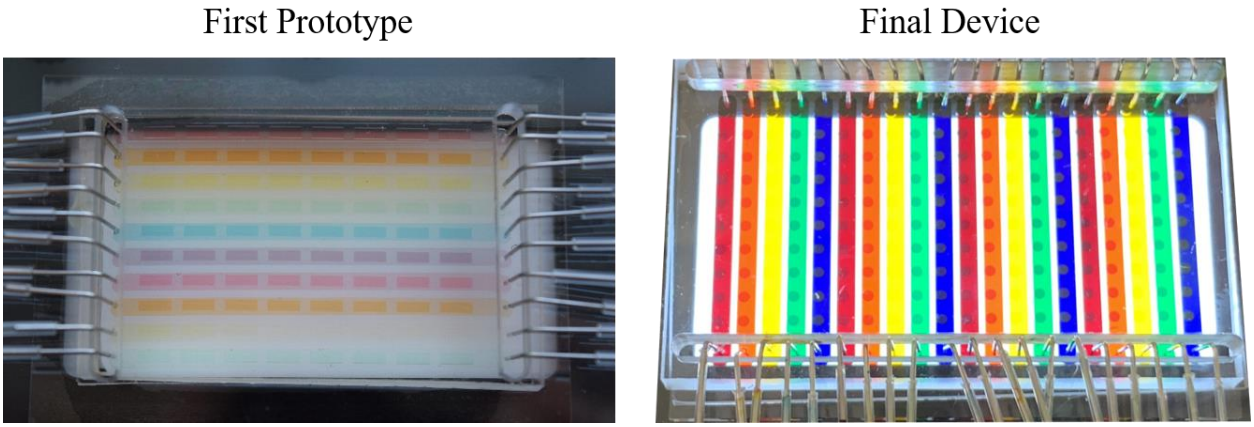

Figure 4-1: Comparison of the first prototype of the 3D culture chamber device to the final version

I also implemented the use of these commercially made "bubble traps", which are a device that intercepts the external tubing leading to the microfluidic device and removes air bubbles from the media before it reaches the device. The bubble trap contains a micro-porous PTFE membrane,

which hydrophobic properties expels bubbles out of the fluid while repelling the aqueous liquid through the outlet that is connected to the inlet of the desired device. Companies such as Omnifit, Elveflow, and Darwin microfluidics are some examples of companies that provide bubble traps devices for purchase. I would also note that as the device got further optimized the use of bubble traps were not completely a necessity, but more used as an added precautionary prevention step. The invention of a more robust clamping system made the necessity of the bubble traps more obsolete. Which leads us to the final challenge I would like to highlight - the clamping system of the culture chamber device (**Figure 4-2**).

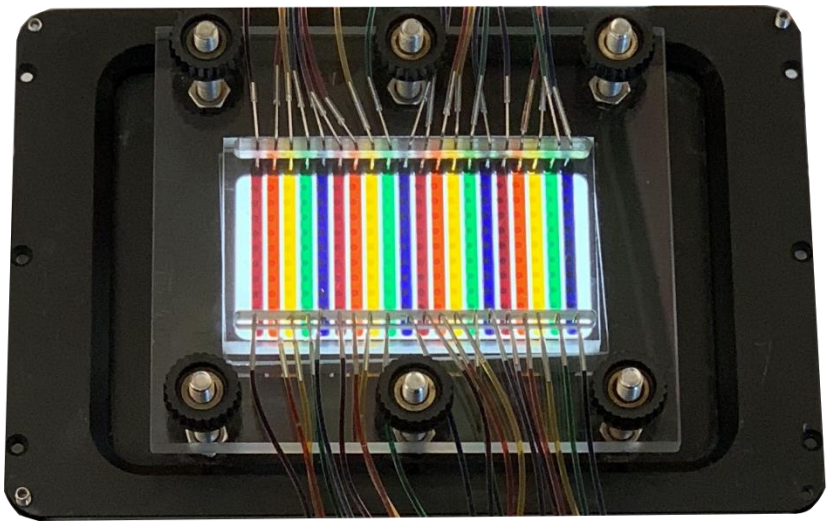

Figure 4-2: Photo of 3D culture chamber device equipped with clamping system

In order to accommodate the use of temperature sensitive hydrogel such as Matrigel, the device was designed to consist of two non-permanently bonded parts to allow for easy embedding of the organoid filled, temperature-sensitive Matrigel. However, the use of a non-permanently bonded system also created a system that was very leakage-prone. If the culture system was not clamped enough, leakage of media out of the device could occur or at the minimum cross-talk between the channels and different treatment groups could occur. To prevent any potential cross-talk or leakage, the material and spacing and overall design of the plastic top and screw system

were optimized to prevent as much leakage as possible. However, once this was solved, I had issues with the bottom glass slide breaking from the clamping pressure, which was ultimately fixed through the use of two commercially available 1mm thick glass sides stacked together or the use of a custom-made glass side that was 1.5mm thick; both solved the problem and still allowed for proper imaging resolution. An additional prevention of using a handheld plasma wand (ETP BD-20AC Laboratory Corona Treater) on both the channel and chamber layers before the device is cultured with organoids, adds an additional surface treatment to the PDMS to allow for additional semi-permeant adhesion when the two parts are put together. Conveniently, this surface treatment is not as strong as using a fully plasma chamber, so removal of the two parts after the experiment is over is still easily obtainable.

The additional of a stronger, more enhanced clamping system contains the ability to easily remove the occasional bubble occurrence through the use of pressure. The permanently bonded devices commonly used in the Tay lab and described in **Section 1.4.1** have the ability to remove any obstructive bubbles through the addition of fluidic pressure added to the inlets, while the outlets valves are closed, which ultimately drives any present bubbles from the fluidic channels out through the PDMS and into the outside environment. This technique is a bit more difficult and results in a longer process time for the culture chamber device due to the fact that the thick plastic layer on top of the device blocks the majority of the surface area of the exposed outside PDMS, however it is still very effective and useful.

Finally, multiple prototypes were constructed in order to test if 200 chambers with 20 channels was the maximum capabilities and the most optimized state of this device. For example, we designed and created a ~1,000 chamber device using the same design, however it was difficult to align the two pieces of the device by eye and required a specialized microscope aligning system,

which we currently did not have available in a cell culture hood (**Figure 4-3**). However, if this device was commercially acquired, I believe these process as well as the seeding process could be automated to bring this device to the throughput required for an industry-like setting. However, the device "as is" is currently capable of being integrated in a small laboratory setting without the need of expensive equipment and operated by a sole user.

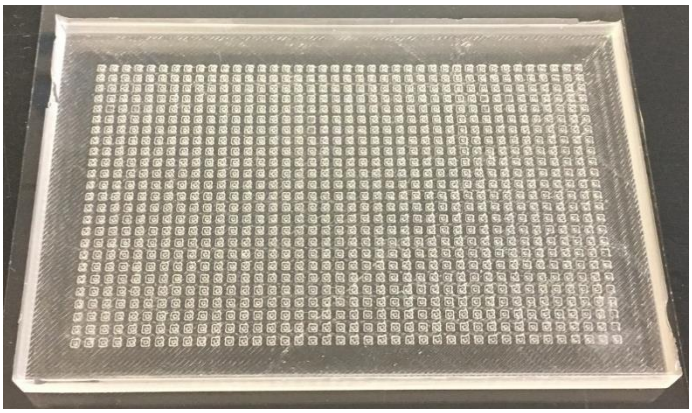

Figure 4-3: Photo of 1,044 well chambers prototype

4.1.2 Novelty and Achievements of OrganoID Overview

First, I would like to again acknowledge Dr. Dana Ishay-Ronen and Dr. Rakefet Ruth Ben-Yishay from Sheba Medical Center for providing the airway lung organoids; Dr. Sonia Kupfer and Margaret Bielski from University of Chicago Medicine for providing the colon organoids; Dr. Chris Weber and Dr. Le Shen from University of Chicago Medicine for providing the adenoid cystic carcinoma (ACC) organoids. Their collaborations were essential in being able to fully examine the platform's full potential beyond the scope of cancer and specifically pancreatic cancer.

Once the platform described in Chapter 2 was established it quickly became apparent that a computational pipeline was needed to thoroughly and accurate dissimilate all the image-based data acquired through out high-throughput platform. Traditional conventical image process methods

such as the 2018 OrganoSeg platform[88] among other commonly used in tradition monolayer cell culture image analysis (e.g. CellProfiler, ImageJ, and Matlab) were unfortunately completely incapable of capturing and analyzing heterogenetic populations of organoids featuring a diversity of size and shapes in a high-throughput manner. Theoretically, one of these methods could be used for a single sample and time point if the correct computational parameters (i.e. threshold, weight variance, size-exclusion threshold, etc.) for that specific image were obtained. However, such parameters required to be tweaked for each specific sample and time point, create a very tedious and time-consuming process. In addition, any interference such us a bubble, random dust or debris particle, or present of a microfluidic chamber or plate edge in the field view quickly voids the use of any of those pipelines.

Other recently published organoid analysis pipelines have turned to the use of transgentically labeled organoids[90] to enable automated tracking, however this completely eliminates the ability to rapidly and inexpensively test a patient-derived tissue or tumor samples directly after its acquisition, which is required for one of this project's primary goals: the discovery of personalized or precision medicine. A few other methods have demonstrated the use of bounding-box methods[89], which are again are limited to more uniform, spherical structures and also incapable of providing specific and exact 2D area dimensions for each organoid.

The platform we created does not have any of the previously described limitations. OrganoID is able to provide automated, thorough and high-throughput analysis of organoid growth from bulk populations to single organoids, compatible with time-lapse analysis, large diversity of morphology detection with multiple types of organoid capabilities, can handle both microfluidic and tradition plate-based platforms, and is unaffected by non-organoid interferences such as bubbles, debris, or poor lighting. OrganoID contains a large portfolio of abilities to provide

analyses from organoid count, total or single organoid area, distributions, and side by side analyses with fluorescent data in a simple “one click” initiation to an entire experiment/s worth of organoid image data.

4.2 Final Thoughts and Future Outlooks

To conclude, three dimensional organoids offer the possibility of a model that can physiologically and genetically replicate the morphology and characteristics of a mammalian tissue. Current biological modeling is limited to either 2D cell lines, which contain limited representation of the actual tissue, or expensive and time-consuming patient xenograft models. I present the completion of an entire platform equipped with a fully functional and automated organoid culturing and dynamic stimulation system followed by a pre-packaged program to rapidly and robustly analyze massive amounts of organoid image data to develop new methods to better enable the use of organoids to be used in a variety of research fields such as biological testing of chemically synthesized compounds, studying complex cellular interactions of organs in development processes, and developing personalized cancer or genetic disease therapies. The highly reproducible, standardized, automated system allows for easy testing of any number of dynamic conditions, while the continuous visual monitoring allows complete analysis of all cellular reactions, which ultimately expands and suppresses the capabilities of current 3D culture technology.

A caveat of the use of organoid culture systems includes the absence of immune signaling and inability to test the tumor’s interactions with immune cells and response to immuntherapies[11]. Many studies were published during my time in graduate school and presented the ability to co-

culture organoids with immune cells[24], patient-specific fibroblasts[69] or stroma components for microtumor environment recreation, as well as microbiome[20,101] and viruses[102,103]. In terms of cancer and the discovery of personalized chemotherapies, the addition of stroma cells is important in examining how the stroma impacts drug response and previous genetic studies of the stroma have correlated it to different clinical outcomes. Further studies testing our platform's ability to accommodate organoid co-cultures could expand the capabilities, as well as the type and amount of data able to be obtained in one experiment, while overall continuously improving the realistic characteristic of this human tumor model system.

To holistically summarize the overall drive and need to continuously seek new complex and accurate human model systems in conjugation with sophisticated platforms to accelerate and efficiently use such systems in the realm of cancer, I will conclude with the presentation of a quote from a review[104] published by Feigin et al. in the *Cold Spring Harbor Laboratory Press* for the 2017 Symposia on Quantitative Biology:

"The ability to faithfully model complex processes lies at the heart of experimental biology. Although a reductionist approach necessarily reduces this complexity, it is nevertheless required for untangling the contributions and interactions of the various system components. It has long been appreciated that cancer is a complex process that involves positive and negative interactions between tumor cells, normal host tissue, and the associated cells of the tumor microenvironment… the ability to model, manipulate, and predict the therapeutic response of an individual's disease outside their body represents the promise of precision medicine."

REFERENCES

1. Boj, S. F. *et al.* Organoid Models of Human and Mouse Ductal Pancreatic Cancer. *Cell* **160**, 324–338 (2016).
2. Bredenoord, A. L., Clevers, H. & Knoblich, J. A. Human tissues in a dish: The research and ethical implications of organoid technology. *Science.* **355**, eaaf9414 (2017).
3. Clevers, H. Modeling Development and Disease with Organoids. *Cell* **165**, 1586–1597 (2016).
4. Boj, S. F. *et al.* Model organoids provide new research opportunities for ductal pancreatic cancer. *Mol. Cell. Oncol.* **3**, e1014757 (2016).
5. Broutier, L. *et al.* Human primary liver cancer–derived organoid cultures for disease modeling and drug screening. *Nat. Med.* **23**, 1424–1435 (2017).
6. Gao, D. *et al.* Organoid Cultures Derived from Patients with Advanced Prostate Cancer. *Cell* **159**, 176–187 (2014).
7. Sachs, N. *et al.* Long-term expanding human airway organoids for disease modeling. *EMBO J.* **38**, e100300 (2019).
8. Roerink, S. F. *et al.* Intra-tumour diversification in colorectal cancer at the single-cell level. *Nature.* **556**, 457–462 (2018).
9. Lee, S. H. *et al.* Tumor Evolution and Drug Response in Patient-Derived Organoid Models of Bladder Cancer. *Cell.* **173**, 515–528 (2018).
10. Kopper, O. *et al.* An organoid platform for ovarian cancer captures intra- and interpatient heterogeneity. *Nat. Med.* **25**, 838–849 (2019).
11. Fiorini, E., Veghini, L. & Corbo, V. Modeling Cell Communication in Cancer With Organoids: Making the Complex Simple. *Front. Cell Dev. Biol.* **8**, 166 (2020).
12. Drost, J. & Clevers, H. Organoids in cancer research. *Nat. Rev. Cance.r* **18**, 407–418 (2018).
13. Lou, Y.-R. & Leung, A. W. Next generation organoids for biomedical research and applications. *Biotechnol. Adv.* **36**, 132–149 (2018).
14. Tuveson, D. & Clevers, H. Cancer modeling meets human organoid technology. *Science.* **364**, 952–955 (2019).
15. Artegiani, B. *et al.* Fast and efficient generation of knock-in human organoids using

homology-independent CRISPR–Cas9 precision genome editing. *Nat. Cell Biol. 2020 223* **22**, 321–331 (2020).

16. Kelava, I. & Lancaster, M. A. Dishing out mini-brains: Current progress and future prospects in brain organoid research. *Dev. Biol.* **420**, 199–209 (2016).
17. Quadrato, G. *et al.* Cell diversity and network dynamics in photosensitive human brain organoids. *Nature.* **545**, 48–53 (2017).
18. Mansour, A. A. *et al.* An in vivo model of functional and vascularized human brain organoids. *Nat. Biotechnol.* **36**, 432–441 (2018).
19. van der Vaart, J. & Clevers, H. Airway organoids as models of human disease. *J. Intern. Med.* **289**, 604–613 (2021).
20. Puschhof, J. *et al.* Intestinal organoid cocultures with microbes. *Nat. Protoc. 2021 1610* **16**, 4633–4649 (2021).
21. Han, Y. *et al.* Identification of SARS-CoV-2 inhibitors using lung and colonic organoids. *Nature.* **589**, 270–275 (2021).
22. Geurts, M. H., van der Vaart, J., Beumer, J. & Clevers, H. The Organoid Platform: Promises and Challenges as Tools in the Fight against COVID-19. *Stem Cell Reports.* **16**, 412–418 (2021).
23. Post, Y. *et al.* Snake Venom Gland Organoids. *Cell.* **180**, 233-247.e21 (2020).
24. Tsai, S. *et al.* Development of primary human pancreatic cancer organoids, matched stromal and immune cells and 3D tumor microenvironment models. *BMC Cancer*. **18**, 335 (2018).
25. WC, van S. *et al.* Human cancer cell lines: Experimental models for cancer cells in situ? For cancer stem cells? *Biochim. Biophys. Acta.* **1795**, 92–103 (2009).
26. Stock, K. *et al.* Capturing tumor complexity in vitro: Comparative analysis of 2D and 3D tumor models for drug discovery. *Sci. Rep.* **6**, 1–15 (2016).
27. Kamb, A. What's wrong with our cancer models? *Nat. Rev. Drug Discov.* **4**, 161–165 (2005).
28. Pampaloni, F., Reynaud, E. G. & Stelzer, E. H. K. The third dimension bridges the gap between cell culture and live tissue. *Nat. Rev. Mol. Cell Biol.* **8**, 839–845 (2007).
29. Willey, C. D., Gilbert, A. N., Anderson, J. C. & Gillespie, G. Y. Patient-Derived Xenografts as a Model System for Radiation Research. *Semin. Radiat. Oncol.* **25**, 273–80

(2015).

30. Pancreatic Cancer Facts - Hirshberg Foundation for Pancreatic Cancer Research. Available at: https://pancreatic.org/pancreatic-cancer/pancreatic-cancer-facts/. (Accessed: 25th October 2021)
31. Cowley, M. J. *et al.* Understanding pancreatic cancer genomes. *J. Hepatobiliary. Pancreat. Sci.* **20**, 549–556 (2013).
32. Romero-Calvo, I. *et al.* Human Organoids Share Structural and Genetic Features with Primary Pancreatic Adenocarcinoma Tumors. *Mol. Cancer Res.* **17**, 70–83 (2018).
33. Sachs, N. *et al.* A Living Biobank of Breast Cancer Organoids Captures Disease Heterogeneity. *Cell.* **172**, 373–386 (2018).
34. Ren, J. *et al.* A novel morphometry system automatically assessing the growth and regeneration of intestinal organoids. *Biochem. Biophys. Res. Commun.* **506**, 1052–1058 (2018).
35. Sasaki, N. & Clevers, H. Studying cellular heterogeneity and drug sensitivity in colorectal cancer using organoid technology. *Curr. Opin. Genet. Dev.* **52**, 117–122 (2018).
36. Zhang, C. *et al.* Ultra-multiplexed analysis of single-cell dynamics reveals logic rules in differentiation. *Sci. Adv.* **5**, eaav7959 (2019).
37. Junkin, M. *et al.* High-Content Quantification of Single-Cell Immune Dynamics. *Cell Rep.* **15**, 411–422 (2016).
38. Albayrak, C. *et al.* Digital Quantification of Proteins and mRNA in Single Mammalian Cells. *Mol. Cell.* **61**, 914–924 (2016).
39. Tay, S. *et al.* Single-cell NF-[kgr]B dynamics reveal digital activation and analogue information processing. *Nature.* **466**, 267–271 (2010).
40. Kellogg, R. A., Tian, C., Lipniacki, T., Quake, S. R. & Tay, S. Digital signaling decouples activation probability and population heterogeneity. *Elife.* **4**, e08931 (2015).
41. Kellogg, R. A. & Tay, S. Noise Facilitates Transcriptional Control under Dynamic Inputs. *Cell.* **160**, 381–392 (2015).
42. Heltberg, M., Kellogg, R. A., Krishna, S., Tay, S. & Jensen, M. H. Noise Induces Hopping between NF-κB Entrainment Modes. *Cell Syst.* **3**, 532-539.e3 (2016).
43. Kellogg, R. A., Tian, C., Etzrodt, M. & Tay, S. Cellular Decision Making by Non-Integrative Processing of TLR Inputs. *Cell Rep.* **19**, 125–135 (2017).

44. Kellogg, R. A., Gómez-Sjöberg, R., Leyrat, A. A. & Tay, S. High-throughput microfluidic single-cell analysis pipeline for studies of signaling dynamics. *Nat. Protoc.* **9**, 1713–1726 (2014).
45. Lin, J. *et al.* Ultra-sensitive digital quantification of proteins and mRNA in single cells. *Nat. Commun.* **10**, 1–10 (2019).
46. Watterson, W. J. *et al.* Droplet-based high-throughput cultivation for accurate screening of antibiotic resistant gut microbes. *Elife.* **9**, 1–22 (2020).
47. Phan, H. Van *et al.* Fixed single-cell RNA sequencing for understanding virus infection and host response. *bioRxiv.* 2020.09.17.302232 (2021). doi:10.1101/2020.09.17.302232
48. Unger, M. A., Chou, H.-P., Thorsen, T., Scherer, A. & Quake, S. R. Monolithic Microfabricated Valves and Pumps by Multilayer Soft Lithography. *Science.* **288**, 113–116 (2000).
49. Thorsen, T., Maerkl, S. J. & Quake, S. R. Microfluidic Large-Scale Integration. *Science.* **298**, 580–584 (2002).
50. Dutta, D., Heo, I. & Clevers, H. Disease Modeling in Stem Cell-Derived 3D Organoid Systems. *Trends Mol. Med.* **23**, 393–410 (2017).
51. Sasai, Y., Eiraku, M. & Suga, H. In vitro organogenesis in three dimensions: self organising stem cells. *Development.* **139**, 4111–4121 (2012).
52. Chan, A. S., Yan, H. H. N. & Leung, S. Y. Breakthrough Moments: Organoid Models of Cancer. *Cell Stem Cell.* **24**, 839–840 (2019).
53. Breslin, S. & O'Driscoll, L. Three-dimensional cell culture: The missing link in drug discovery. *Drug Discov. Today.* **18**, 240–249 (2013).
54. Cheon, D.-J. & Orsulic, S. Mouse Models of Cancer. *Annu. Rev. Pathol. Mech. Dis.* **6**, 95–119 (2011).
55. Marasso, S. L. *et al.* Optimized design and fabrication of a microfluidic platform to study single cells and multicellular aggregates in 3D. *Microfluid. Nanofluidics.* **21**, 1–14 (2017).
56. Jung, D. J. *et al.* A one-stop microfluidic-based lung cancer organoid culture platform for testing drug sensitivity. *Lab Chip.* **19**, 2854–2865 (2019).
57. Kim, J. A., Hong, S., Rhee, J. & Rhee, W. J. Microfluidic three-dimensional cell culture of stem cells for high-throughput analysis Conflict-of-interest statement. *World J Stem Cells.* **11**, 803–816 (2019).

58. Takebe, T., Zhang, B. & Radisic, M. Synergistic Engineering: Organoids Meet Organs-on-a-Chip. *Cell Stem Cell.* **21**, 297–300 (2017).
59. Herland, A. *et al.* Quantitative prediction of human pharmacokinetic responses to drugs via fluidically coupled vascularized organ chips. *Nat. Biomed. Eng.* **4**, 421–436 (2020).
60. John, H. & Paulson, A. Robotic fluidic coupling and interrogation of multiple vascularized organ chips. *Nat. Biomed. Eng.* **4**, 407–420 (2020).
61. Czerniecki, S. M. *et al.* High-Throughput Screening Enhances Kidney Organoid Differentiation from Human Pluripotent Stem Cells and Enables Automated Multidimensional Phenotyping. *Cell Stem Cell* **22**, 929–940 (2018).
62. Shah, M. A. & Schwartz, G. K. The relevance of drug sequence in combination chemotherapy. *Drug Resist. Updat.* **3**, 335–356 (2000).
63. Palmer, A. C., Sorger Correspondence, P. K. & Sorger, P. K. Combination Cancer Therapy Can Confer Benefit via Patient-to-Patient Variability without Drug Additivity or Synergy. *Cell.* **171**, 1678–1691 (2017).
64. Lee, M. J. *et al.* Sequential Application of Anticancer Drugs Enhances Cell Death by Rewiring Apoptotic Signaling Networks. *Cell.* **149**, 780–794 (2012).
65. Shirure, V. S. & George, S. C. Design considerations to minimize the impact of drug absorption in polymer-based organ-on-a-chip platforms. *Lab Chip.* **17**, 681–690 (2017).
66. Neal, J. T. *et al.* Organoid Modeling of the Tumor Immune Microenvironment. *Cell.* **175**, 1972–1988 (2018).
67. Dijkstra, K. K. *et al.* Generation of Tumor-Reactive T Cells by Co-culture of Peripheral Blood Lymphocytes and Tumor Organoids. *Cell.* **174**, 1586-1598.e12 (2018).
68. Öhlund, D. *et al.* Distinct populations of inflammatory fibroblasts and myofibroblasts in pancreatic cancer. *J. Exp. Med.* **214**, 579–596 (2017).
69. Biffi, G., Öhlund, D. & Tuveson, D. Building up the tension between the epithelial and stromal compartment in pancreatic ductal adenocarcinoma. *Cell Death Differ.* **23**, 1265–1266 (2016).
70. Barnett, R. M. & Vilar, E. Targeted Therapy for Cancer-Associated Fibroblasts: Are We There Yet? *JNCI J. Natl. Cancer Inst.* **110**, 2017–2019 (2018).
71. Benam, K. H. *et al.* Small airway-on-a-chip enables analysis of human lung inflammation and drug responses in vitro. *Nat. Methods.* **13**, 151–157 (2015).

72. Gómez-Sjöberg, R., Leyrat, A. A., Pirone, D. M., Chen, C. S. & Quake, S. R. Versatile, fully automated, microfluidic cell culture system. *Anal. Chem.* **79**, 8557–8563 (2007).
73. Tay, S. *et al.* Single-cell NF-kB dynamics reveal digital activation and analogue information processing. *Nature.* **466**, 267–271 (2010).
74. Neils, C., Tyree, Z., Finlayson, B. & Folch, A. Combinatorial mixing of microfluidic streams. *Lab Chip.* **4**, 342–350 (2004).
75. Jensen, E. C. *et al.* Digitally programmable microfluidic automaton for multiscale combinatorial mixing and sample processing. *Lab Chip.* **13**, 288–296 (2013).
76. Fujii, M. *et al.* Human Intestinal Organoids Maintain Self-Renewal Capacity and Cellular Diversity in Niche-Inspired Culture Condition. *Stem Cell.* **23**, 787–793 (2018).
77. Kretzschmar, K. & Clevers, H. Organoids: Modeling Development and the Stem Cell Niche in a Dish. *Dev. Cell.* **38**, 590–600 (2016).
78. Driehuis, E. *et al.* Oral Mucosal Organoids as a Potential Platform for Personalized Cancer Therapy. *Cancer Discov.* **9**, 852–871 (2019).
79. Clevers, H. & Tuveson, D. A. Organoid Models for Cancer Research. *Annu. Rev. Cancer Biol.* **3**, 223–234 (2019).
80. Garreta, E. *et al.* Rethinking organoid technology through bioengineering. *Nat. Mater.* **20**, 145–155 (2020).
81. Pettinato, G. *et al.* Spectroscopic label-free microscopy of changes in live cell chromatin and biochemical composition in transplantable organoids. *Sci. Adv.* **7**, (2021).
82. Kim, S. *et al.* Comparison of Cell and Organoid-Level Analysis of Patient-Derived 3D Organoids to Evaluate Tumor Cell Growth Dynamics and Drug Response. *SLAS Discov.* **25**, 744–754 (2020).
83. Dekkers, J. F. *et al.* High-resolution 3D imaging of fixed and cleared organoids. *Nat. Protoc.* **14**, 1756–1771 (2019).
84. Hof, L. *et al.* Long-term live imaging and multiscale analysis identify heterogeneity and core principles of epithelial organoid morphogenesis. *BMC Biol.* **19**, 1–22 (2021).
85. Bailey, S. R. & Maus, M. V. Gene editing for immune cell therapies. *Nat. Biotechnol.* **37**, 1425–1434 (2019).
86. Ang, L. T. *et al.* A Roadmap for Human Liver Differentiation from Pluripotent Stem Cells. *Cell Rep.* **22**, 2190–2205 (2018).

87. Riss, T., Trask, O. J. & Jr. Factors to consider when interrogating 3D culture models with plate readers or automated microscopes. *Vitr. Cell. Dev. Biol.* **57**, 238–256 (2021).
88. Borten, M. A., Bajikar, S. S., Sasaki, N., Clevers, H. & Janes, K. A. Automated brightfield morphometry of 3D organoid populations by OrganoSeg. *Sci. Rep.* **8**, 1–10 (2018).
89. Kassis, T., Hernandez-Gordillo, V., Langer, R. & Griffith, L. G. OrgaQuant: Human Intestinal Organoid Localization and Quantification Using Deep Convolutional Neural Networks. *Sci. Rep.* **9**, 1–7 (2019).
90. Kok, R. N. U. *et al.* OrganoidTracker: Efficient cell tracking using machine learning and manual error correction. *PLoS One* **15**, e0240802 (2020).
91. Ronneberger, O., Fischer, P. & Brox, T. U-net: Convolutional networks for biomedical image segmentation. in *International Conference on Medical image computing and computer-assisted intervention* **9351**, 234–241 (Springer Verlag, 2015).
92. Clevert, D.-A., Unterthiner, T. & Hochreiter, S. Fast and Accurate Deep Network Learning by Exponential Linear Units (ELUs). *4th Int. Conf. Learn. Represent. ICLR 2016 - Conf. Track Proc.* (2015).
93. Schuster, B. *et al.* Automated microfluidic platform for dynamic and combinatorial drug screening of tumor organoids. *Nat. Commun.* **11**, 1–12 (2020).
94. Canny, J. A Computational Approach to Edge Detection. *IEEE Trans. Pattern Anal. Mach. Intell.* (1986).
95. Munkres, J. Algorithms for the Assignment and Transportation Problems. *J. Soc. Ind. Appl. Math.* **5**, 32–38 (1957).
96. Bloice, M. D., Stocker, C. & Holzinger, A. Augmentor: An Image Augmentation Library for Machine Learning. *J. Open Source Softw.* **2**, 432 (2017).
97. Kingma, D. P. & Ba, J. Adam: A Method for Stochastic Optimization. *3rd Int. Conf. Learn. Represent. ICLR 2015 - Conf. Track Proc.* (2014).
98. He, K., Zhang, X., Ren, S. & Sun, J. Delving Deep into Rectifiers: Surpassing Human-Level Performance on ImageNet Classification.
99. Virtanen, P. *et al.* SciPy 1.0: fundamental algorithms for scientific computing in Python. *Nat. Methods 2020 173* **17**, 261–272 (2020).
100. Walt, S. van der *et al.* scikit-image: image processing in Python. *PeerJ* **2**, e453 (2014).
101. Williamson, I. A. *et al.* A High-Throughput Organoid Microinjection Platform to Study

Gastrointestinal Microbiota and Luminal Physiology. *CMGH* **6**, 301–319 (2018).

102. Mulay, A. *et al.* SARS-CoV-2 infection of primary human lung epithelium for COVID-19 modeling and drug discovery. *Cell Rep.* **35**, 109055 (2021).
103. Krüger, J. *et al.* Drug Inhibition of SARS-CoV-2 Replication in Human Pluripotent Stem Cell–Derived Intestinal Organoids. *CMGH* **11**, 935–948 (2021).
104. Feigin, M. E. & Tuveson, D. A. Challenges and Opportunities in Modeling Pancreatic Cancer. *Cold Spring Harb. Symp. Quant. Biol.* **LXXXI**, 031104 (2017).